Quasi-dynamic modelling of shared mooring lines for floating wind turbines

Master Thesis

Cecilia Saccone

Quasi-dynamic modelling of shared mooring lines for floating wind turbines

Master Thesis

by

Cecilia Saccone

Student Name	Student Number
Saccone Cecilia	5351995

Supervisors: Dr. ir. E. E. Bachynski
Dr. ir. A. C. Viré
Dr.ing. S. Schreier
Dr. ir. K. Larsen

TU Delft

NTNU
Norwegian University of Science and Technology

Preface

This master thesis is part of the requirements for the master's degrees in Offshore Engineering and Dredging at the Technical University of Delft and Technology-Wind Energy at the Norwegian University of Science and Technology.

The work has been conducted in collaboration between the Technical University of Delft and the Department of Marine Technology at the Norwegian University of Science and Technology (NTNU) in Trondheim, Norway. The supervision of Dr. ir. Erin Bachynski and Dr. ir. Kjell Larsen has been provided from NTNU and Dr. ir. Axelle Viré and Dr. ir. Sebastian Schreier have been supervising the work from TU Delft.

I consider myself lucky to have worked under the supervision of such dedicated and knowledgeable researchers. This work would not have been possible without the guidance and assistance I received. I am grateful to my professors for constantly challenging me throughout this thesis and teaching me how to not give up throughout challenges, but rather persist until the desired result is achieved. I would like to express my gratitude to Erin Bachynski, for, from the very first moment, supporting the idea of doing a thesis with floating wind platforms and guiding me in the topic research and for assisting me in using SIMA. To Sebastian Schreier, for your valuable feedback and for sharing your passion and vast knowledge about mooring lines with me. Thank you to Kjell Larsen for your support and constant and insightful contributions. Thank you to Axelle Viré, for chairing the committee, and for pushing towards a critical thinking. Thank you all for your availability, valuable ideas, for sharing your knowledge and for giving me the opportunity of carrying out this work.

Cecilia Saccone
Delft, October 2022

Abstract

The idea of shared mooring systems has been introduced in the offshore wind farm industry as an effort to lower the overall installation costs for floating offshore wind farms. The reason for building such plants is that using floating turbines allows them to move to deeper waters, reducing visual and environmental impact and allowing footprint reduction, with the downside being an increase in the total installation costs.

Because shared mooring lines create couplings between neighbouring turbines, the use of shared mooring lines adds complexity to the design and modelling of offshore floating wind farms. So far, these systems have been investigated and analyzed using either quasi-static or fully dynamic models. With the goal of using a method that can be more accurate in terms of dynamic behavior of the mooring lines than the quasi-static one and less time-consuming than the fully dynamic one by using a system with less degrees of freedom, this project seeks to further explore the idea of shared mooring lines within a quasi-dynamic model.

A quasi dynamic system is not as complex as the dynamic model but more rigorous than the quasi-static one because it includes terms related to the drag and inertia of the mooring lines. Inertial loads on mooring lines can alter the tension of the mooring line at the fairlead, while drag forces on mooring lines will dampen platform motions, especially for slowly varying motions. These are the two reasons why it is critical to include these effects in the model. In this case inertial terms have not been considered, focusing mainly on including drag terms for both the anchor and shared lines together with the geometric and elastic stiffnesses.

To begin with, the quasi-dynamic model has been applied to a two-turbine system, constrained to move only horizontally in surge as a model assumption. The model has been implemented in Matlab as a two-degree-of-freedom system.

The ultimate goal of this research is to see if this approach can be used instead of conducting a thorough dynamic analysis. As a result, in addition to the Matlab model, an equivalent system in SIMA has been built to perform a full dynamic analysis and allow comparison of the two models' findings.

Based on the model results, it appears possible to obtain good accuracy for both motion amplitudes and tension values in a shorter amount of time than a full-dynamic analysis. Indeed, some correlation has been observed between the results obtained with the quasi-dynamic model and the full dynamic one, especially at lower forcing frequencies.

Contents

1 Introduction

The concept of shared mooring systems has been introduced in the offshore wind farm industry as an attempt to reduce the total installation costs for floating offshore wind farms. Figure 1.1 shows a shared mooring line system.

The reason for realizing such plants is that the use of floating turbines instead of bottom-founded ones, allows to move to deeper waters, thus diminishing the problems of visual and environmental impact and allowing footprint reduction, with the downside, however, of a substantial increase in costs.

The use of shared moorings introduces a complexity in the design and modelling of offshore floating wind farms, since the use of shared mooring lines creates couplings between neighbouring turbines, whose displacements are hence influenced by each other. These systems have so far been studied and analyzed using either quasi-static or fully dynamic models. The former is a simplified model that is suitable when the focus is mostly on the displacements of the interconnected turbines rather than on the dynamic behaviour of the mooring lines, which is often required for more in depth analysis of these systems. The latter captures the full dynamic behavior of the mooring lines but it is computationally very expensive, especially for large scale wind farms.

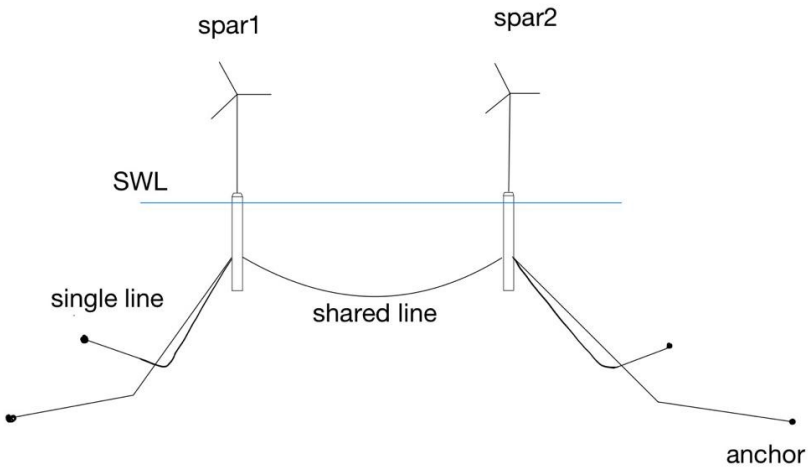

Figure 1.1: Illustration of a shared mooring system

This project seeks to further investigate the concept of shared mooring lines within a quasi-dynamic model, with the intention of using a method that can be more accurate in terms of dynamic behaviour of the mooring lines than the quasi-static one, as well as less time consuming than the fully dynamic one.

A quasi dynamic system is a halfway point between the two previously mentioned models, not as complex as the dynamic one but more rigorous than the quasi-static model, since it also takes into account terms related to the drag and inertia of the mooring lines. Drag forces on mooring lines will have a damping effect on the platform motions, especially for the slowly-varying motions, while inertial loads of the mooring line can change the mooring line tension at the fairlead. These are two reasons why it is important to have these effects included in the model.

The quasi-dynamic model, to begin with, has been applied to a two-turbine system which have been constrained to move only horizontally in surge as a model assumption for ease of analysis. Surge is also one of the main degrees of freedom affected by the catenary mooring system. The model has been implemented in Matlab, as a two degree of freedom system (see chapter 5). The objective is to look at how the two turbines behave and investigate the full dynamics of the mooring lines using the quasi-dynamic model. The ultimate purpose of the project is to investigate if this approach can be used instead of doing a thorough dynamic analysis. For this reason, parallel to the Matlab model, an equivalent system has been built in SIMA (Simulation Workbench for Marine Applications) to perform a full dynamic analysis and to allow comparison between the findings of the two models.

There are already some projects and activities based on the concept of employing shared mooring lines or shared anchors. Among these are the Hywind Tampen project form Equinor and the Honeymooring concept by Semar.

The Hywind Tampen project, shown in Figure 1.2 and developed by Equinor in the Norwegian North Sea, employs shared anchors. This 88 MW project will use 19 anchors for 11 turbines [Equ22]. This is considered a significant decrease from equinor's Hywind Scotland project where five turbines are held by 15 anchors [Equ22].

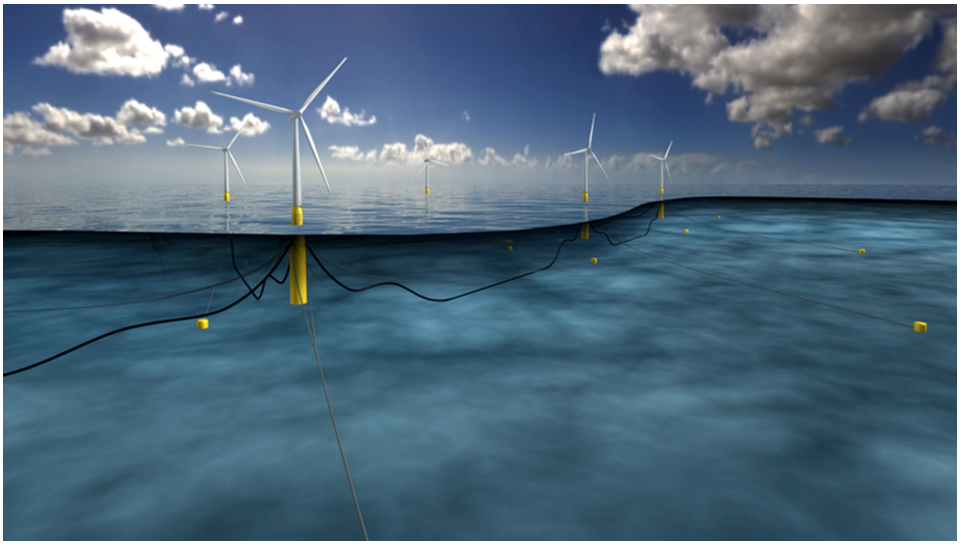

Figure 1.2: Hywind Tampen project by equinor [Equ22]

On the other side, the innovation of the Honeymooring methodology is to connect floating wind turbines in a "honeycomb" network (see Figure 1.3), enabling new methods of deploying well-proven mooring technology in novel and more efficient anchor-sharing combinations. Ac-

cording to Semar, this configuration enables the mooring of floating wind turbines in a network utilizing shared buoys, synthetic fiber lines, and anchors, in a way that it is expected for the system to save up to 50% on hardware costs when compared to typical mooring options based on steel chains [OED22].

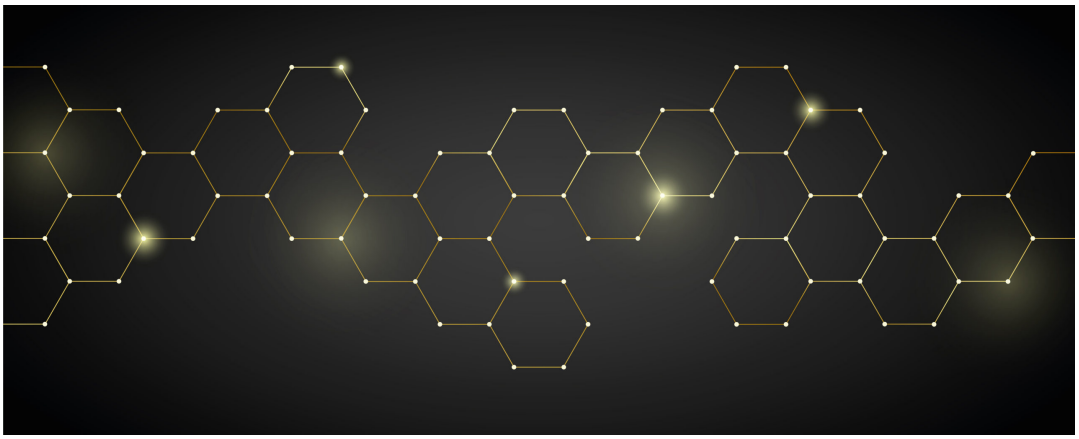

Figure 1.3: Honeymooring concept by Semar [SEM], layout

Figure 1.4 reported below clearly show how turbines and buoys are placed in the honeycomb pattern. Each buoy connects three wind turbines and each wind turbine connects three buoys. The mooring system is realised with low-cost fiber lines and standardized anchor systems are used. This project's value proposition includes improved revenue, lower CAPEX (Capital Expenditure) and OPEX (Operating expenses), lower CO2 emissions, and less seabed damage [SEM]. Additionally, the design accommodates any floater design and provides sufficient vessel clearance [SEM].

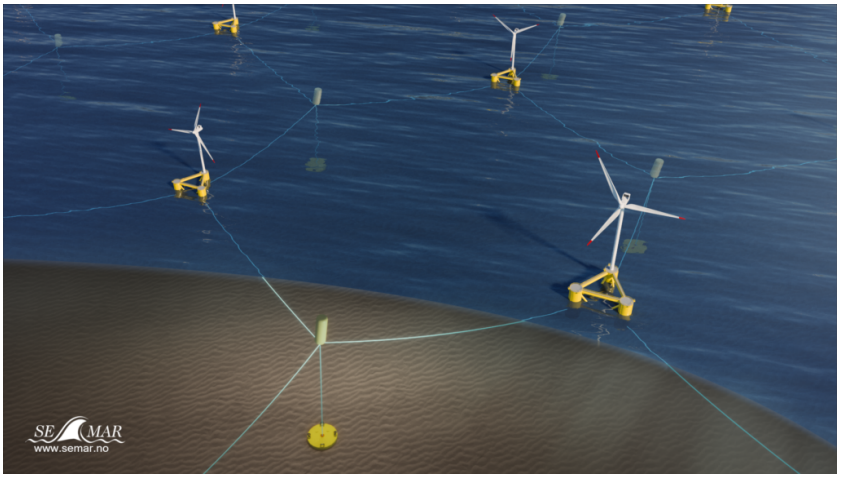

Figure 1.4: Honeymooring concept by Semar [SEM]

2

Background

2.1. Shared mooring systems

As wind energy technology advances, the trend has been moving more and more towards the use of larger turbines in deeper waters. In the last 20 years, offshore wind turbines have seen a remarkable development because they enabled the constructions of more extensive wind farms, with fewer constraints imposed by the availability of areas and by geographical obstacles, which could affect the wind resource (such as trees, buildings).

Most of the offshore wind farms are bottom fixed and realized in waters not deeper than 50 m [CPS18]. In all sites with intermediate ($60 - 120$ m) and high water depths ($200 - 400$ m), traditional support structures for wind turbines, as monopiles, jackets and tripods, are not suitable. This because they would imply excessive costs for great water depths [CH19].

To widen the choice of possible installation sites for wind turbines, floating turbines have been introduced, to be able to install them in deeper waters using mooring systems and anchors to keep them in place. For this reason, floating offshore farms started to be developed and moorings are starting to become a substantial part of the total costs for an offshore wind farm.

Usually in the realization of an offshore wind farm project there are several cost items to be considered. First of all, the construction costs, consisting of manufacturing and installation, which include the turbines, the foundations, the sub-stations, cabling and grid connection costs, must be taken into account. Then there are the operational costs, which include administrative, managerial and maintenance costs. All of these can increase when dealing with floating wind farms, both due to the increased complexity of the structures and to the greater risks associated with this technology.

Therefore, one of the biggest challenges holding back the growth of the floating wind industry is the high cost of realization. The major cost contributions are due to the floating platforms and mooring systems. This because, in deeper waters, the required mooring line length becomes larger, implying higher costs. For this reason, at the moment, the focus is mainly on trying to find ways that make this solution more economically attractive. One of the potential options to lower the total costs in the farm would be to use shared moorings between adjacent turbines, such that neighbouring floating platforms can share part of their mooring lines and eventually also share the same anchors.

In [CH19], Patrick Connolly and Matthew Hall, perform the design and a cost analysis of a four-turbine wind farm, adopting three different shared-mooring configurations and considering four different water depths. The turbines are four pilot-scale 5 MW NREL turbines with

the DeepCwind semisubmersible as support structure, same configuration used in this project. The cost model used is a simplified representation of both the material and installation costs. The mooring line costs are calculated using a coefficient of $\$0.42/$kN-m times the total length of the line and the maximum steady state tension. The anchoring costs instead are computed with a load-based and per anchor component. The results from [CH19] are reported in the figures below. They show that savings are attainable for different design concepts at water depths of 400 m and above, see Figure 2.1 and Figure 2.2. Because a big part of the cost savings in shared moorings comes from not having to lay mooring lines all the way to the seabed, increasing the water depth shows this benefit. Additionally, it should be noted that these cost projections are modest because the FOWTs in the layouts that are taken into account by the authors of the paper are placed 10 rotor diameters apart to reduce wake losses. Less shared mooring line length would be needed for smaller spacings, which would reduce more the cost of moorings.

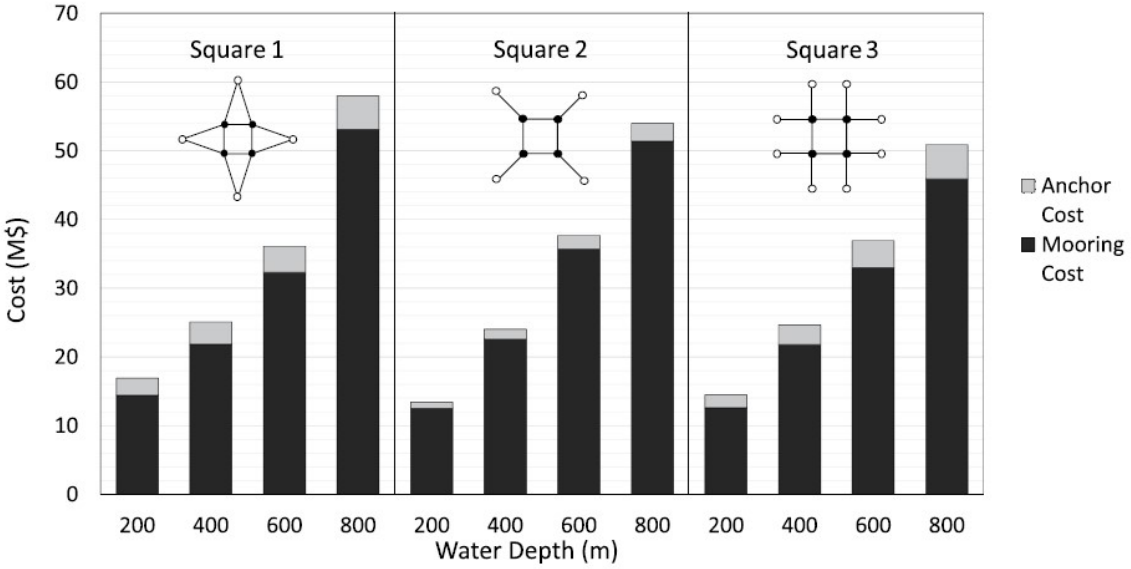

Figure 2.1: Total mooring system cost by configuration from [CH19]

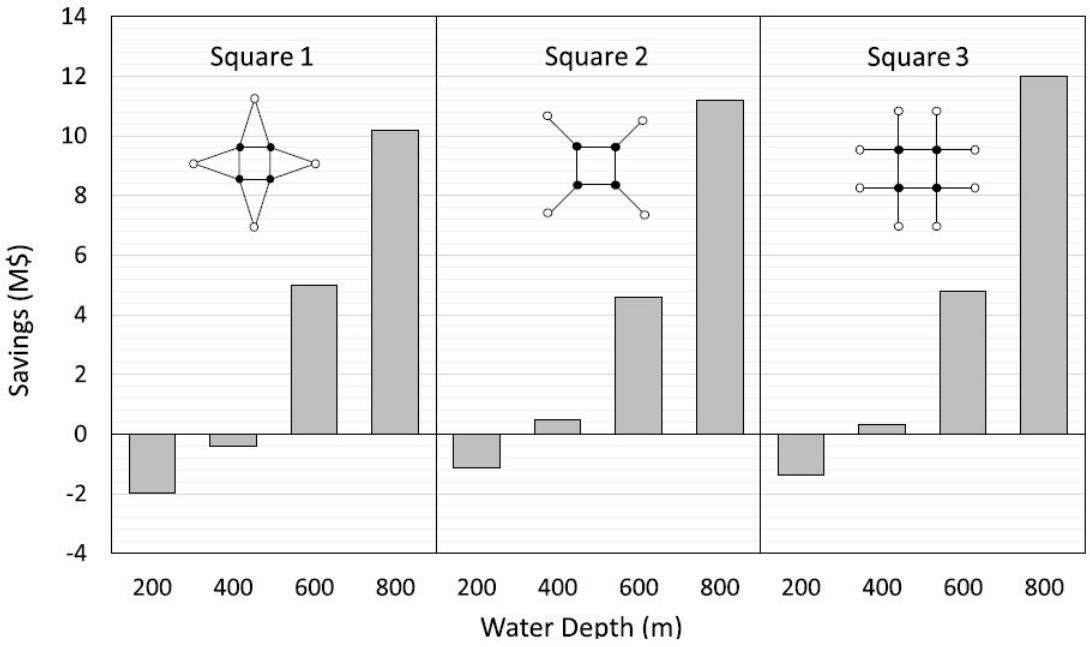

Figure 2.2: Cost savings over single FOWT design by configuration [CH19]

The reason why the system with the configuration with the larger number of anchors and mooring lines ”Square 3”, has the lowest cost is because it corresponds to the one that has the lowest tensions, see Figure 2.3. Since this configuration has a higher ratio between the number of lines and the number of FOWTs $(12/4)$, compared for example to the configuration ”Square 2” which has the lower ration between the number of lines and FOWTs $(8/4)$ it has lower tensions in the lines which determines also a lower mooring line and anchor costs, which both depend on the tension in the lines.

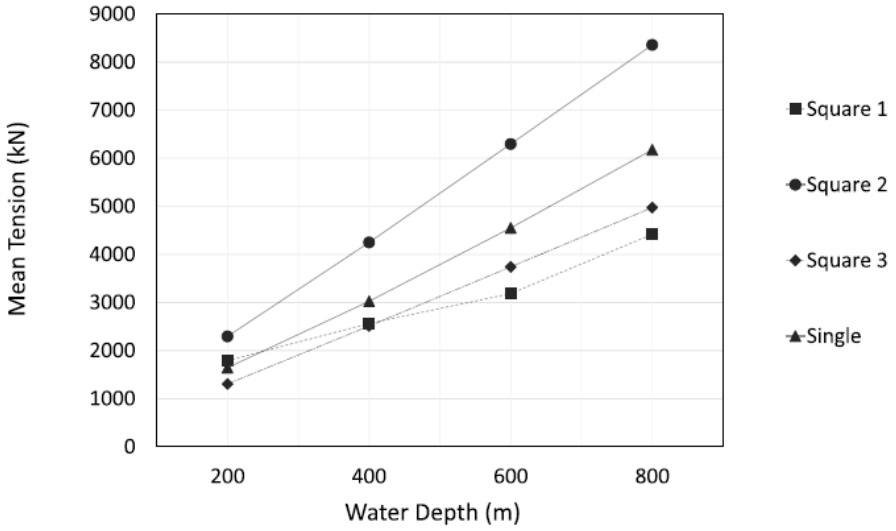

Figure 2.3: Mean Tension values by configuration [CH19]

Looking at Figure 2.1 and Figure 2.2, by selecting appropriate mooring line properties, platform displacements and mooring line tensions may be kept low, and significant cost reductions

over individually-moored farms are attainable at water depths above 400 m. To put these results into perspective, it is worth mentioning that for the current floating offshore wind turbine industry the deep water range includes water depths between 200 and 300 m. As a result, cost savings will be realized when the floating wind industry installs wind farms in deeper waters. Cost reductions are also predicted to be increased by using site-specific design, decreasing FOWT spacing, and increasing farm size.

As already mentioned, the use of shared mooring lines would reduce the total length of the mooring lines both by reducing the number of lines required to keep the turbines in place, and avoiding that all lines have to run all the way down to the sea bed. Furthermore, the wind farm footprint could be reduced and also the number of anchors, which are a further source of considerable costs and represent a crucial component in the installation process. On the other hand, stronger anchoring could be required, which might also make predicting costs more difficult. Unfortunately, shared mooring lines introduce new design and modelling challenges.

Connecting wind turbines through shared moorings will complicate the dynamic behaviour of the wind farm, due to the introduction of additional coupling effects. This relates, in the context of wind turbines, to the analysis of the system displacements caused by time-varying forcing terms. Shared mooring lines connect the turbines together with the possibility of creating unwanted motions. Each shared mooring line is a coupling link. This means that the motions of the turbines that are connected to the same mooring line are influenced by eachother. Therefore, with many shared mooring lines the effect would be to couple many degrees of freedom which must be taken into account for the dynamic analysis of the whole farm.

The introduction of coupling effects between the turbines implies that there will be other natural frequencies of oscillation associated to the coupled DOFs. With the shared configuration, the natural frequency ranges change and could broaden [Con18]. The linking of the FOWTs with common moorings implies that the coupled DOFs of the system will have natural frequencies of oscillation. If there are multiple interconnected FOWTs each free to travel in any direction, there will be numerous natural frequencies of oscillation. If the input force (wave loads and wind loads) excites one or more of these natural frequencies, the response of the wind farm could be significant. In other words, the chance of mechanical resonance increases by adding shared moorings between FOWTs. The result would be an increase in the Floating Offshore Wind Turbines (FOWTs) displacements, whose mitigation is one of the relevant aspects to take into account for the design of floating offshore wind farms. This might become an issue, particularly for surge displacements, whose frequency is in the low frequency range. The main design goal of FOWTs, however, is also to limit the load effects on the structure. To reduce power cable stresses and curvature, or to diminish the loads in the mooring system or on the tower, which are influenced by the displacements of the FOWTs.

The mooring system is what must provide station keeping by restraining the motions of the platform within some specific limits. When assessing the feasibility of a given mooring design, the ability to limit motions is an important factor to consider. Hence, it is important to try to avoid excessive relative displacements between the turbines, especially for the power cables which are not intended to displace excessively and given the high cost of installation that they require. This is because large displacements may result into additional stress and bending in the power cables.

The understanding of the dynamics of these systems is important to properly model the loads on the anchors and on the turbines. This is fundamental also to estimate the costs. Consequently, it is necessary to have simulations and models to analyse more deeply these coupling effects, in an accurate and efficient way.

As shown in Figure 1.1 a shared mooring line configuration consists of a line that is sus-

pended between two adjacent turbines. This line, unlike the other ones that are anchored to the ground, is left hanging between the two turbines and it assumes a different shape. While the anchor lines assume the conventional catenary shape, the shared line has a central sag resulting from the weight of the line itself, which, for heavy line, can also be described by the catenary equations.

2.2. Existing literature on shared moorings

The mooring system, as already mentioned, is intended to limit the displacements of a floating offshore wind turbine, and therefore its design is fundamental to the reliability of the whole wind farm.

Shared moorings are in the first stages of development. They have potential to reduce the number of mooring lines and even anchors, but research about their applications is still ongoing. As a matter of fact, there are no existing examples of floating offshore wind farms with shared mooring lines that have already been installed.

Connolly and Hall [CH19] present an algorithm to perform a preliminary sizing of a shared mooring system for pilot-scale floating offshore wind farms with the main intention to demonstrate that there could be cost savings. Four turbines are considered, arranged in three different rotational symmetric layouts (square) for four different water depths (see Figure 2.4).

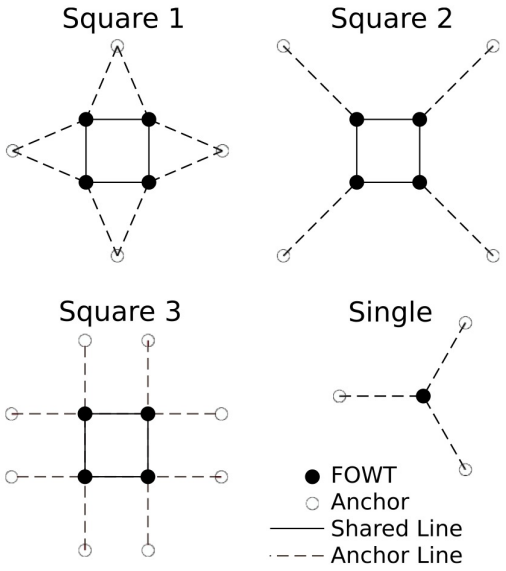

Figure 2.4: Shared mooring FOWT (Floating Offshore Wind Turbines) configuration from [CH19]

The steady state analysis performed in this paper takes into account only steady wind thrust forces and a quasi-static mooring line model. The effects of waves, currents and unsteady wind are neglected in this phase. The algorithm represents the mooring lines having a linear force-displacement relationship over the small wind-induced displacements. A quasi-static mooring line model is used to determine anchor spacings, line lengths, required line weights.

A fully dynamic mooring analysis would be necessary to include the effects of unsteady environmental conditions, but for this preliminary design exploration case the authors do not think it is necessary.

The analysis performed shows that by choosing the appropriate mooring line properties, platform displacements and water depth, mooring line tensions can be kept low and significant

cost savings over the individually-moored wind turbine wind farms are achievable at water depths higher than 400 m. This is quite intuitive if we think that with higher water depths, the lack of need to run the chains all the way to the sea bed is an advantage.

Regarding these results and improvements to this approach, one of the first things to be considered is that by carrying out a quasi-static analysis, steady-state results are obtained. Dynamic displacements and mooring line tensions must be computed for these types of wind turbine arrays.

Goldschmidt and Muskulus [GM15] found that by using shared moorings considerable cost reductions can be achieved, but only up to a certain farm size. Depending on the type of configuration the number of FOWTs until which the cost reduction is reached varies from 3 to 4 in the triangular and rectangular set-up and stays 3 for the row layout, see Figure 2.5. This is because the requirements due to the loads in the mooring chains and anchors and the resulting costs increase with the number of FOWTs in these type of systems.

The catenary mooring system, in this case, is modeled using the catenary equation. For calculations in the frequency domain the mooring system is simplified by a linearized stiffness matrix. For the solution in the time domain a quasi-static catenary model is used which is coupled to the overall hydrodynamic analysis to solve to the response of the floater.

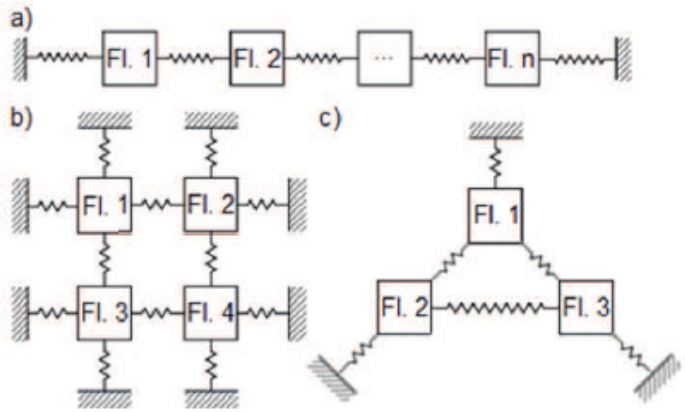

Figure 2.5: Wind farm layouts: a) row, b) rectangular, c) triangular considered in [GM15]

M. Hall and S. Wilson [Wil+21] introduce a linearized model for the force-displacement response of shared moorings, including couplings. The aim is to provide a general method for creating shared mooring designs, which compared to single moorings have more design variables. Furthermore, the coupling between adjacent turbines makes the achievement of the equilibrium positions more challenging, which is why it has been included in the model.

The model considers the wind turbines as point masses, while the mooring lines are modelled as mass-less linear springs, see Figure 2.6. Each floating platform can move in x and y directions.

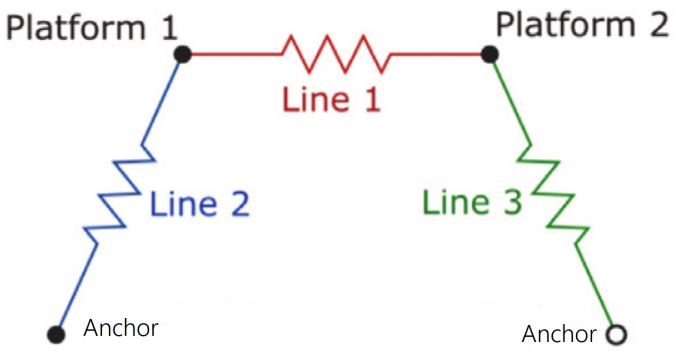

Figure 2.6: Hypothetical array of wind turbines adapted from [Wil+21]

The original figure from [Wil+21] included a third platform in place of one of the anchors. Figure 2.6 has been adapted from [Wil+21] because assuming that it was a top view of the array of turbines, a system having three platforms and only one anchor would have led to no steadiness and it would have been a weather-vane system. Therefore, the figure has been re-interpreted as an elevation of an array of two turbines with a shared line and one on the platforms replaced with an anchor.

The aim of this work is to optimize the layout of the wind turbines in order to find the best shared configuration that gives the lightest arrangement in terms of tensions in the lines.

One of the outcomes of this analysis is that the more a turbine is moored by shared lines instead of anchor lines (mooring lines that connect the single floater to the anchor on the seabed), the less restrained their movement will be.

One of the suggestions made by the authors is to try to use a model for the mooring lines that gives a better estimation of the dynamics of the line itself, since dynamic mooring line loads are particularly important for shared mooring floating wind turbines.

Connolly [Con18] investigates the potential for and effects of mechanical resonance in shared mooring configurations for floating offshore wind farms.

For the frequency-domain analysis the mooring lines are modelled as simplified mass-spring systems. For the time-domain analysis a quasi-static mooring line model is used to simulate the catenary mooring lines in order to calculate the platform displacements and mooring line tensions.

A mooring design algorithm is developed to determine the effective stiffness required by an individual line to maintain the total displacement lower than a specific limit. Then it defines, on a set of parameters, the quasi-static mooring line which will satisfy this stiffness. The shape of the mooring line is found using a secant solver.

A quasi-static model is used to simulate the catenary mooring-lines and calculates the tension in the mooring line at each end by solving for the catenary shape and then summing the force over a discrete set of points along the line. It is assumed that the line is stationary at every time step. Therefore any damping or added mass due to the motion of the mooring lines is not accounted for. Also inertial loads due to dry mass are not accounted for in this approach.

Linearity is assumed in this model, which makes computations easier and allows accurate results for small displacements. However, when the platforms are displaced, the amount of mooring line which hangs and the shape of the line itself, changes, and the forces change as well. These changes are not necessarily linear and to avoid these non linearities that the

model will not be able to consider, the mooring lines have to be designed with conservative design choices. Using a non linear model could ease the design process by not needing to be so rigid on certain parameters and being able to make more realistic choices.

The quasi static mooring line model is based on the unloaded positions of each FOWT. When the wind turbines are subjected to a steady wind force, they are displaced several meters and this has a significant effect on the stiffness of the mooring lines. Due to these displacements the lines are in a different catenary shape than expected. For example the mooring lines of the turbines that are upwind (1 and 3 in figure Figure 2.7) will see an increase of the stiffness in their lines, because they come close to being taut. For the ones on the other side of the farm (0 and 2 in Figure 2.7), the FOWT are moved closer to the anchors and their effective stiffness in the lines decreases. In conclusion, when subjected to a steady wind force the FOWTs are displaced enough to have a significant effect on the stiffness of the mooring lines. The increase in stiffness for each mooring line as described above is expected to become less linear the more the line is close to being taut and this causes discrepancy with the linear assumption made.

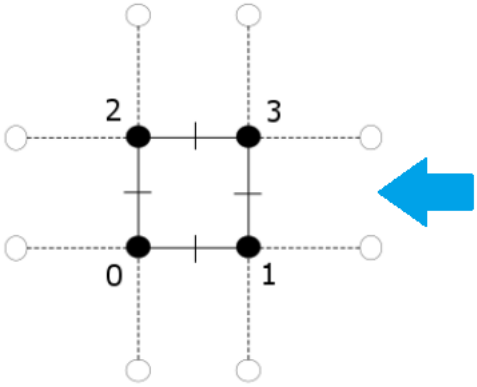

Figure 2.7: 2-by-2 FOWT farm configuration from [Con18], wind blows from the right to the left as the blue arrow indicates

It is also mentioned that when the number of coupled DOF increases, the number of natural frequencies increases as well. Therefore, when the different modes are excited, there could be a higher risk of mechanical resonance from the wave forcing.

2.3. Conclusion

By taking into consideration what has been discussed so far, one of the improvements that can be done in this field, is in the mooring design process, taking into account dynamic effects. A fully dynamic analysis might be computationally expensive and long to perform, therefore to avoid this, a quasi-dynamic model can be implemented to have more accurate results than the quasi-static analysis, which has been the most commonly used tool until now to get an estimation of the behavior of these types of systems in a short amount of time compared to a fully dynamic analysis.

3

Theory

3.1. Catenary Mooring Systems

As it has been said before, mooring systems are designed for the station keeping of the floating wind turbines to withstand environmental loads, pulling them back to the equilibrium when they are displaced.

A mooring system consists of three parts: an anchor system, a mooring line and a defined layout. The latter depends on a number of factors such as the local environmental conditions, soil properties, type of floater, water depth and seafloor conditions. However, these aspects also affect the choice of anchor and mooring line.

There are different types of mooring lines such as catenary and taut, and also different materials with which these can be manufactured (steel chains, nylon cables etc.). The catenary system has a larger footprint on the seabed compared to the taut mooring system in terms of having a larger seabed area.

The environmental loads that act on a floating wind turbine are taken up by different elements, such as inertia and hydrostatic restoring forces, damping and finally by the mooring lines. These loads have different magnitude and directions and the most important ones that have to be taken into account for the mooring line design are wind, waves and current as shown in Figure 3.1.

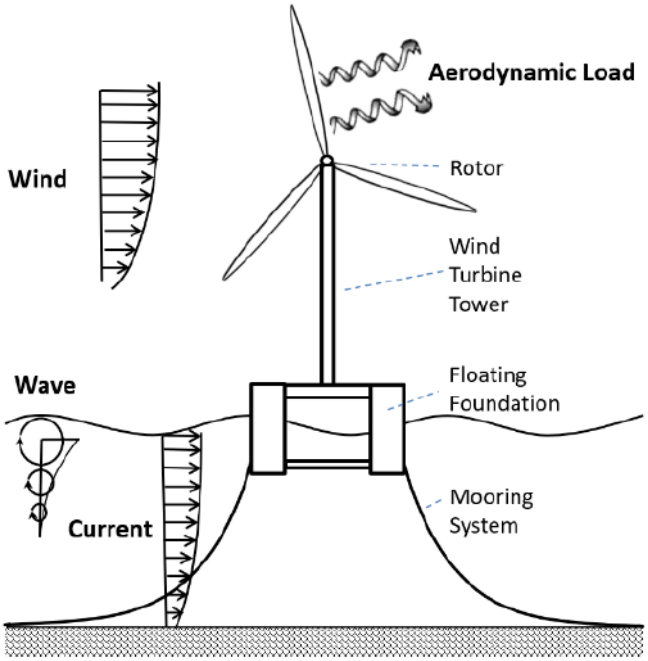

Figure 3.1: Environmental loads acting on a Floating Offshore Wind Turbine [Ma+21]

The goal is to design the mooring lines to withstand the environmental loads so that the strength and fatigue requirements are met by all mooring components.

The loads that act on a floating structure can cover different frequency ranges.

- Steady loads
- Low-frequency loads
- First order wave-frequency loads
- Operation loads such as wind turbine loads 1P and 3P

Steady loads, as mean wind, current and mean wave forces, move the structure causing a displacement from equilibrium which is counterbalanced by the restoring force of the mooring lines.

Low-frequency loads include the wave-drift second order forces. These loads are associated with the frequencies of wave groups occurring in irregular waves. The contribution from a given pair of wave components from a wave group has frequency equal to the difference between the frequencies of the wave components in the pair. Wave component pairs that are near each other in frequency give low frequency load contributions; these determine the slowly varying part of the wave drift load, which can excite slow drift motion of the floater and the mooring system.

First order wave frequency loads contribute to the maximum mooring line tensions and fatigue damage. However, since the presence of a mooring system introduces a high natural period in the horizontal plane, there are risks of low frequency resonant excitation from second order difference frequency effects. This effect is then enhanced by the slowly varying wind force. The first order, wave forces are linearly proportional to the wave height and contain the same frequencies as the waves.

The operation loads are divided into wind load, 1P (rotor rotational speed), and 3P (blade passing frequency). These loads are generated by the wind pressure and depend on the inflow turbulence and frontal area of the blades. The 1P load is generated by the mass and the

aerodynamic imbalance of the rotor, and it is the one that causes fatigue damage to the main shaft, gearbox, and tower. The 3P load, which results in power pulsation and is dangerous for grid security, is brought on by wind shear and tower shadow effects when blades pass through the front of the tower.

In order to understand where these frequencies are placed in the typical total frequency spectrum of a floating turbine with respect to each other, the following figure has been reported:

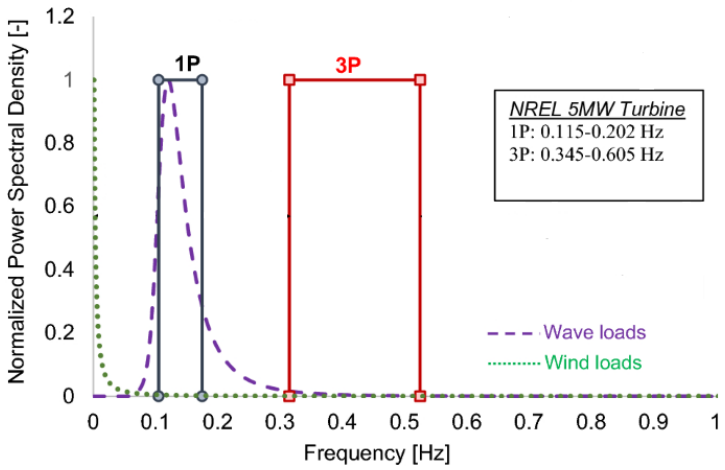

Figure 3.2: Excitation frequency ranges for the 5MW NREL offshore wind turbine [Bha+13]

As it can be seen in the figure above, the low frequencies (from 0.05 to 0 Hz) will fall in the wind turbulence frequency range, which could represent a potential source for excitation of the natural frequencies of the system. This emphasises the importance of having a reliable mooring line-dynamic model, relatively easy and fast to implement, to better estimate the possibility of resonance in a shared mooring configuration [Mag14].

In this analysis catenary mooring lines have been selected. These are characterized by a hyperbolic profile between the fairlead and the touchdown point due to their self-weight with part of the line laying on the sea bed in the static equilibrium position. The shape is shown in Figure 3.3.

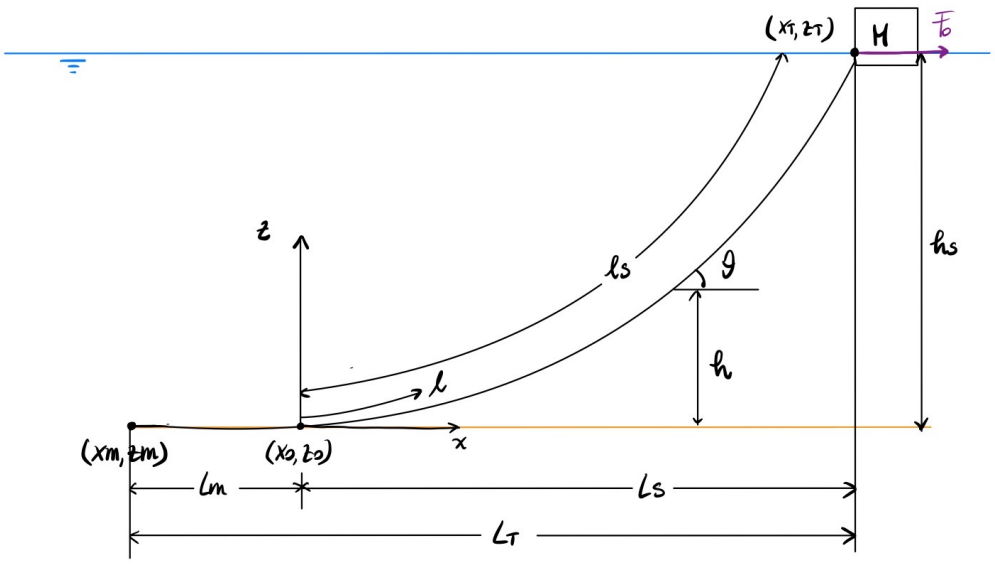

Figure 3.3: Catenary mooring line scheme

In the image above, the main geometrical parameters of a single mooring line are presented :

- l_s, the total suspended length
- h_s, the water depth (assuming that the fairleads are at the waterline)
- F_0 mean horizontal force from wind,wave and pre-tension
- (x_T, z_T) coordinates of the fairlead
- (x_0, z_0) coordinates of the touchdown point
- (x_m, z_m) coordinates of the anchor point
- L_T, the anchor radius
- w, the chain wet weight per unit length

3.1.1. Governing equations of mooring line

Considering a small element of the mooring line in a 2-D plane as shown in the figure below, it is possible to write the equilibrium equations considering all the forces acting on the single element. In this case the elasticity of the cable has been taken into account, since the elastic material properties can make a significant difference to the tension levels.

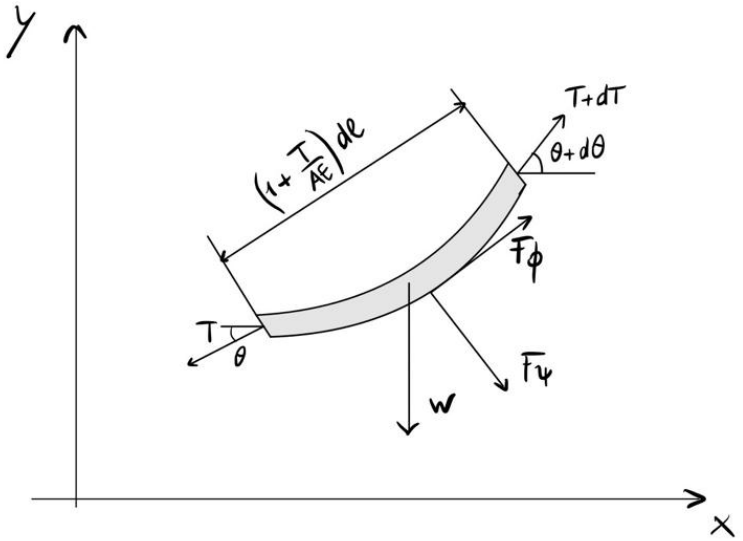

Figure 3.4: Force and displacement on an element of a mooring line [Ma+19]

In the free body diagram, the axial stretch of the line will result in $dl(1+\frac{T}{AE})$, where AE is the axial stiffness per unit length, T is the effective tension along the line, $d\psi(l)$ is the displacement in the direction normal to the mooring line, $d\phi(l)$ is the displacement in the direction tangential to the mooring line and w is the submerged weight per unit length.

Bending and torsional stiffnesses are neglected, since a chain element is considered. F represents the hydrodynamic force acting on the mooring line element with a mass m. In the tangential and normal directions the equilibrium equations are as follows [Ma+19]:

$$-T + (T + dT)\cos d\theta - w \sin\theta dl + F_\phi \left(1 + \frac{T}{AE}\right) dl = m\frac{d^2\phi(l)}{dt^2} \tag{3.1}$$

$$(T + dT)\sin d\theta - w\cos\theta dl - F_\psi \left(1 + \frac{T}{AE}\right) dl = m\frac{d^2\psi(l)}{dt^2} \tag{3.2}$$

F_ψ and F_ϕ are the hydrodynamic forces in the normal and tangential directions, which can be derived from Morison's equation. The other forces included in the previous equations are the inertia forces in the normal and tangential directions.

These equations, with appropriate boundary conditions on the floating structure's attaching point and seabed conditions, are the governing differential equations for a mooring line considering both mooring line dynamics and elasticity.

3.1.2. Mooring line statics

If no dynamics are considered, ignoring damping and inertia forces, the statics of the mooring line can been solved. In fact, when only the statics of the mooring line are taken into account, the catenary equations can be defined.

Here below the static equilibrium equations are reported, for a mooring line element as the one shown in Figure 3.4.

$$\frac{d\phi}{ds} = \frac{w}{T}\cos\phi \tag{3.3}$$

$$\frac{dT}{ds} = w \sin\phi \tag{3.4}$$

The following equations are the ones that link the horizontal (x) and vertical (y) distances to the mooring line length s and angle ϕ:

$$dx = ds(1 + \frac{T}{AE}) \cos\phi \tag{3.5}$$

$$dy = ds(1 + \frac{T}{AE}) \sin\phi \tag{3.6}$$

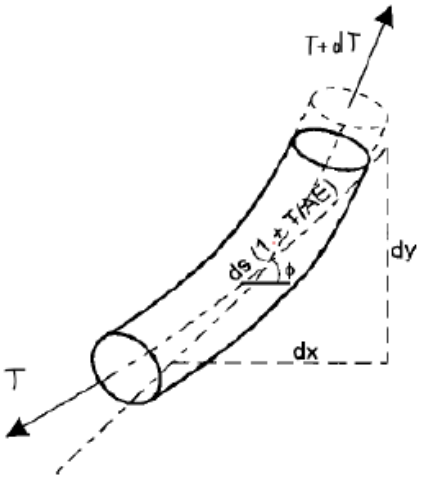

Figure 3.5: Mooring line element wit axial stretch

Solving analytically the previous equations the ”catenary solutions” that include the effects of elasticity are the following [LJM21]:

$$x(s) = \frac{Hs}{EA} + \frac{H}{w} \sinh^{-1}(\frac{V}{H}) \tag{3.7}$$

$$y(s) = \frac{ws^2}{EA}\left[\frac{V}{ws} - \frac{1}{2}\right] + \frac{H}{w}\left[\sqrt{1 + \left(\frac{V}{H}\right)^2} - 1\right] \tag{3.8}$$

where s is the suspended length of the cable, w is the weight in water of the chain per unit length and V and H are the vertical and horizontal components of the line tension.

To determine the suspended line length and the static shape of the line, Equation 3.7 and Equation 3.8 combined with the following other two expressions, are solved in an iterative way, with an initial guess for the distance between anchor and touchdown point. In Equation 3.10, L is the total untrained length of the cable.

$$X = \frac{H}{w} \sinh^{-1}(\frac{wL}{H}) + \frac{HL}{AE} \tag{3.9}$$

$$L = 1/w\sqrt{T^2 - H^2} \tag{3.10}$$

By combination of several equations, without considering the elasticity of the line ($\frac{T}{EA} << 1$), the following expression can be found:

$$X_l = L + \frac{H}{w} \cdot \cosh^{-1}\left(1 + \frac{w \cdot y}{H}\right) - \sqrt{y \cdot \left(y + \frac{2H}{w}\right)} \tag{3.11}$$

$$y = \frac{H}{w} \cdot \left[\cosh\left(\frac{w \cdot x}{H}\right) - 1\right] \tag{3.12}$$

Suspended catenary equations

Here below have been reported the catenary equations in the case of a suspended catenary line [LJM21].

$$x(s) = \frac{Hs}{EA} + \frac{H}{w}\left[\sinh^{-1}\left(\frac{V}{H}\right) - \sinh^{-1}\left(\frac{V - ws}{H}\right)\right] \tag{3.13}$$

$$y(s) = \frac{ws^2}{EA}\left[\frac{V}{ws} - \frac{1}{2}\right] + \frac{H}{w}\left[\sqrt{1 + \left(\frac{V}{H}\right)^2} - \sqrt{1 + \left(\frac{V - ws}{H}\right)^2}\right] \tag{3.14}$$

When s is equal to the total suspended length of the line, Equation 3.13 and Equation 3.14 give respectively the horizontal and vertical distance between the top ends of the line.

In the figure below, the general case of a suspended catenary is represented.

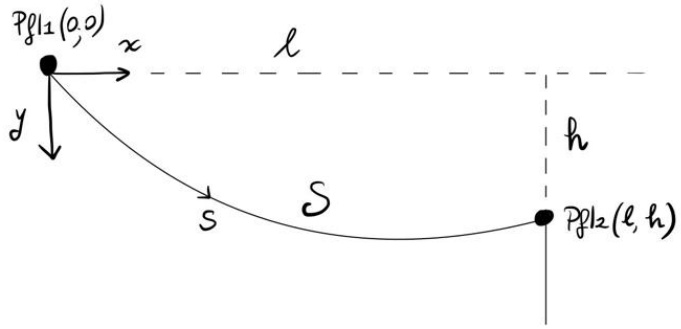

Figure 3.6: Illustration of a shared line system in the catenary plane

Lower case s defines the coordinate along the suspended line while capital S indicates the total suspended length of the line.

3.1.3. Mathematical models for catenary mooring systems

Mathematical models for mooring systems identify and represent the relationship that exists between system parameters, variables, and environmental inputs such as wave, wind and currents.

Among the parameters and properties of the system are:

- the number of lines

- position of the anchors on the bottom (x_m, z_m)
- the initial length of the line
- the point of connection with the floater (fairleads) (x_T, z_T)
- the diameter of the lines
- material properties as mass density, elasticity
- pre-tension

The variables, on the other hand, are:

- the suspended length l_s
- the strain, which indicates how much the line has stretched
- the tension in the mooring line T
- the point where it touches the ground (touch-down point) (x_0, y_0)
- the length of the line, which can vary due to the elasticity of the line, directly related to strain
- speed and acceleration of the mooring line

Mooring line systems are susceptible to a variety of loads due to their placement in water with changing loads as well to the motions at the fairleads. Current forces generate drag on the line and tension forces within the lines.

There are different possible options in which mooring lines can be mathematically modeled, depending on the level of accuracy of the model desired and the computational costs to be faced. The following are the different mathematical methodologies that can be used to model mooring line systems sorted from the least realistic and computationally least expensive to the most detailed, numerically most complex and with the higher computational costs. The distinction lies in the different fidelity of the models, in the sense of how much of the physical problem is accounted for.

- Static linear model
- Quasi-static model
- Quasi-dynamic model
- Dynamic model

If only the static shape and forces of the hanging chain line are of interest, the static model is effective. If very small motions of the floaters are considered, the mooring line stiffness can be assumed constant and the static approach can be extended to small and slow motions. If the motions then become larger, the change in the mooring line stiffness needs to be taken into account and therefore the quasi-static approach should be adopted. If in addition to this the damping and the inertia terms have to be taken into account because of higher frequency loads, but the motions can still be considered relatively small, then the quasi-dynamic approach can be adopted. Finally if the whole dynamics of the system in terms of non-linear drag, inertial loads and non linear stiffness are included then the full dynamic model should be used.

Static linear model

The simplest mooring line model that can be used is a linear spring model linearized around a given floater location and orientation. This model determines the equilibrium between constant or mean environmental loads and the restoring force, which is calculated considering the mooring system as a mass-spring system. The spring considered is a linear spring. The

equation of the model is $F = k \cdot x$, where F is the restoring force, k is the mooring (tangential) stiffness and x is the displacement of the floater with mass M and added mass A. The displacement of the mass is used to calculate the tension in the mooring line, knowing the stiffness. With this method non linear static or dynamic effects are not captured.

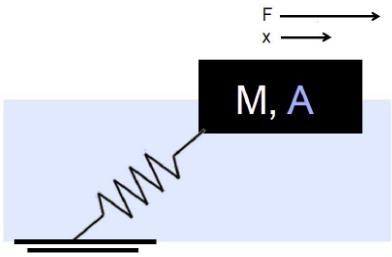

Figure 3.7: Mass-spring model

Quasi-static model

The quasi-static model expands the linearized one by updating the line forces for every given position and orientation of the floater. In the quasi-static model it is assumed that the line immediately reaches its new static equilibrium state for the updated position of the floater, which does not happen in reality. The motion of the system is considered linear and uniform between two static positions (see Figure 3.8). However what changes for every new position, are the suspended length and the part laying on the seabed between the beginning and the end of the calculation. Therefore, given a displacement of the fairlead, the new shape is found knowing the catenary equation. More typically given the forces on the line, the displacement that gives the static equilibrium is found.

The model is defined as quasi-static because it assumes that the mooring line is stationary at every time step, for which the loads are assumed constant. This means that any possible damping or added mass due to the motion of the mooring line itself is not taken into account. Also it does not predict snap loads.

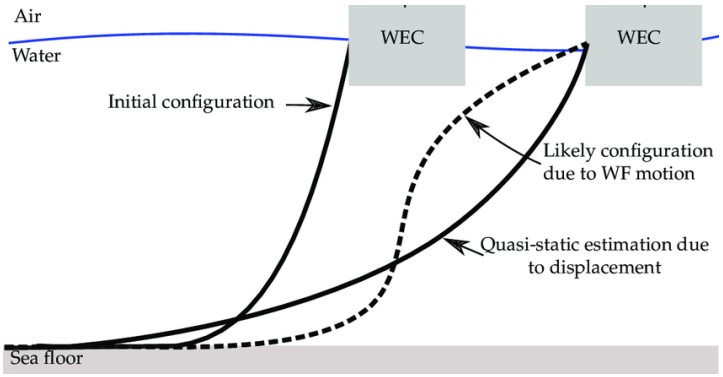

Figure 3.8: Comparison quasi-static shape [JSW06]

Neither the linear spring nor quasi-static model takes the cable dynamics and hydrodynamics into account.

Quasi-dynamic model

The quasi-dynamic model includes drag and inertia forces, compared to the previous methods. It models each line as a single DOF spring-dashpot system, see Figure 3.9. This system considers inertia and drag forces due to the line motion in addition to the elastic and geometric stiffness already considered in the quasi-static model.

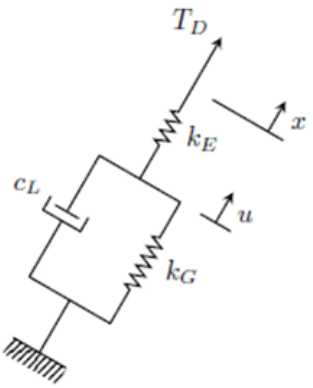

Figure 3.9: Quasi-dynamic scheme [Heg20]

The dynamic tension can then be derived using the following expression [Heg20]:

$$T_D = k_E[x(t) - u(t)] = c^*\dot{u}(t)|\dot{u}(t)| + k_G u(t) \tag{3.15}$$

which can be considered as a variant of Morison's equation. In Equation 3.15 $u(t)$ represents the generalized displacement of the line while k_G is the geometric stiffness. The generalized damping coefficient c^* can be found using the quasi-static line configuration as the shape function. This process for the linear damping coefficient is presented in subsection 5.1.3. On the other hand, in this project in the quasi-dynamic model the inertia term $\omega^2 m^* x(t)$ has been neglected.

Dynamic model

The full dynamic analysis considers the mooring line as a whole of finite elements consisting of a lumped mass and a spring-damper system (Finite Element Method). The motion of each element is calculated using Newton's second law, where all the forces acting on the element are considered, added mass, damping and stiffness.

Dynamic analysis has the potential to be the most accurate one, since it includes all dynamic effects as inertial loads, hydrodynamics, sea bed interaction but it requires higher computational cost, especially for large scale wind farms. With this model the number of degrees of freedom of the system is much larger compared to the previous ones. For each mooring line the FEM divides the cable into multiple elements and the accuracy of the model increases with increased number of elements. Therefore this type of analysis can reach high computational complexity due to the high number of degrees of freedom.

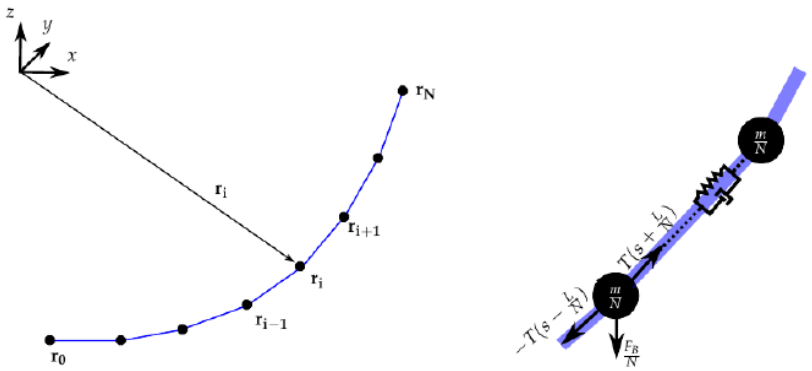

Figure 3.10: Dynamic model representation

3.1.4. Modelling choice

After presenting the different modelling approaches the differences between them, from the simplest to the most sophisticated and complex, are easily deductible.

In this specific study, the quasi-dynamic approach is investigated. The reason is to propose an approach for modelling shared mooring lines that is between the quasi-static and the fully dynamic one that has not yet been used for this specific type of system and will provide sufficiently accurate results in a faster time frame.

4

Case study

The system that has been modelled for this project includes two semi-submersible floating wind turbines, each having three mooring lines, one shared between the two turbines and two anchored to the sea bed. The system thus defined is shown in the following figure:

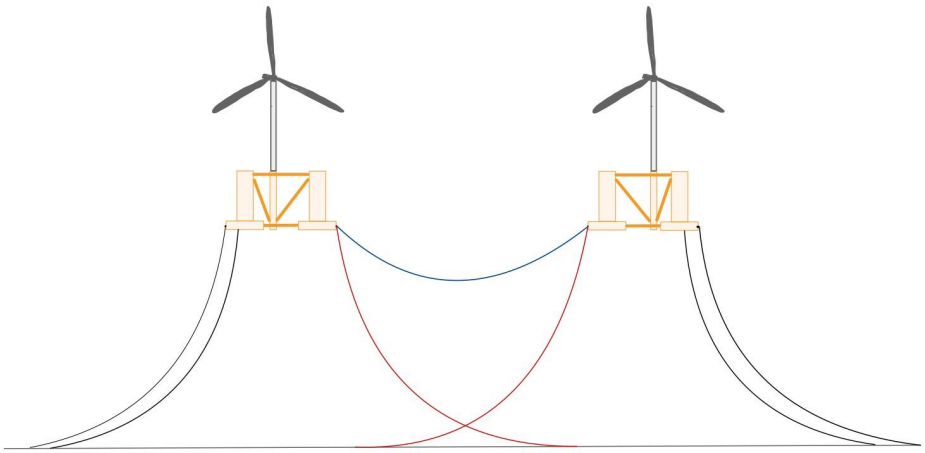

Figure 4.1: Representation of the model with the OC4 semi-submersible with (blue line) and without (red lines) the shared mooring line

The red lines represent the conventional mooring configuration, while the blue line represents the shared mooring one.

4.1. Structure type

In this project the OC4 semi-submersible, whose design has been developed for the DeepCwind project, has been used. The reason why this type of structure has been chosen is to be able to benchmark the results with the ones found from Connolly in [Con18] in his shared mooring system model.

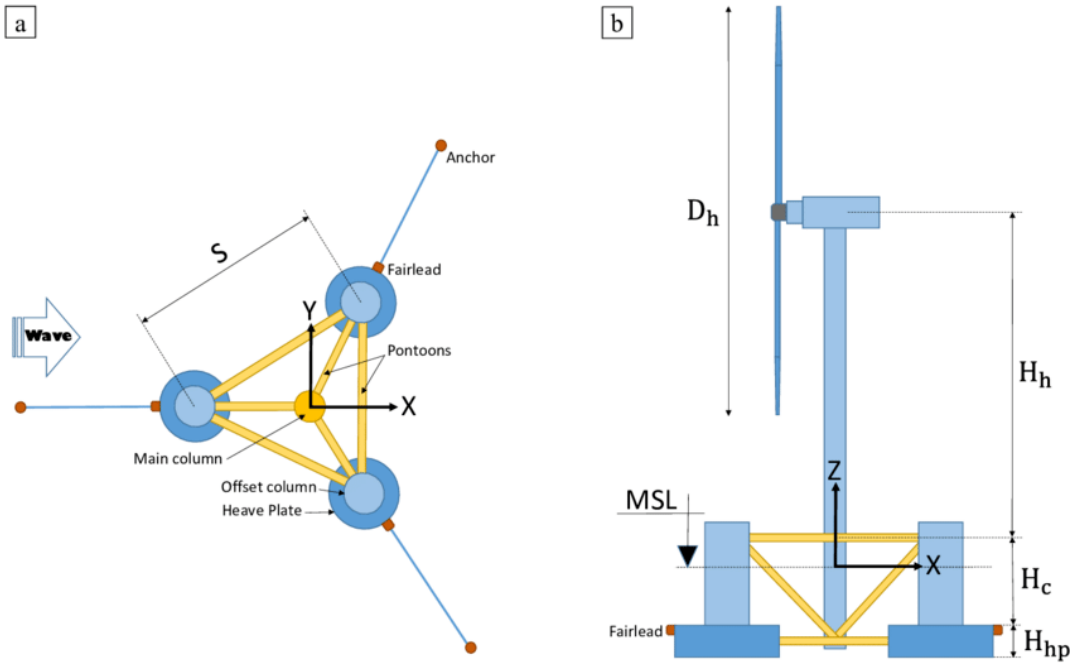

Figure 4.2: DeepCwind floating wind system design

The OC4 stands for Offshore Code Comparison Collaboration Continuation project, and this structure is part of a project created to build aero-hydro-servo-elastic models. In this project four different types of wind turbine systems are analysed, of which three are bottom-fixed and one floating. In the previous project OC3, of which OC4 is the continuation, the floating system was a spar concept while for the OC4 the system is the DeepCwind semi-submersible.

This type of substructure, as shown in Figure 4.2, consists of a small column attached to the tower and three offset columns connected to the main column through a series of smaller diameter pontoons and cross members. This structure, compared for example to a spar-type, is characterized by relatively large motions. This because the spar unlike the semi-submersible has a small water-plane area and therefore small responses to wave forces.

The semi-submersible has on the other side a straightforward installation and it is flexible regarding the water depth choice. In addition, it is a buoyancy stabilized floating structure, see Figure 4.3, compared to the spar type which is a ballast stabilized structure. The fact that the semisubmersible is a buoyancy stabilized type of structure is due to its larger water-plane area. More specifically, the water-plane area is the key contribution to the restoring moment of the floater because in the event of rotational displacement, having a large second moment of area with respect to the rotational axis, due to a large water plane area, provides a stabilising righting moment, ensuring the balance of the system.

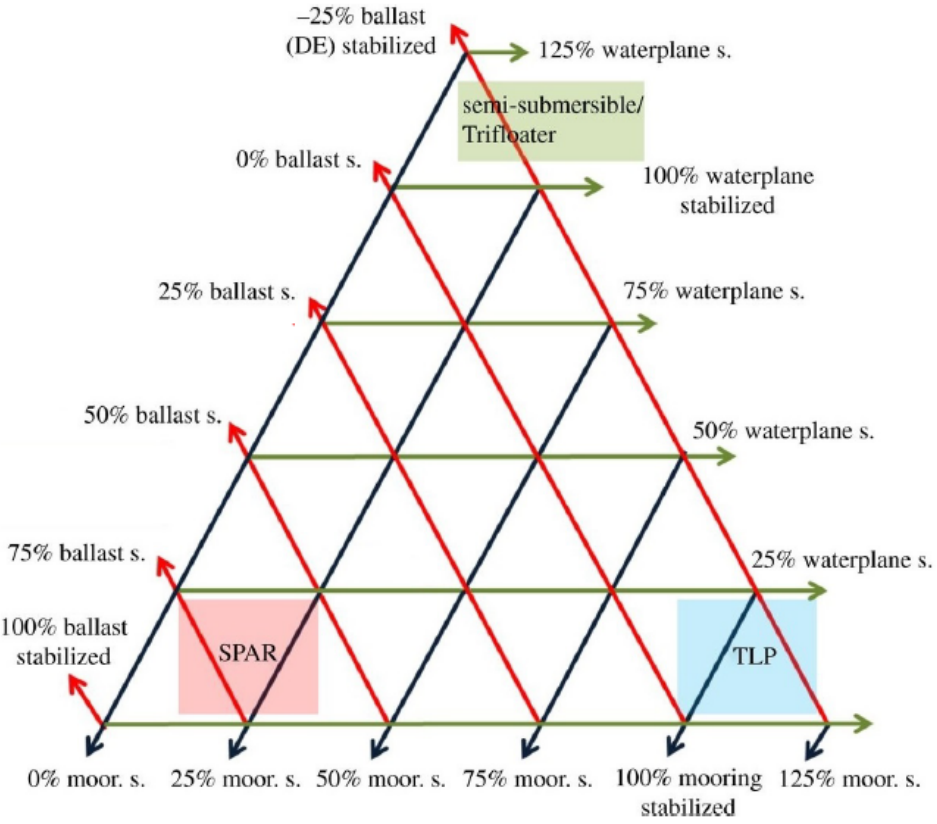

Figure 4.3: Stability triangle for floating structures [LKC18]

In the following tables, the floating platform structural properties are presented.

Depth of platform base below SWL (total draft)	20 m
Elevation of main column (tower base) above SWL	10 m
Elevation of offset columns above SWL	12 m
Spacing between offset columns	50 m
Length of upper columns	26 m
Length of base columns	6 m
Depth to top of base columns below SWL	14 m
Diameter of main column	6.5 m
Diameter of offset (upper) columns	12 m
Diameter of base columns	24 m
Diameter of pontoons and cross braces	1.6 m

Table 4.1: Platform geometry from [Rob+14]

Platform mass, including ballast	1.3473E+7 kg
CM location below SWL	13.46 m
Platform roll inertia about CM	6.827E+9 kg-m2
Platform pitch inertia about CM	6.827E+9 kg-m2
Platform yaw inertia about CM	1.226E+10 kg-m2

Table 4.2: Platform Structural Properties from [Rob+14]

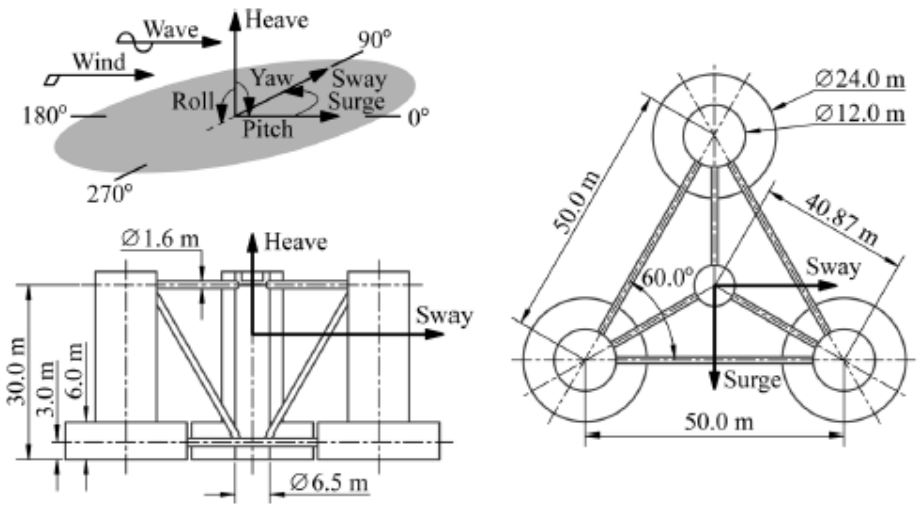

Figure 4.4: Coordinate system and dimensions of the DeepCwind semi-submersible platform [Cou+13]

4.1.1. Wind Turbine

The turbine used in the model is the National Renewable Energy Laboratory (NREL) offshore 5-MW baseline wind turbine.
In the following tables, the properties of the wind turbine are presented.

Rating	5 MW
Rotor Orientation, Configuration	Upwind, 3 blades
Rotor, Hub Diameter	126 m, 3 m
Hub Height	90 m
Rotor Mass	110,000 kg
Nacelle Mass	240,000 kg
Tower Mass	347,460 kg
Hub Mass	56,780 kg

Table 4.3: Gross Properties of the NREL- 5 MW Baseline Wind Turbine adapted from [Jon+09]

In both the quasi-dynamic Matlab and the full dynamic SIMA models the wind turbines are included as lumped masses. In the first model the mass of the rotor-nacelle assembly together with the mass of the floater and tower are summed and referred to as M_1 and M_2 (see Figure 5.1 and Equation 5.1). In the second model, the rotor-nacelle assembly mass is included as a lumped mass placed on top of the tower located itself on top of the semi-submersible.

4.1.2. Mooring line system

Here below are reported the mooring line data from the DeepCwind project, in terms of system properties. In Table 4.5, the lengths of the lines chosen for this model are reported. These values have been taken from Connolly [Con18], which were found through his mooring design algorithm. The reference [Rob+14] specifies that the mooring system is constituted by three catenary lines, however the type of chain is not specified.

Number of mooring lines for each floater	3
Angle between adjacent lines	120°
Depth to anchors below SWL	200 m
Depth to fairleads below SWL	14 m
Mooring line diameter	0.0766 m
Submerged mass per unit length	108.63 kg/m
Dry mass per unit length	113.35 kg/m
Axial stiffness of the Mooring line	7.536e+08 N

Table 4.4: Mooring system properties adapted from [Rob+14]

Type	L_{total} (m)
Anchor	772
Shared	1296

Table 4.5: Quasi-static mooring line parameters used in [Con18]

To get the submerged weight of the line per unit length then, the submerged mass per unit length has been used and multiplied by the acceleration of gravity $g = 9.81$ m/s^2, which leads to a value of $w = 1.0656e + 03$ N/m.

The final mooring line configuration has been found by performing the static analysis in SIMA and the parameters have been reported in the table below.

Total distance between floaters	X_{tots}	1255.1 m
Horizontal tension shared line	Tx_{shared}	$1.4677e + 06$ N
Vertical tension shared line	Tz_{shared}	$6.905e + 05$ N
Axial tension shared line	T_{shared}	$1.622e + 06$ N
Horizontal tension anchor line	Tx_{anchor}	$1.4657e + 06$ N
Suspended length anchor line	S	733.3 m
Vertical tension anchor line	Tz_{anchor}	$7.8148e + 05$ N
Axial tension anchor line	T_{anchor}	$1.661e + 06$ N
Anchor radius	X_{tota}	741.6 m
Horizontal distance fairlead touchdown point	Xa	702.9 m
Length of line laying of the seabed	S_0	38.6 m

Table 4.6: Configurations before and after static analysis in SIMA

In the figure below all parameters of the shared and anchor lines have been reported.

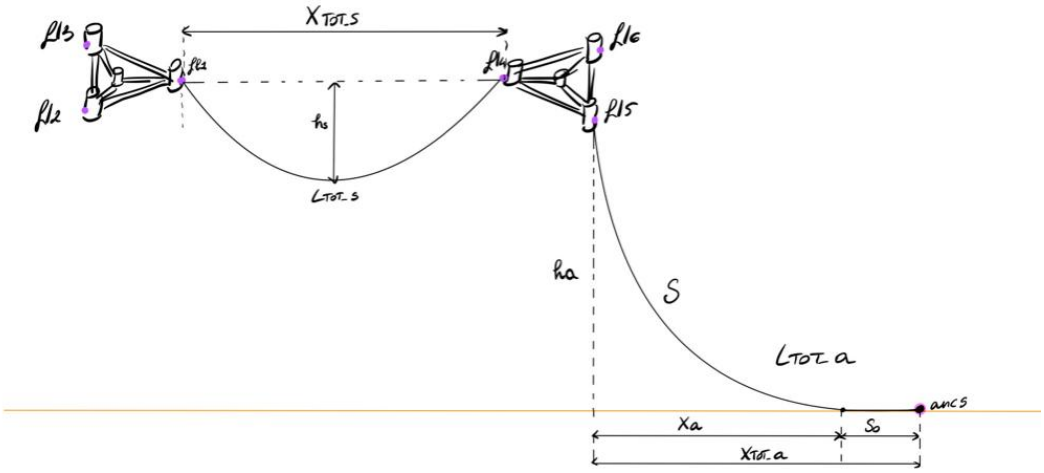

Figure 4.5: Final static configuration of the mooring lines for both shared and anchor lines

5 Method

5.1. Quasi-dynamic Matlab Model

The equivalent model of the system in terms of lumped masses, dampers and springs is shown below:

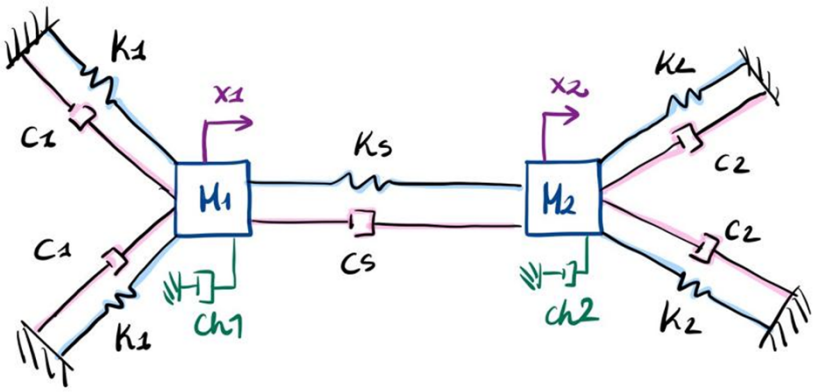

Figure 5.1: Equivalent 2 DOFs Matlab model

In the figure shown above, $M1$ and $M2$ are the lumped masses for the two wind turbines both constrained to move only horizontally in surge, DOFs x_1 and x_2. The two masses are equal and include the masses of the floating structure, the tower, the rotor-nacelle assembly and the added mass.

$$M = M_{rot} + M_{nac} + M_{hub} + M_{tow} + M_{semisub} + M_{added} \tag{5.1}$$

Mass of the nacelle	M_{nac}	240000 kg
Mass of the rotor	M_{rot}	110000 kg
Mass of the hub	M_{hub}	56780 kg
Mass of the tower	M_{tow}	347460 kg
Mass of the semisubmersible	$M_{semisub}$	$1.3473e+07$ kg

Table 5.1: Mass values used for the model from [Rob+14]

The added mass for the semi-submersibles in surge, M_{added} in Equation 5.1, is a frequency dependent term and the values can be found in Figure 5.2. More precisely, the above mentioned graph reports the hydrodynamic added mass for the three translation modes as a function of oscillation frequency from [Rob+14]. Because of the semisubmersible's symmetries, the surge-surge element of the frequency-dependent added-mass matrices, A11, is identical to the sway-sway element, A22.

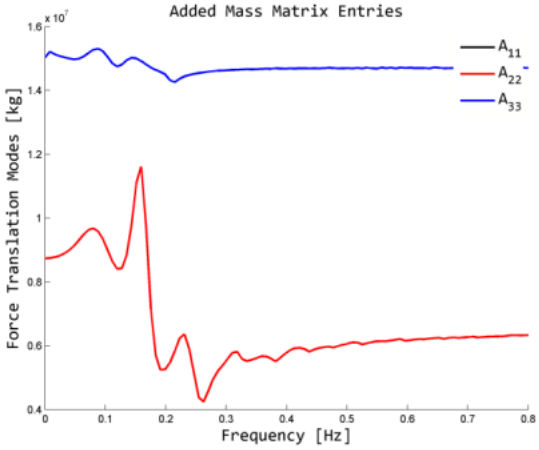

Figure 5.2: Hydrodynamic added mass for the OC4-DeepCwind semisubmersible [Rob+14]

Whereas, k_1, k_2 and k_s are the stiffnesses of the springs representing the mooring line stiffnesses, c_1, c_2, c_s and c_h are the damping coefficients of the dashpots representing the drag from the mooring lines and the floaters' hull. Indices $1, 2$ identify the anchor lines and s represents the shared line.

Each of the five mooring lines have been modelled using an equivalent model to the quasi-dynamic mathematical scheme previously described and shown in Figure 3.9. In this way the total number of DOFs of the system becomes two. The equivalent model for the lines is defined in Figure 5.3b as follows:

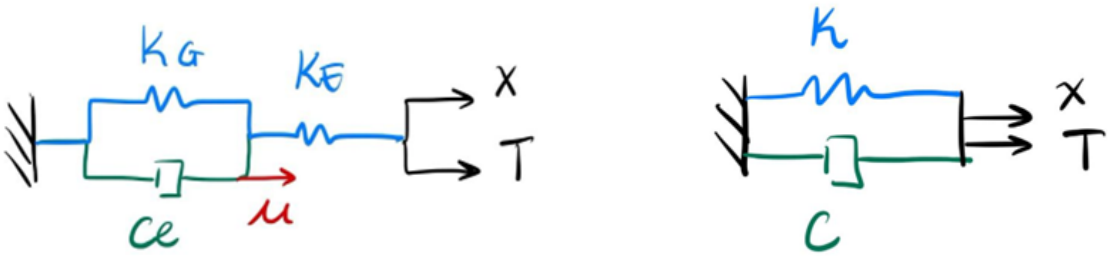

(a) Quasi-dynamic model **(b)** Equivalent model to quasi-dynamic model

Figure 5.3: Quasi-dynamic model and its equivalent

Where k_E, k_G, c_e are respectively the elastic stiffness, the geometric stiffness and the linearized damping coefficient. k and c are the equivalent stiffnesses and damping coefficients defined as:

$$k = k_E \left[1 - \frac{k_E(k_G + k_E)}{(k_G + k_E)^2 + (c_e\omega)^2} \right] \tag{5.2}$$

$$c = \frac{c_e k_E^2}{(k_G + k_E)^2 + (c_e \omega)^2}] \tag{5.3}$$

The calculations that led to Equation 5.2 and Equation 5.3 are reported in Appendix A.

To compute the values of the stiffnesses k and damping coefficients c the expressions for the geometric stiffness k_G, elastic stiffness k_E and linearized damping c_e need to be determined for both the shared line and the anchor lines.

The basis of this model is to assume that when the WTs move the line moves quasi-statically with a catenary shape. The model adds to the calculations an estimation of the damping of the lines by taking into account that the line when oscillates it has a change in its catenary shape. The process is based on the calculation of the drag caused by the change in the catenary shape in a portion of the line and then this is integrated along the whole length.

5.1.1. Equations of motion

Before starting to discuss all the different terms, the equations of motion have been reported.

The equations of motion have been obtained using the free body diagrams from Figure 5.1, and by writing the equilibrium between the forces acting on each body. The EOMs obtained are as follows:

$$\begin{cases} M_1\ddot{x}_1 = -2k_1 \cos^2(\alpha)x_1 - 2c_1 \cos^2(\alpha)\dot{x}_1 - c_{h,1}\dot{x}_1 - k_s(x_1 - x_2) - c_S(\dot{x}_1 - \dot{x}_2) + F_1 \\ M_2\ddot{x}_2 = -2k_2 \cos^2(\alpha)x_2 - 2c_2 \cos^2(\alpha)\dot{x}_2 - c_{h,2}\dot{x}_2 - k_s(x_2 - x_1) - c_S(\dot{x}_2 - \dot{x}_1) + F_2 \end{cases} \tag{5.4}$$

The $\cos(\alpha)$ term comes from the inclined springs and dash-pots, whose contribution is in the plane of the line, inclined of α with respect to the global x-direction, as seen in Figure 6.2.
F_1 and F_2 in Equation 5.4 are two harmonic forces that have been applied to the system, with a varying forcing frequency ω.
In order to obtain a force that could represent a wave of significant scale to excite the system, the amplitudes of the forcing terms F_{10} and F_{20} have been determined by looking at the first order wave force transfer function, which is reported below.

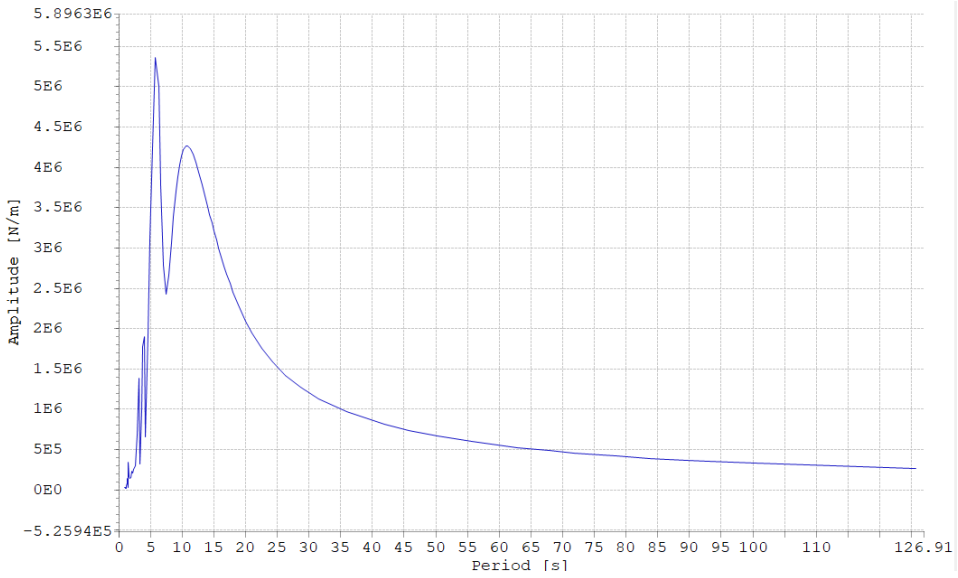

Figure 5.4: First order wave force transfer function from [Rob+14]

More specifically, this graph shows the force RAO, i.e. the force normalized per meter wave amplitude. Each point indicates the amplitude of a wave forcing correspondent to a certain period for a 1 m wave amplitude. For instance in the specific case of having a forcing term with a period of 10 s, looking at the graph it corresponds to a force amplitude of $4E6$ N with a 1 m wave amplitude. To exert on the floaters a force that is equivalent to a regular wave of reasonable height as a 3 m one, it is sufficient to multiply the force amplitude with a factor if 1.5 to obtain the correspondent forcing amplitude per wave amplitude.

To write this system of equations in the matrix form, the mass matrix **M**, the damping matrix **B** and the stiffness matrix **C** have been reported below:

$$\mathbf{M} = \begin{pmatrix} M_1 & 0 \\ 0 & M_2 \end{pmatrix} \tag{5.5}$$

where the terms M_1 and M_2 in Equation 5.4 in the equations of motion include both the added mass terms M_{added1} and M_{added2} and the effective masses of the floater, tower and nacelle as shown in Equation 5.1.

The stiffness matrix C has been defined as:

$$\mathbf{C} = \begin{pmatrix} 2k_1 cos^2\alpha + k_s & -k_s \\ -k_s & 2k_2 cos^2\alpha + k_s \end{pmatrix} \tag{5.6}$$

while the damping matrix B:

$$\mathbf{B} = \begin{pmatrix} 2c_1 cos^2\alpha + c_s + c_{h1} & -c_s \\ -c_s & 2c_2 cos^2\alpha + c_s + c_{h1} \end{pmatrix} \tag{5.7}$$

c_h is the hydrodynamic damping of the floaters, the subscript h stands for the hull of the floater. This term, like the added mass, is frequency dependent and therefore it has been chosen looking at the following graph, and taking the value corresponding to the forcing frequency. However, these values do not take into account any viscous damping of the hull.

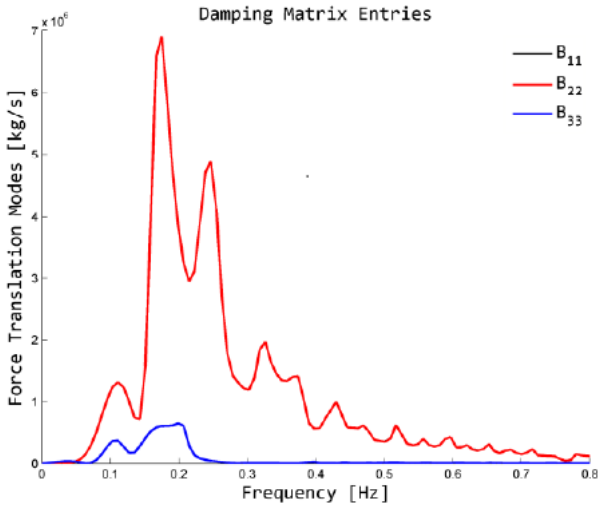

Figure 5.5: Hydrodynamic damping for the OC4-DeepCwind semisubmersible [[Rob+14]]

The final expression of the EOM becomes:

$$\mathbf{M}\begin{bmatrix} \ddot{x}_1 \\ \ddot{x}_2 \end{bmatrix} + \mathbf{B}\begin{bmatrix} \dot{x}_1 \\ \dot{x}_2 \end{bmatrix} + \mathbf{C}\begin{bmatrix} x_1 \\ x_2 \end{bmatrix} = \mathbf{F} \tag{5.8}$$

where **F** is the forcing vector defined as:

$$\begin{bmatrix} F_1 \\ F_2 \end{bmatrix} \tag{5.9}$$

The expressions for F_1 and F_2 are $F_{10}\cos(\omega t)$ and $F_{20}\cos(\omega t + \phi)$. The shift angle ϕ has been chosen to be π.

At this point the following step is to solve the equations for the unknowns using the expressions for k and c shown in the previous paragraph, Equation 5.2 and Equation 5.3.

5.1.2. Elastic and Geometric stiffnesses

The elastic stiffnesses k_E can be found as:

$$k_E = \frac{EA}{l} \tag{5.10}$$

Where l is the total length of the line, E is the modulus of elasticity and A is the cross-sectional area. Depending on the different length of the shared and anchor lines, two different values for this coefficient have been found:

$$\begin{aligned} k_{Eanchor} &= \frac{EA}{l_{anchor}} = 9.7617e+05\text{N/m} \\ k_{Eshared} &= \frac{EA}{l_{shared}} = 5.8148e+05\text{N/m} \end{aligned} \tag{5.11}$$

The shared line which has a bigger length has a smaller elastic stiffness while the anchor lines have a higher elastic stiffness.

As for the geometric stiffness, since the model has been linearized, the expression for the k_G can be defined as:

$$k_G = \frac{1}{\partial x / \partial T_x} \tag{5.12}$$

This term is defined as the change in geometry of the top end of the line due to a variation of the horizontal tension, without including any elasticity term. Equation 5.12 assumes two different expressions for the shared and the anchor lines.

The expression for the horizontal coordinate of the shared line that has been differentiated with respect to the horizontal tension at the fairlead is:

$$x(s) = s - \frac{1}{6}(\frac{w}{T_0})^2 s^3 \tag{5.13}$$

where s is the coordinate along the suspended line, w is the weight in water per unit length and T_0 is the horizontal component of the tension at the fairlead as shown in Figure 5.6.

Equation 5.13 is the horizontal coordinate found using the towline approximation for the shared line. A towline is a cable used to pull along different types of objects for marine operations (e.g. positioning of floating structures). The assumption of using the towline equations for the shared line has its origin in the fact that a towline is generally a long line with a high axial tension as is the shared lines between the two turbines.

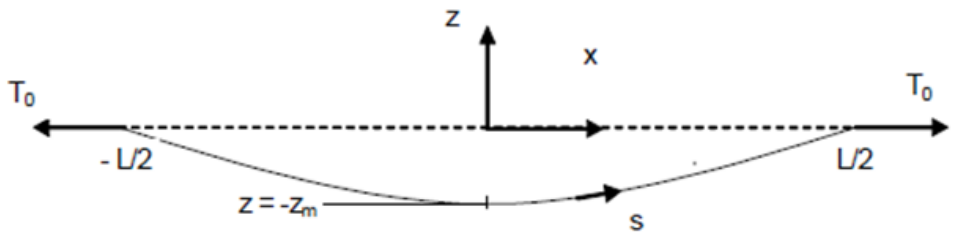

Figure 5.6: Shared line system

The expressions for the geometric stiffnesses using Equation 5.13 is:

$$k_G = \frac{1}{\partial x(s)/\partial T_x} = \frac{12T_0^3}{(wL)^2 L} = 1.53e + 04\text{N/m} \tag{5.14}$$

On the other hand, regarding the anchor lines, the expression of the horizontal coordinate that has been used to compute the geometric stiffness is:

$$X_l = l + \frac{T_x}{w}\,\text{acosh}(1 + \frac{wy}{T_x}) - \sqrt{y(y + \frac{2T_x}{w})} \tag{5.15}$$

where l is the total length of the line, T_x is the horizontal component of the tension at the fairlead, w is the submerged weight per unit length and y is the water depth as shown in Figure 5.7.

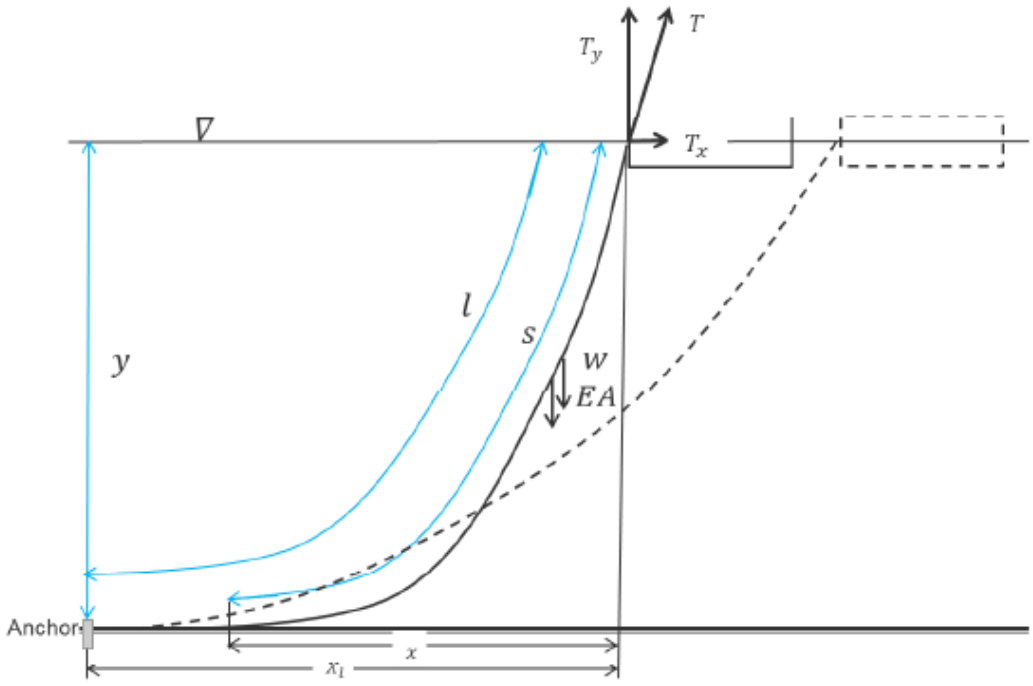

Figure 5.7: Illustration of the notation defining the anchor line characteristics

Equation 5.15 has been differentiated with respect to T_x and the following has been found:

$$k_G = \frac{1}{\partial x(s)/\partial T_x} = \frac{w}{\text{acosh}(\frac{wh}{T_x} + 1) - \frac{2}{\sqrt{1+\frac{2T_x}{wh}}}} = 9.644e + 04\ N/m \tag{5.16}$$

which corresponds to expression (5.20) from [Ma+19].

The reason why Equation 5.15 has been used instead of the expression for the horizontal coordinate x given by Equation 3.7 is that to to define the stiffness k two requirements have to be met such as:

- a defined earth-fixed point
- a line that can be lifted from off the from the seabed

and Equation 5.15 is the only expression that takes into account both that the line is not fixed at the touch down point and therefore, that the suspended length can change and it also assumes an earth fixed point with respect to which the stiffness expression can be computed.

For these reasons Equation 5.15 is the most complete expression to use to estimate the geometric stiffness for the anchor lines.

5.1.3. Linearized damping coefficients

The last thing to be determined to be able to complete the equivalent model are the linearized damping coefficients for the shared and anchor lines.

Shared line

In order to use the towline approximation for the expression of the vertical coordinate z (as defined in Figure 5.6), in the computation for the damping coefficient, the following calculation has been carried out.

According to the towline expressions the sag of the line, z_m is defined as:

$$z_m = \frac{wL^2}{8T_0} \tag{5.17}$$

To see how much this is close to what would happen using the catenary equations, a numerical simulation has been carried out. More specifically, the catenary expression for the suspended line Equation 3.13 and Equation 3.14 have been used in Matlab to simulate the change in shape when the floaters move both 5 m apart from each other. When the floaters move the sag of the line changes, decreasing. This change in vertical coordinate has been found and then compared to the one obtained using Equation 5.17. What happens is shown in the figure below with a Matlab plot.

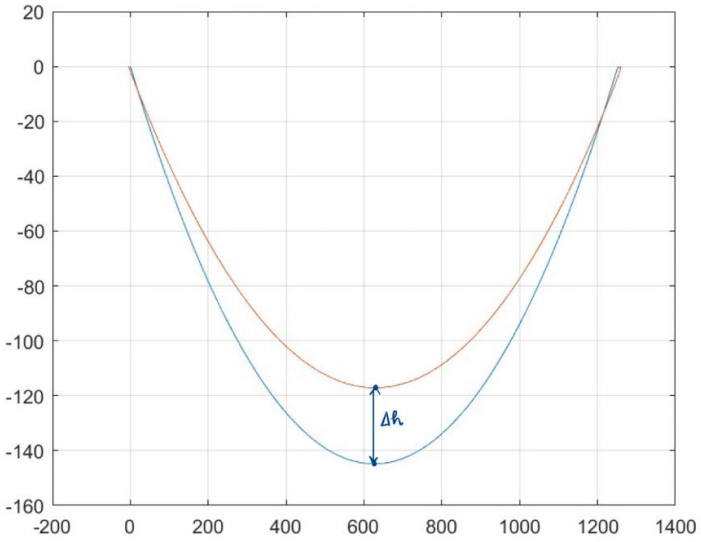

Figure 5.8: Change in the sag of the line when fairleads displace of 5 m each

Carrying out the numerical simulation the change in sag that has been obtained is equal to $\Delta h = h_1 - h_0 = 144.7 - 117.03 = 27.67$m, while using Equation 5.17 $z_{m1} - z_{m0} = 152.445 - 126.66 = 25.76$ m. The obtained results show that the difference between the variation of the sag using the catenary equation and the towline approximation is around 7%. This value is lower than 10% difference which makes the approximation acceptable. It is therefore possible to use this approximation for the vertical coordinate as well.

For the shared line using the towing line simplification considering only half of the line, the following formula has been used:

$$z(x) = \frac{1}{2}\frac{wx^2}{T_0} - \frac{\omega L^2}{8T_0} = \frac{W}{8T_0}\left(ux^2 - L^2\right) \tag{5.18}$$

Imposing a motion amplitude u_a and a velocity amplitude $\dot{u}_a = u_a\omega$ to the top of the line, implies that the line will move vertically upwards with an amplitude $z_a(z)$ as shown in Figure 5.9 in blue.

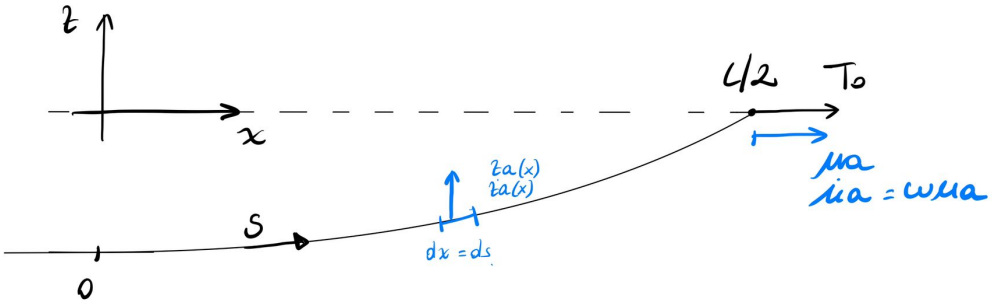

Figure 5.9: Half towline coordinate system

The equilibrium of the drag force along half of the line has been determined in order to estimate the drag resistance along the shared line. In order to do this, the drag force acting

on a small portion of the line dx as well as the drag forces acting on each of the line's edges T_d have been estimated, as shown in the figure below.

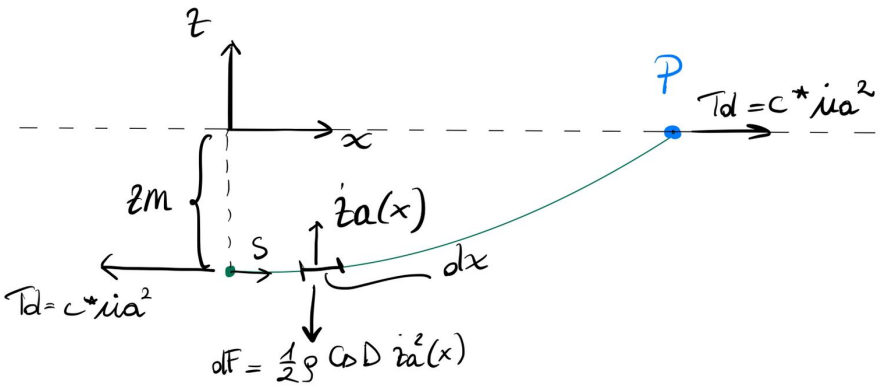

Figure 5.10: Drag force balance on half of towline

Because the line is considered to be a long high tensioned line, the vertical component of the drag force at the top of the line has been neglected, and the x coordinate has been defined to be coinciding with the s coordinate along the suspended length. Furthermore, there is no vertical component at the bottom of the line because it is completely horizontal at the sag.

Taking all of this into consideration, the first step was to find the expression for $za(x)$, which was defined above. The following steps have been taken.

$$\frac{dz(x)}{du} = \frac{dz(x)}{dT_0} \cdot \frac{dT_0}{du} \tag{5.19}$$

The first term $\frac{dz(x)}{dT_0}$ can be found by differentiating the expression of $z(x)$ (Equation 5.18) with respect to the horizontal component of the tension at the top of the line T_0:

$$\frac{dz(x)}{dT_0} = \frac{w\left(L^2 - 4x^2\right)}{8T_0^2} \tag{5.20}$$

While the second term $\frac{dT_0}{du}$ represents the geometric stiffness k_G. Therefore the expression becomes:

$$\frac{dz(x)}{du} = \frac{w}{8T_0^2}\left(L^2 - hx^2\right) \cdot k_G \tag{5.21}$$

Which gives the following expression for $z_a(x)$:

$$z_a(x) = \frac{w}{8T_0^2}\left(L^2 - 4x^2\right) k_G u_a \tag{5.22}$$

The next step is to write the moment equilibrium of the drag forces with respect to point P, which is illustrated in blue in Figure 5.10, taking everything what has been discussed into account.

$$
\begin{aligned}
&-T_d z_m + \int_0^{L/2} dF dx = 0 \\
&T_d \frac{wL^2}{8T_0} = \int_0^{L/2} K_D \left[\frac{w}{8T_0^2}\left(L^2 - 4x^2\right) K_G\right]^2 \dot{u_a}^2 x dx \\
&c^* \dot{u_a}^2 \frac{wL^2}{8T_0} = K_D K_G^2 \left(\frac{w}{8T_0^2}\right)^2 \dot{u_a}^2 \int_0^{L/2} \left(L^2 - 4x^2\right) x dx \\
&c^* = K_D k_G^2 \left(\frac{w}{8T_0^2}\right)^2 \cdot \frac{L^6}{24} \cdot \frac{8T_0}{wL^2}
\end{aligned}
\tag{5.23}
$$

Since $k_G = \frac{12T_0^3}{w^2 L^3}$ the expression for c^* becomes:

$$
c^* = K_D \frac{T_0^3}{w^3 L^2} \frac{3}{4} \tag{5.24}
$$

To get the expression for the linearized damping coefficient c_e, it is necessary to linearize the expression for $\dot{u_a}^2$. In this case, a deterministic linearization has been carried out since the forcing term applied to the system is a harmonic function that simulates regular waves. If an irregular force had been applied to the system instead, a stochastic linearization would have been necessary.

$$
\begin{aligned}
T_d &= \frac{3}{4} K_D \frac{T_0^3}{w^3 L^2} \dot{u_a}^2 \\
\frac{3}{4} K_D \frac{T_0^3}{w^3 L^2} \dot{u_a} \frac{8}{3\pi} - \dot{u_a} &= c_e \dot{u_a} \\
c_e &= \frac{3}{4} K_D \frac{T_0^3}{w^3 L^2} \dot{u_a} \frac{8}{3\pi}
\end{aligned}
\tag{5.25}
$$

Where $K_D = 1/2 \rho C_D D$ and $\dot{u_a} = u_a \omega$, where ω is the frequency of the system which corresponds to the frequency of the forcing term.

Anchor lines

To find the expression of the linear damping coefficient for the anchor lines the procedure outlined in [LS90] has been followed. The starting point is expression for the drag force in the tangential direction ϵ, defined as follows:

$$
F_D(\omega) = \frac{T}{q} f CDN (\dot{u_n})^P = \frac{T}{q} f CDN f(\beta)^2 (\dot{\epsilon})^2 \tag{5.26}
$$

where the factor f and $f(\beta)$ are defined respectively as from [LS90]:

$$
f = \frac{1}{u_n^p \left(\epsilon^* = 0\right)^2 s} \int_0^s \left[u_n \left(l, \epsilon^*\right)\right]^2 dl \tag{5.27}
$$

and

$$
f(\beta) = \frac{du_n^p}{d\varepsilon} = \left[\beta - \frac{\beta^2 + 4}{4} \ln\left(\frac{\beta + 2}{\beta - 2}\right)\right]^{-1} \tag{5.28}
$$

And $CDN(l) = \frac{1}{2} \rho C_D D$ is the drag coefficient. f from Equation 5.27 is suggested to be set to 0.53 [LS90].

The beta-factor $f(\beta)$ defined in Equation 5.28 represents the relation between the motion at the reference point along the line, where the sag is at its maximum, and the motion at the

top end of the line, see Figure 5.11. In the previous expression the factor β can be found as follows:

$$\beta = \frac{s}{u_n^p\left(\epsilon^* = 0\right)} \tag{5.29}$$

$$u_n^p\left(\epsilon^* = 0\right) = \frac{hx_1}{c} - \frac{H}{q}\left(1 - \frac{x_0}{c}\right) \tag{5.30}$$

$$x_1 = \frac{H}{q}\,\mathsf{ln}\left(\frac{h+c}{x_0}\right) \tag{5.31}$$

where h is the water depth, H is the horizontal component of the tension at the fairlead, c is the distance between the touchdown point and the fairlead, as also shown in Figure 5.11, q is the submerged weight per unit length (usually w) and $x0$ is the anchor radius.

It is possible to obtain a greater understanding of the β coefficient by looking at these expressions. Equation 5.29 shows that β is defined by the ratio between the suspended length s and u_n^P shown also in Figure 5.11, which is the point where the static "sag" of the catenary is. The value expected for β will be greater than one, since the suspended length is larger than the value of the "static sag" of the line. Indeed, the computations show that this value is 15.87.

Equation 5.26, taking into account that $\frac{8}{3\pi}\epsilon_a$ is the linearization factor, as the one used in Equation 5.25 becomes:

$$\begin{aligned} F_D(\omega) = c_e^{\epsilon}\dot{\epsilon} &= \frac{T}{q}0.53CDNf(\beta)^2(\dot{\epsilon})^2 \\ c_e^{\epsilon}\dot{\epsilon} &= \frac{T}{q}0.53CDNf(\beta)^2\frac{8}{3\pi}\dot{\epsilon_a}\dot{\epsilon} \end{aligned} \tag{5.32}$$

The expression for the linearized damping coefficient in the tangential direction can then be found as:

$$c_e^{\epsilon} = \frac{T}{q}0.53CDNf(\beta)^2\frac{8}{3\pi}\dot{\epsilon_a} \tag{5.33}$$

where ϵ_a is the amplitude of the velocity in the tangential direction to the line.

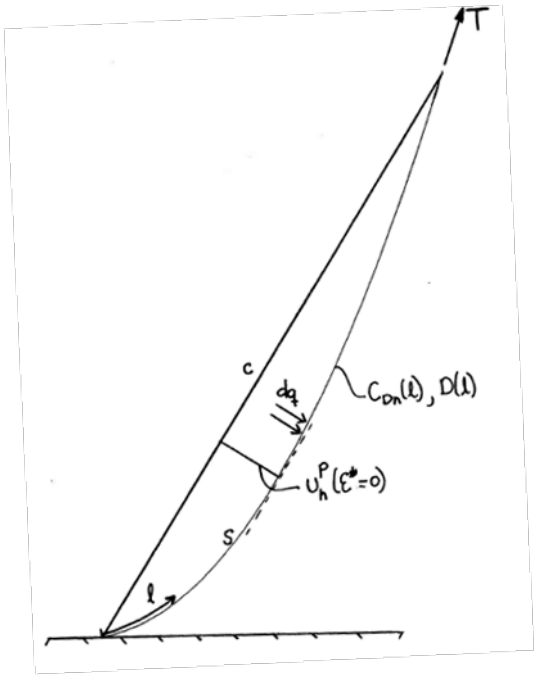

Figure 5.11: Mooring line characteristics from [LS90]

To get the expression for the linearized damping coefficient of our interest, it is necessary to rewrite the expression for the drag force in the horizontal direction u.

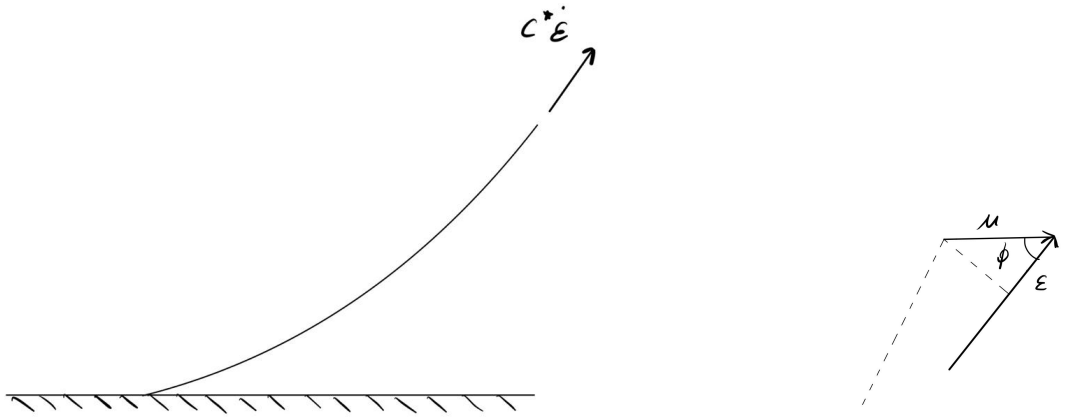

(a) **(b)** Zoom-in of the top end of the line

Figure 5.12

In Figure 5.12b, the directions along which the two drag forces are oriented, F_D^ϵ and F_D^u are shown. ϵ is the direction along the line, while u is the horizontal one. Therefore, looking at Figure 5.12b the following relations can be found:

$$\begin{aligned} \epsilon &= u cos(\phi) \\ \dot{\epsilon} &= \dot{u} cos(\phi) \end{aligned} \tag{5.34}$$

Accordingly, the expression for F_D^u can be found as:

$$F_D^u = F_D^\epsilon \, cos(\phi) = c_e^\epsilon \dot{\epsilon} \, cos(\phi) = \frac{T}{q} 0.53 \, CDN \, f(\beta)^2 \frac{8}{3\pi} \, \dot{\epsilon_a} \, \dot{\epsilon} \, cos(\phi) \tag{5.35}$$

$$F_D^u = \frac{T}{q} \, 0.53 \, CDN \, f(\beta)^2 \frac{8}{3\pi} \, \dot{u_a} \, \dot{u} \, cos(\phi)^3 \tag{5.36}$$

Therefore, taking into account this expression, c_e^u can be found as:

$$\begin{aligned} c_e^u &= \frac{T}{q} \, 0.53 \, CDN \, f(\beta)^2 \, \frac{8}{3\pi} \, \dot{u_a} \, cos(\phi)^3 \\ c_e^u &= \frac{T}{q} \, 0.53 \, CDN \, \left[\beta - \frac{\beta^2 + 4}{4} \ln \left(\frac{\beta + 2}{\beta - 2} \right) \right]^{-2} \, \frac{8}{3\pi} \, \dot{u_a} \, cos(\phi)^3 \end{aligned} \tag{5.37}$$

where β is given by Equation 5.29.
In Equation 5.37 all the terms are:

- T is the total static tension at the top of the line
- q is the submerged weight per unit length of the line
- ω is the frequency of the system (rad/s)
- CDN is the drag factor
- s is the suspended length (733.32 m)
- c is the secant length, found as distance between touchdown point and fairlead (727.5 m)
- x_0 is the horizontal distance between touchdown point and fairlead (703.38 m)
- h is the water depth (200 m)

Beta factor

The factor introduced in Equation 5.28 as $f(\beta) = \frac{du_n^p}{d\varepsilon}$ represents the dynamic transfer function between the top end motion ϵ and a reference point along the line u_n^P, previously defined, where the drag force is calculated . This indicates that a certain positive motion at the top of the line will tighten up the line itself, which will cause the ”sag” of the line to decrease. As a result, the beta factor will be negative because a positive motion at the top will reduce the sag. However, considering the dynamic motion amplitude, this is always positive and therefore the absolute value must be used.

Figure 5.13 shows the trend of the absolute values of the beta function with respect to different values of beta. It is worth noticing that the amplitude at the reference point increases with an increasing β. This makes sense since the line will be ”stiffer” and more responsive to top end motions as the pretension (and β) increases. As can be observed a factor between 1 and 4 is shown by $f(beta)$.

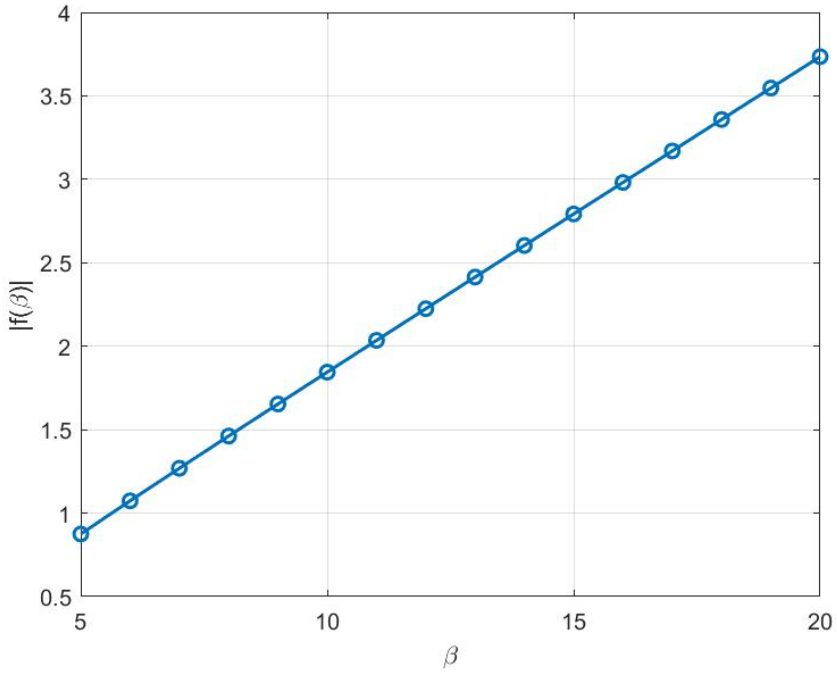

Figure 5.13: Variation of absolute value of beta factor $f(\beta)$ with respect to different values of β

In this particular system the value of β for the anchor line is 15.87, which indicates that the suspended length s is around 16 times the ”sag” of the anchor line. To define a realistic range for the values of beta for this system, different value of β have been computed for different top tensions between $5 - 30$% of MBL (minimum breaking load). For each different tension value the corresponding line characteristics have been computed to find the matching values of β. By assuming that the mooring chain for this system, given its diameter $d = 76$ mm and its submerged weight per unit length $w = 1.065 + 03$ N/m, is of ”R4” quality, the correspondent break load MBL according to the standards of commercial mooring chains is found to be 6001 kN. Hence, the following values of β have been found and plotted against the different tension values in Figure 5.14.

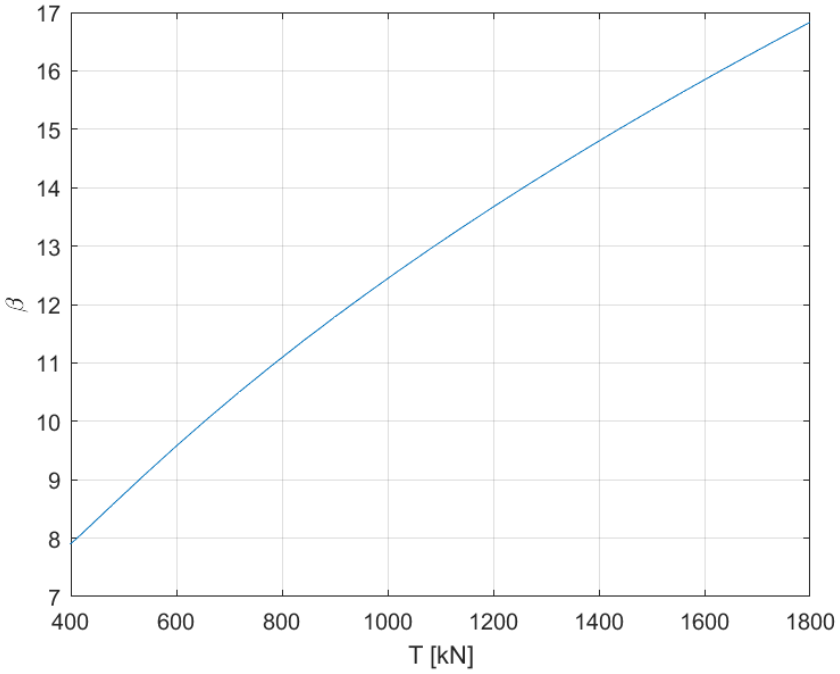

Figure 5.14: Variation of β for range of mean values of top tension for this system

These values represent the expected β for a range of mean values of the top tension for this system. The plot shows both that the value of β increases with the value of the top tension T and also that the relationship between the two variables is not linear as shown in Equation 5.29, Equation 5.30 and Equation 5.31, indeed the graph displays a curve. Lower tension values than 400 kN have not been considered because for very low tensions compared to the pre-tension of the system $T = 1661$ kN, the line shape approaches the shape of hanging vertically and the β is not of interest. In general design of mooring systems is performed such that too low mean tension is avoided. The lowest mean tension is particularly experienced by the downwind line(s). In order to avoid too low tension in these lines, a sufficiently high pretension is selected. Hence, lines will normally not experience very low mean tension and it does not make sense to take that into account for this analysis.

5.1.4. Amplitude of horizontal motion ua

The additional ”internal” degree of freedom u (depicted in Figure 5.3a in red) needs to be determined to find the expressions for the damping coefficients for both shared and anchor lines.

$$u_a = \frac{k_E}{\sqrt{(k_E + k_G)^2 + (c_e \cdot \omega)^2}} \cdot x_a \tag{5.38}$$

Equation 5.38 is the necessary expression for determining the amplitude of horizontal motion at the top of the line, which is needed to calculate the linearized damping coefficients.

The steps to obtain Equation 5.38 are presented in Appendix A.

Anchor lines

In the case of anchor lines Equation 5.38, depending on which anchor line is considered the value of x_a will change between x_{1a} or x_{2a} and the linearized damping coefficient c_e will be

given by Equation 5.37 becoming:

$$u_{1a} = \frac{k_E}{\sqrt{(k_E + k_G)^2 + (c_e \cdot \omega)^2}} \cdot x_{1a} \tag{5.39}$$

for anchor lines on the left-side on the floaters and the following for the anchor lines on the right-side of the floaters:

$$u_{2a} = \frac{k_E}{\sqrt{(k_E + k_G)^2 + (c_e \cdot \omega)^2}} \cdot x_{2a} \tag{5.40}$$

Shared line

For the shared line instead the amplitude of the motion, x_a in Equation 5.38 becomes the absolute value of the difference between the amplitudes of the motions of both floaters, since the line is in the middle of the floaters and the linearized damping coefficient will be given by Equation 5.25:

$$u_{sa} = \frac{k_E}{\sqrt{(k_E + k_G)^2 + (c_e \cdot \omega)^2}} \cdot |x_{1a} - x_{2a}| \tag{5.41}$$

5.1.5. Solving the equations

To be able to carry out in Matlab the numerical analysis of the previously developed model, the equations of motion in Equation 5.4 have to be solved to find the time dependent expressions for the displacements $x_1(t)$ and $x_2(t)$. To do so the second order system has been rewritten as a first-order system, introducing the state vector $\underline{q}$, which reads:

$$\underline{q} = \begin{bmatrix} q_1 \\ q_2 \\ q_3 \\ q_4 \end{bmatrix} = \begin{bmatrix} x_1 \\ x_2 \\ \dot{x}_1 \\ \dot{x}_2 \end{bmatrix} \tag{5.42}$$

and consequently the vector $\dot{\underline{q}}$ results:

$$\dot{\underline{q}} = \begin{bmatrix} \dot{x}_1 \\ \dot{x}_2 \\ \ddot{x}_1 \\ \ddot{x}_2 \end{bmatrix} \tag{5.43}$$

To recast the model to the form $\frac{dq}{dt} = \underline{f}(t, \underline{q})$ to be able to solve the equations of motion with the Matlab $ode4$ solver, the system of equations from Equation 5.4 has been considered together with other two equations:

$$\begin{cases} q_3 = \dot{q}_1 \\ q_4 = \dot{q}_2 \end{cases} \tag{5.44}$$

In this way a coupled second order system has been written as a function of the first order terms. The state space representation of a system replaces an n-th order differential equation, in this case a second order one, with a single first order matrix differential equation. The second order differential equation has been rewritten as a first order system of the form:

$$\frac{d\underline{q}}{dt} = \underline{f}(t, \underline{q}) = (\mathbf{M})^{-1}(-\mathbf{C}^{*}\underline{q} + \underline{F}) \tag{5.45}$$

where the matrix $\mathbf{C}^{*}$, which multiplies the state vector, includes both the terms from the stiffness **C** and damping **B** matrixes. In this way the 2nd order differential system can be solved using Matlab.

It is worth mentioning that the force balance for each time step has been evaluated to verify the computations in the dqdt function implemented in Matlab to solve the differential equations using ode4.

To be able to solve the equations of motion to get the dynamic response of the system in terms on the two degrees of freedom x_1 and x_2 taking into account all the expressions for the stiffnesses and damping coefficients that have been shown above it is necessary to solve the system iteratively. This is because both damping coefficients c_{ea} and c_{es} for the anchor and shared lines are dependant on the amplitudes of the horizontal motions $u_{a,anchor}$ and $u_{a,shared}$ as shown in Equation 5.37 and Equation 5.25, which are in turn determined by the amplitudes of the degrees of freedom x_1, x_2.

Here below, the steps that have been carried out to solve the system have been reported:

1. c_{ea} and c_{es} have been assumed to be 0, stiffnesses coefficients k_1, k_2, k_s have been estimated
2. The system with no damping has been solved finding x_{1a} and x_{2a}
3. u_{1a}, u_{2a} and u_s have been calculated
4. New values of c_{ea} and c_{es} have been found using Equation 5.39, Equation 5.40 and Equation 5.41
5. Stiffness and damping coefficients k_1, k_2, k_s , c_1, c_2 and c_s found using the values of the linearized stiffness terms
6. The system with damping has been solved finding x_{1a} and x_{2a} to update the values for u_{1a}, u_{2a} and u_s
7. New values for c_{ea} and c_{es} have been computed until convergence is reached.

The convergence criteria is based on the computation of the relative change between the damping coefficients until it becomes smaller than a given $\epsilon < 10^{-6}$:

$$\epsilon = |\frac{c_e(i+1) - c_e(i)}{ce(i)}| \tag{5.46}$$

The diagram below highlights the various steps that have been taken to solve the system iteratively.

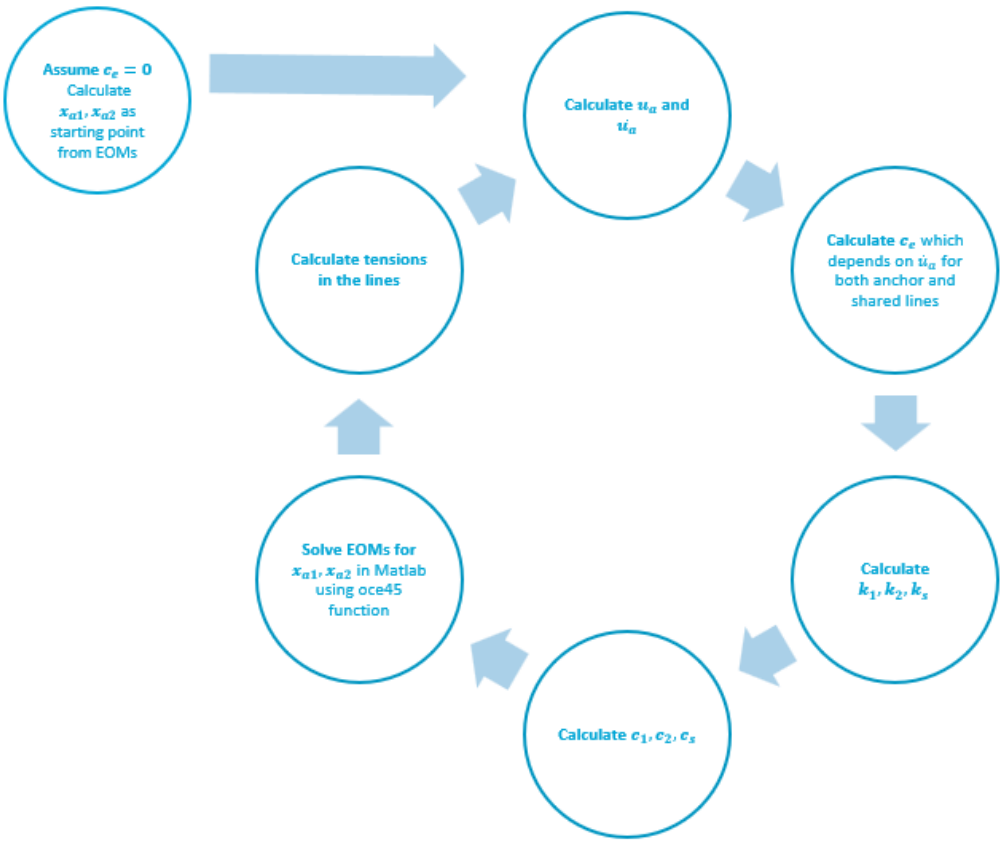

Figure 5.15: Graphical representation of the loop implemented in Matlab to solve the EOMs

However, the system under consideration is a mass-dominated system. This means that the response of the system, which is given by x_1 and x_2 is almost not influenced by the damping but only depends on the forcing frequency. This happens when the excitation frequencies, which in this case are wave frequencies, are higher than the natural frequencies of the system, which are 0.0069 Hz and 0.0089 Hz. For this reason steps 5 and 6 listed above can be skipped in the resolution process, since the values of the motion amplitudes do not change every iteration when the damping coefficients change. This simplifies the model and the calculations significantly, making the code faster and more efficient.

This approach has been verified in Matlab. In the following table, the amplitudes of both the displacements and the velocities for the different frequencies have been reported throughout each loop. Since the velocity and displacement amplitudes of the second floater are identical, because both floaters are subjected to the same forcing amplitudes and only have a phase shift, just the amplitudes of the first floater have been displayed below. The amplitudes for each step in the loop fluctuate illusorily, as seen in in Table 5.2 and Table 5.3, which is why the recalculation was omitted. The frequencies here below are the wave frequencies which are higher compare to the frequency range that is of interest for the mooring analysis.

f [Hz]	xa_1 [m]	xa_12 [m]	xa_1dot [m/s]	xa_12dot [m/s]
0.2	0.172905842	0.345811684	0.217255394	0.434510788
	0.172859981	0.345719962	0.217196947	0.434393894
	0.172860015	0.34572003	0.217196991	0.434393982
	0.172860015	0.34572003	0.217196991	0.434393982
0.166667	0.267985631	0.535971262	0.280550767	0.561101534
	0.267869165	0.53573833	0.280427963	0.560855926
	0.267824084	0.535648167	0.280380284	0.560760568
	0.267824221	0.535648442	0.280380429	0.560760858
	0.26782422	0.535648441	0.280380429	0.560760857
0.142857	0.159632669	0.319265339	0.143251331	0.286502662
	0.159623433	0.319246866	0.143243591	0.286487182
	0.15962337	0.319246739	0.143243492	0.286486984
	0.15962337	0.319246739	0.143243492	0.286486984
0.125	0.30176756	0.603535119	0.236991627	0.473983254
	0.301730152	0.603460304	0.236960979	0.473921959
	0.301723185	0.603446369	0.236954562	0.473909125
	0.301723182	0.603446364	0.236954561	0.473909123
	0.301723182	0.603446364	0.236954561	0.473909123
0.111111	0.411394215	0.822788429	0.286883127	0.573766254
	0.411329305	0.822658611	0.286839904	0.573679808
	0.411294762	0.822589525	0.28681863	0.57363726
	0.411294766	0.822589531	0.286818628	0.573637257
	0.411294766	0.822589531	0.286818628	0.573637257
0.1	0.681075437	1.362150874	0.427879266	0.855758531
	0.680969486	1.361938971	0.427809947	0.855619893
	0.6809095	1.361818999	0.42776417	0.85552834
	0.680909228	1.361818456	0.427764017	0.855528033
	0.680909229	1.361818458	0.427764017	0.855528034
0.090909	0.814963848	1.629927697	0.464759145	0.92951829
	0.814856488	1.629712975	0.464695947	0.929391894
	0.814822072	1.629644144	0.464669112	0.929338224
	0.81482158	1.629643159	0.464668845	0.92933769
	0.814821581	1.629643162	0.464668846	0.929337692
0.083333	0.940863535	1.881727071	0.492610354	0.985220708
	0.940792197	1.881584394	0.492569236	0.985138473
	0.940951577	1.881903154	0.492635976	0.985271952
	0.940950738	1.881901475	0.492635562	0.985271124
	0.94095074	1.881901479	0.492635563	0.985271126
0.076923	0.883302632	1.766605265	0.426014323	0.852028647
	0.883240966	1.766481933	0.425988708	0.851977417
	0.883313528	1.766627055	0.426040512	0.852081024
	0.883313185	1.76662637	0.426040329	0.852080659
	0.883313185	1.766626371	0.42604033	0.852080659
0.071429	0.962325669	1.924651337	0.433014112	0.866028224
	0.962279518	1.924559036	0.432996317	0.865992634
	0.962419657	1.924839315	0.433076437	0.866152874
	0.96241931	1.924838619	0.433076266	0.866152532
	0.96241931	1.92483862	0.433076266	0.866152532

Table 5.2

f [Hz]	xa_1 [m]	xa_12 [m]	xa_1dot [m/s]	xa_12dot [m/s]
0.066667	1.17081607	2.34163214	0.49044214	0.980884281
	1.170803695	2.34160739	0.490432033	0.980864066
	1.171259754	2.342519508	0.490595492	0.981190984
	1.17125918	2.34251836	0.490595268	0.981190536
0.0625	1.2233586	2.446717199	0.480419351	0.960838702
	1.223342516	2.446685033	0.48040793	0.960815861
	1.223748212	2.447496424	0.480536772	0.961073544
	1.223747763	2.447495526	0.480536611	0.961073223
0.058824	0.938128687	1.876257374	0.347061055	0.694122109
	0.93814391	1.87628782	0.347054709	0.694109419
	0.938272368	1.876544735	0.347097375	0.694194751
	0.938272303	1.876544607	0.347097348	0.694194697
0.055556	1.080882248	2.161764497	0.378257566	0.756515132
	1.080871705	2.16174341	0.37825053	0.756501061
	1.080968668	2.161937336	0.37829904	0.756598081
	1.080968571	2.161937141	0.378298997	0.756597995
0.052632	1.299926436	2.599852871	0.428201414	0.856402827
	1.299877097	2.599754193	0.428189433	0.856378865
	1.299972828	2.599945656	0.428227046	0.856454092
	1.299972628	2.599945255	0.42822698	0.856453961
0.05	1.395999763	2.791999527	0.438575792	0.877151583
	1.39607774	2.79215548	0.438594354	0.877188708
	1.396544323	2.793088646	0.438699514	0.877399028
	1.396544256	2.793088512	0.438699497	0.877398993
0.047619	1.394153241	2.788306482	0.415425794	0.830851589
	1.394336682	2.788673365	0.415486523	0.830973046
	1.39496632	2.78993264	0.4156771	0.8313542
	1.39496641	2.78993282	0.415677125	0.83135425
0.045455	1.024908815	2.04981763	0.292725319	0.585450637
	1.024908203	2.049816405	0.292739845	0.58547969
	1.025009824	2.050019648	0.29280157	0.58560314
	1.025009816	2.050019632	0.292801565	0.58560313
0.043478	1.45939815	2.918796301	0.396771773	0.793543546
	1.459791087	2.919582174	0.396872815	0.79374563
	1.46081023	2.921620461	0.397137076	0.794274153
	1.460810573	2.921621146	0.397137163	0.794274327
0.041667	1.571179435	3.14235887	0.411351689	0.822703377
	1.571653702	3.143307405	0.411469307	0.822938614
	1.572932767	3.145865534	0.411750105	0.82350021
	1.572933242	3.145866484	0.411750195	0.82350039
0.04	1.625591201	3.251182402	0.408571583	0.817143166
	1.626104526	3.252209052	0.408694122	0.817388244
	1.627474884	3.254949767	0.408980068	0.817960135
	1.627475369	3.254950739	0.408980149	0.817960298

Table 5.3

6

Validation in SIMA

6.1. SIMA

SIMA also known as Simulation Workbench for Marine Applications, is a simulation and analysis program for marine operations and floating structures developed by SINTEF Ocean. This workbench is built on a software for non-linear time domain analysis from modelling to results. These can be immediately and easily comprehended by the users thanks to 3D and 2D representations. Other features covered by the SIMA software are simulation and engineering analysis of marine operations, feasibility evaluation and detection of problematic circumstances. Among its applications is Offshore wind: an accurate physical representation of both fixed and floating offshore wind turbines can be created using SIMA's modeling capabilities.

SIMA uses the calculation engines SIMO and RIFLEX. SIMO is a software that carries out time domain simulations of multi-body hydrodynamic systems (rigid multi-body coupled time-domain analysis) together with the analysis of marine operations and station-keeping analysis. RIFLEX, carries out the finite element model analysis of slender marine structures like risers and mooring lines. In this specific case the semi-submersibles with the towers and the lumped masses have been modelled as SIMO bodies and the mooring lines as slender elements with RIFLEX.

6.2. SIMA model

As already mentioned above, an analogous SIMA model to the Matlab one has been created, in order to benchmark the results obtained with the quasi-dynamic model.

As shown in Figure 6.1 the model in SIMA, unlike the Matlab model, is a three dimensional one. In order to compare the two models, the model in SIMA has been simplified in order to make it as similar as possible to the Matlab one. In addition to using the same values for the masses (both models present the OC4 semisubmersible and the 5MW NREL wind turbine) and the same mooring line properties, also taken from the OC4 project (see Table 4.4), both the rotor and the blades have been removed from the two turbines and the masses of these have been included on top of the towers as two lumped masses. The system is made of four SIMO bodies, two OC4 semisumbersibles floating platforms and the two lumped masses defined as MASS and MASS1 which have the following values:

- $M_{nacelle} = 2.4e + 05$ kg
- $M_{rotor} = 1.1e + 05$ kg

- $M_{hub} = 56780$ kg

which summed give a value of $M = 4.06e + 05$ kg . The two semisubmersibles have been placed with respect to each other at a distance of 1257.6 m found by static calculations in Maltab as will be explained in section 7.1.

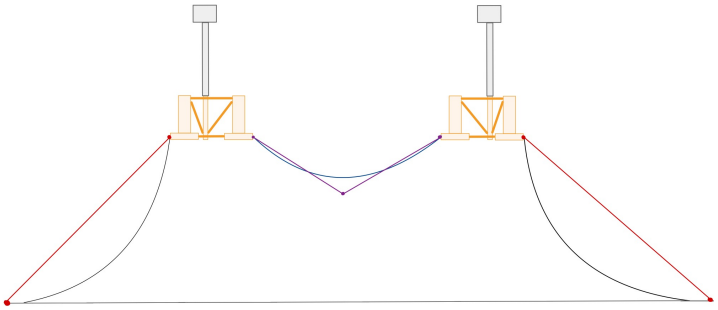

Figure 6.1: Different modelling options for mooring lines in SIMA

On the other side, the anchor lines as well as the tower-mass and the tower-floater connections have been modelled with RIFLEX. In Appendix B, Table B.2 are presented the different lines modelled in the system. The table has multiple columns in which the types, start and end nodes and lengths of lines are reported. All the nodes are then also reported in Appendix B in Table B.1.

The different line types of lines are:

- mooring
- mooring shared half
- semidum
- tower_lt

The first two types are respectively the ones adopted for the anchor lines and for the shared line. Both types have the same properties as listed in Table 4.4 with the exception of the length, that in the mooring type is 772 m, which is the length chosen for the anchor lines and in the mooring shared half type is 648 m, which corresponds to half of the shared line length 1296 m. The other two type of lines are ”dummy” lines created to model the connections between the tower and the semisubmersible (semidum) and between the elements of the tower (tower_lt).

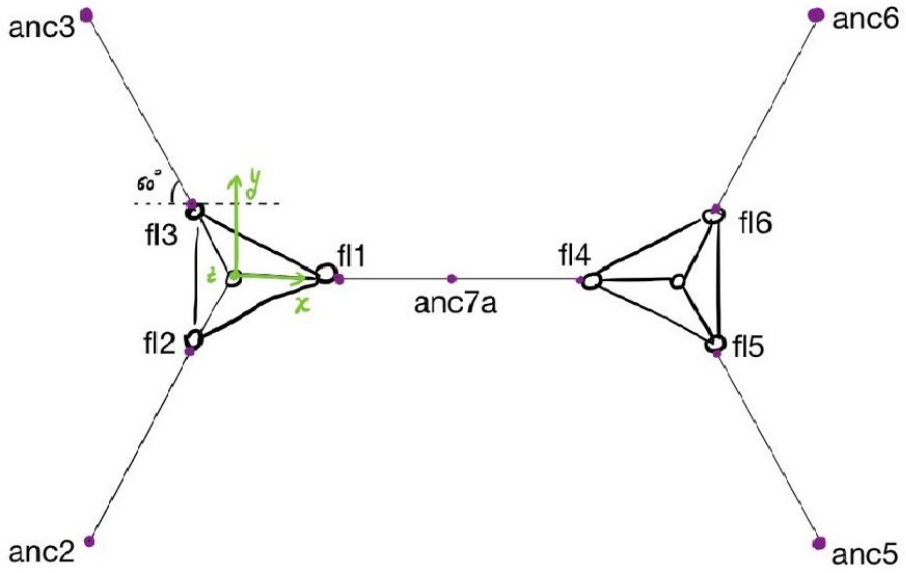

Figure 6.2: Top view of the system in SIMA including nodes

As it is visible in Figure 6.4, all the mooring lines are initially modelled as straight lines. Regarding the anchor lines, to have them assuming the desired catenary shape the nodes representing the anchors have been defined by two different positions: the initial and the prescribed one. The initial position is the position of the node if the anchor line would be stretched in its full length at the fairlead level ($z = -14$ m). Whereas, the prescribed position is the one that the anchor is supposed to assume on the sea bed when the static equilibrium of the system is reached. The latter is then predicted with a preliminary analysis in the Matlab model using the value of the anchor radius. The procedure is explained more in depth in the next chapter section 7.1.

Regarding the shared line, different modelling options have been tried. The first option was to model the shared line as one straight line whose ends were two fictitious nodes whose prescribed positions would have been the fairleads. The second option was to model the shared line as two separate lines of length equal to half of the actual length of the shared line $1296/2 = 648m$, in a V shape, as depicted in purple in Figure 6.1. In this case the supernode in the middle would have been modelled as free. The second option has been the preferred one as it is shown below. The initial position of the free node anc7a as been derived using the following scheme :

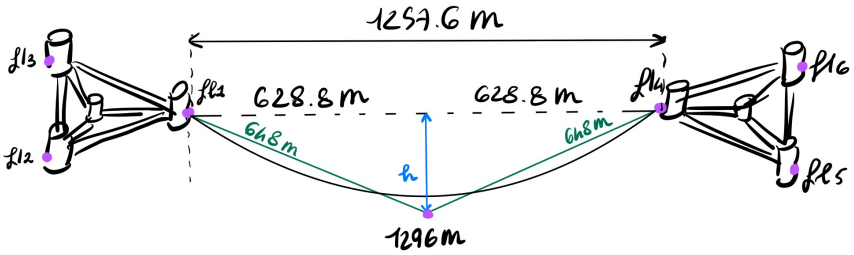

Figure 6.3

This shows that the initial x-coordinate corresponds to half of the distance between the two floaters and the initial z-coordinate (h) has been determined as $\sqrt{648^2 - 628.8^2} = 170.57$ m.

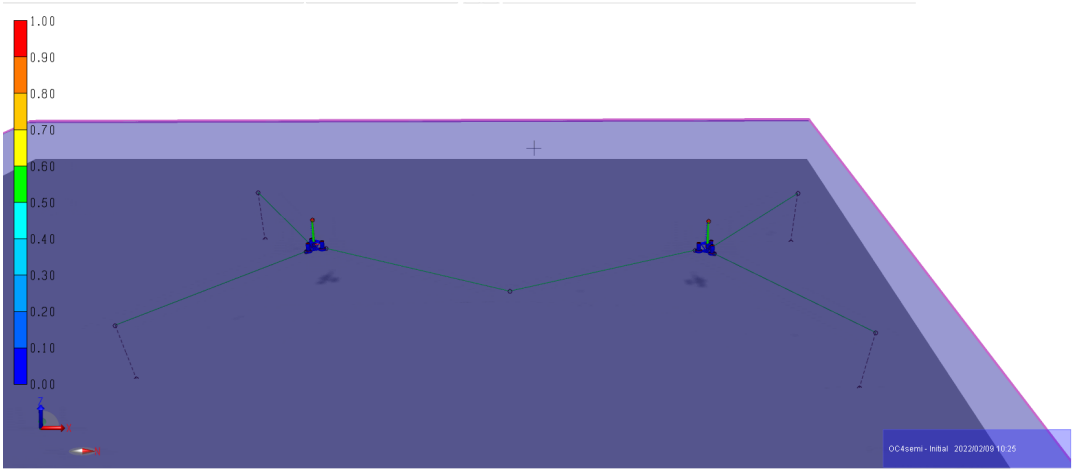

Figure 6.4: Visualization of the model set-up in SIMA

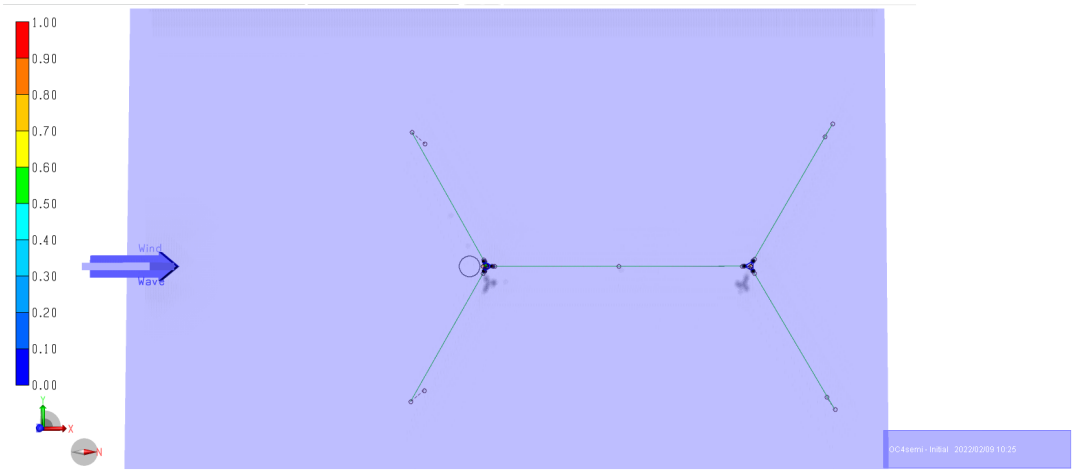

Figure 6.5: Visualization of the model set-up in SIMA from the top

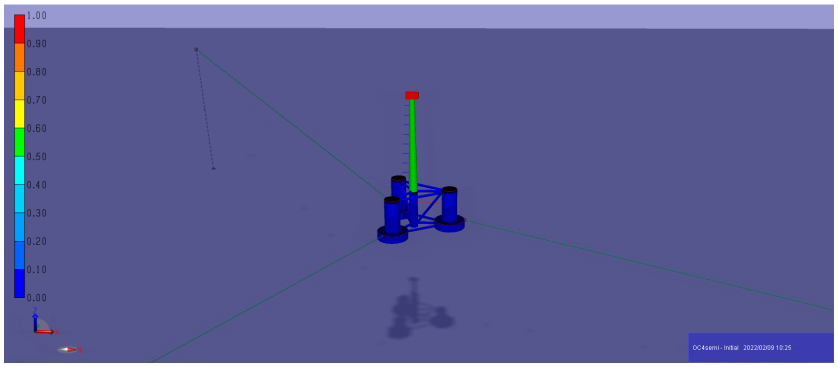

Figure 6.6: Visualization of the single turbine in SIMA

Once the model was set the static analysis has been carried out giving the following final static configuration:

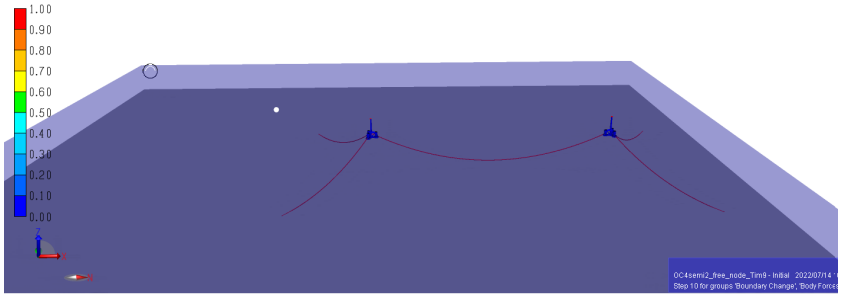

Figure 6.7: Final static configuration obtained in SIMA

6.2.1. Static Analysis in SIMA

Numerically, the static equilibrium in SIMA is found by application of an incremental loading procedure with equilibrium iterations at each load step. This means that the static configuration at each load step is found by iterative solution.

The loads are implemented incrementally in load groups. The load groups are defined in the static calculation parameters. In this case the load groups that have been applied to this system and in the following order are: volume forces i.e. buoyancy and weight, specified displacements i.e. displacements from the stress-free configuration to the final position of nodal points, boundary change and body forces (floater forces).

E.g. given the load group of volume forces with 10 load steps, at the first step SIMA would apply $1/10$ of the buoyancy and $1/10$ of the weight and try to achieve equilibrium, then at the next step it will apply $2/10$ of the buoyancy and $2/10$ of the weight and so on for every step and load groups.

In the following chapter the results of the static analysis in SIMA have been reported.

7

Results

7.1. Static analysis results

The first thing to be done to define the system is to establish the static equilibrium configuration in terms of tensions in the mooring lines, distance between the turbines and anchor positions, which has been presented in subsection 4.1.2. The initial configuration is supposed to ensure the static equilibrium of the system in terms of tensions in the lines at the fairleads for both the Matlab and SIMA models.

Initially, for the static analysis the parameters given in Table 4.1 in [Con18] have been used, not only to have an already verified starting point but also to have results to benchmark the models. These parameters were the lengths of both anchor and shared lines, the distance between the turbines and the anchor positions. The values of the length of the lines and of the anchor radii are also reported here below in Table 7.1. These have been found through his mooring design algorithm which uses a quasi-static model. The mooring line data to which Connolly refers to is also the one from the DeepCwind project already presented above in Table 4.4.

Type	$L_{waterplane}$ (m)	L_{total} (m)
Anchor, 2-by-2	726	772
Shared, 2-by-2	1260	1296
Anchor, 3-by-3	938	976
Shared, 3-by-3	1260	1282

Table 7.1: Table of quasi-static mooring line parameters from Connolly [Con18] for both 2-by-2 and 3-by-3 FOWT grid configurations

In the table above the water-plane length $L_{waterplane}$ of the lines represents the distance, in the plane of the line, between the fairlead and the anchor from the top while L_{total} is the total length of the lines and these values have been reported for both set-ups presented above.

During the static analysis then some modifications have been done to the design choices made by Connolly and the final values that have been used are reported in Table 7.2, in the ”Initial” column. These have been found by using the catenary equations for both the shared and the anchor lines, in order to ensure equilibrium between the tensions at the fairleads.

More specifically, by using all the parameters from [Con18], there was a big imbalance in the axial tensions of the mooring lines at the fairleads and both turbines were moving around 20 m inwards, causing the shared line to go down to the seabed. These results suggested

the presence of several problems such as a too short shared line length, a too large distance between the turbines, an excessive weight of the lines or an incorrect location of the anchors that were not providing enough tension to balance the shared line.

The objective of the static analysis in SIMA is to ensure that the floaters don't have to move significantly to reach their equilibrium with respect to the initial position that they have in SIMA, that enough chain is laying on the seabed and that the sag of the shared line is not too large.

Therefore, the total unstretched lengths of the shared and anchor lines were kept as the ones from Table 7.1, together with the wet weight and the axial stiffness. The initial sag of the line was fixed to be $h = 136$ m and the rest of the parameters found by imposing the same horizontal tensions at the fairleads of each floater through the catenary equations.

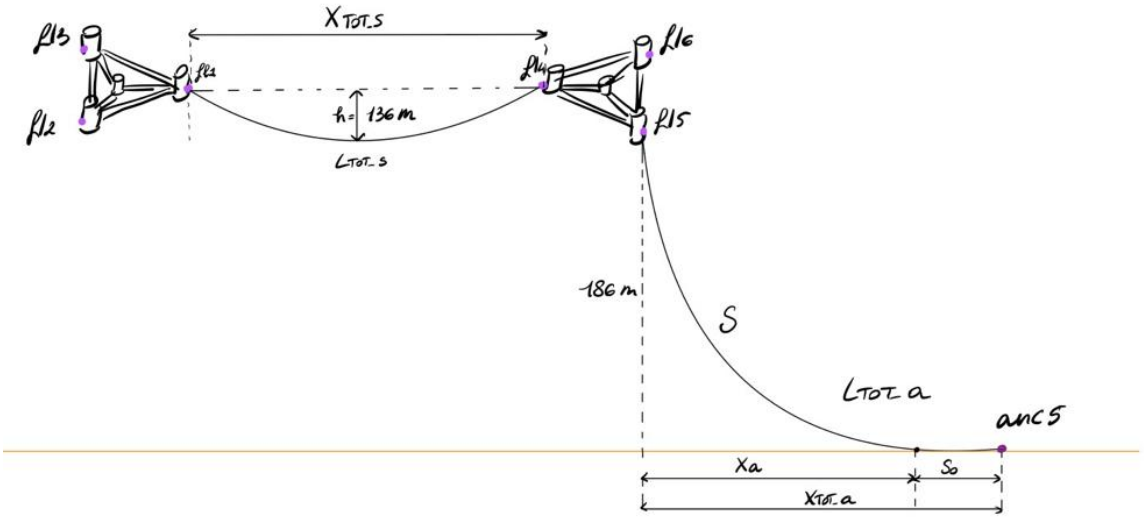

Figure 7.1: Scheme of the starting configuration of the system

After deriving through Matlab the initial static configuration in terms of spacing between the turbines and the positions of the anchors on the seabed, the static analysis in SIMA has been run to check if it would effectively ensure the equilibrium of the system in terms of tensions at the fairleads and without making the floaters displace. The results that were obtained appeared to be very similar to the starting values calculated via Matlab with the catenary equations. These values have been reported in Table 7.2 in the "Final" column.

		Final	Initial
Total distance between floaters	X_{tots}	1255.1 m	1257.6 m
Horizontal tension shared line	Tx_{shared}	$1.4677e+06$ N	$1.572e+06$ N
Vertical tension shared line	Tz_{shared}	$6.905e+05$ N	$6.905e+05$ N
Axial tension shared line	T_{shared}	$1.622e+06$ N	$1.71e+06$ N
Horizontal tension anchor line	Tx_{anchor}	$1.4657e+06$ N	$1.572e+06$ N
Suspended length anchor line	S	733.3 m	763.92 m
Vertical tension anchor line	Tz_{anchor}	$7.8148e+05$ N	$8.14e+05$ N
Axial tension anchor line	T_{anchor}	$1.661e+06$ N	$1.77e+06$ N
Anchor radius	X_{tota}	741.6 m	741.4 m
Horizontal distance fairlead touchdown point	Xa	702.9 m	733.36 m
Length of line laying of the seabed	S_0	38.6 m	8.07 m

Table 7.2: Configurations before and after static analysis in SIMA

Looking at the table above, it is visible that the final distance between the turbines has decreased because the two floaters have moved towards each-other and that the amount of anchor line laying on the seabed has increased from 8 m to about 38 m.

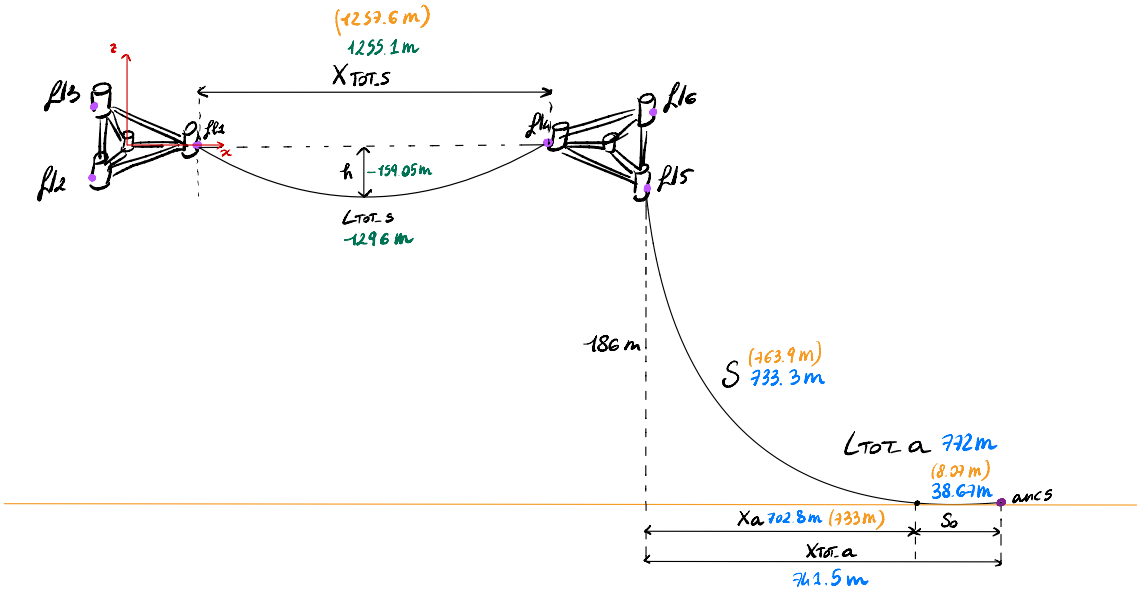

Figure 7.2: Final static configuration of the mooring lines in blue for anchor line and green for the shared line, in yellow starting configuration

Here below have been reported two tables that summarise the results obtained with the static analysis carried out in SIMA. Table 7.3 displays the final positions in terms of all six

degrees of freedom of the two SIMO bodies (OC4semi1 and OC4semi2) modelled in SIMA. However, the values that are of interest are those of surge, as the model moves mainly in the x-direction. Table 7.4 shows the total forces and moments acting on the system in the x,y,z directions.

BODY	Surge [m]	Sway [m]	Heave [m]	Roll [deg]	Pitch [deg]	Yaw [deg]
oc4semi1	1.256	-0.2044E-02	-0.2666	-0.3434E-04	0.2181	0.8625E-04
oc4semi2	1.3	-0.1316E-04	-0.2666	-0.1337E-05	0.6527	0.2718E-04

Table 7.3

	FX [kN]	FY [kN]	FZ [kN]	MX [kNm]	MY [kNm]	MZ [kNm]
oc4semi1	-0.7038	-0.6887E-01	186.1	0.5058E-01	29.02	0.3199E-01
oc4semi2	-2.108	-0.5803E-03	186.1	-0.1827E-02	-49.20	0.1440E-01

Table 7.4

At the end of the static analysis each semisubmersible moved around 1 m and the total resultant forces acting on the system in the x-direction FX is close to 0.

At this point the dynamic analysis has been carried out using this configuration as a starting point in both models.

7.2. Eigenvalue analysis

Before proceeding with the dynamic analysis, the eigenvalue analysis has been performed in both models and in this section the results have been reported and discussed.

In SIMA the natural frequencies have been obtained by running the eigenvalue analysis in the software and the results obtained for the two DOFs that are of interest are the following:

$$\begin{aligned} \omega_{n,1} &= 0.0075 \text{ Hz} \\ \omega_{n,2} &= 0.0098 \text{ Hz} \end{aligned} \tag{7.1}$$

In Matlab the natural frequencies have been obtained using the Matlab function *eig* which gives as outputs both eigenvalues (D) and eigenvectors (T). The natural frequencies have then been calculated as $\omega_n = \sqrt{D}/(2\pi)$, and the results are displayed below.

$$\begin{aligned} \omega_{n,1} &= 0.0069 \text{ Hz} \\ \omega_{n,2} &= 0.0089 \text{ Hz} \end{aligned} \tag{7.2}$$

As the difference between the values is roughly 10%, the derived natural frequencies of the two models are fairly comparable.

Regarding the eigenvectors and the eigenmodes the values computed in Matlab have been reported in Table 7.5, while the results from SIMA have been plotted and shown in Figure 7.3, Figure 7.4, Figure 7.5 and Figure 7.6 in order to visualize the modes.

eigenvector 1	eigenvector 2
-0.707106781	-0.707106781
-0.707106781	0.707106781

Table 7.5: Eigenvectors computed in Matlab

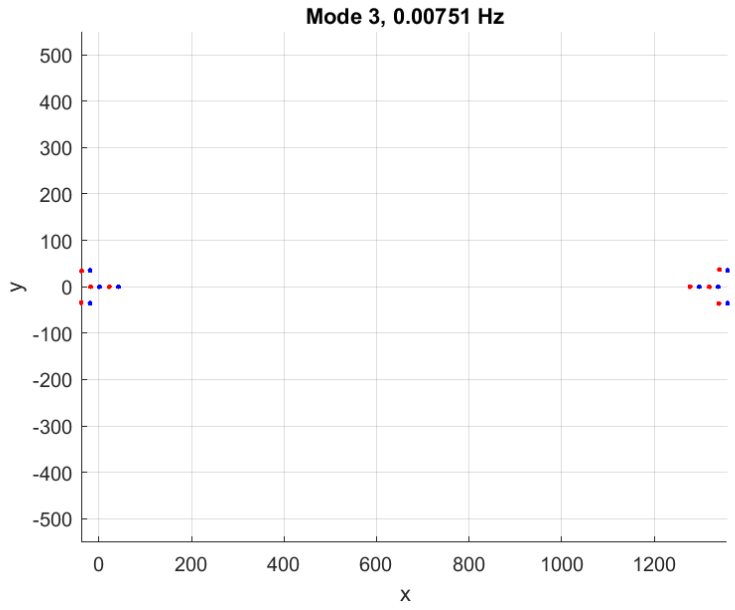

Figure 7.3: Visualization in the x-y plane of first mode corresponding to $\omega_n = 0.0075$ Hz, computed by SIMA

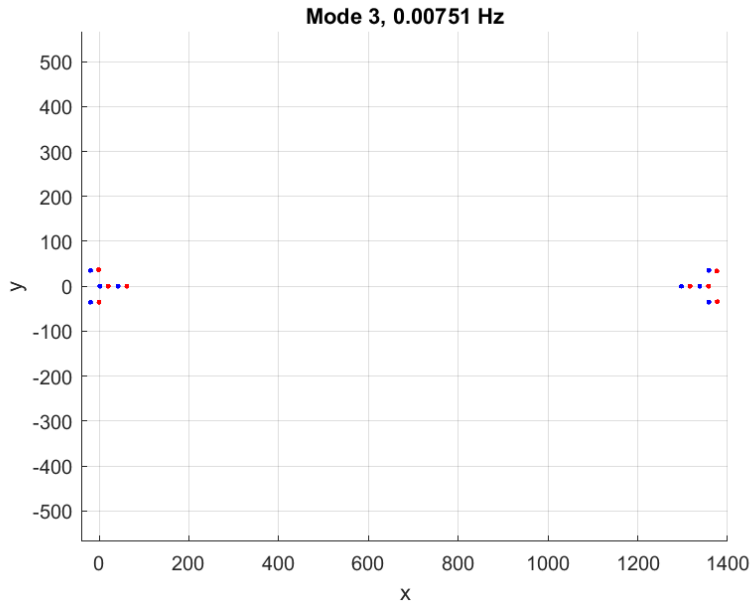

Figure 7.4: Visualization in the x-y plane of first mode corresponding to $\omega_n = 0.0075$ Hz, computed by SIMA

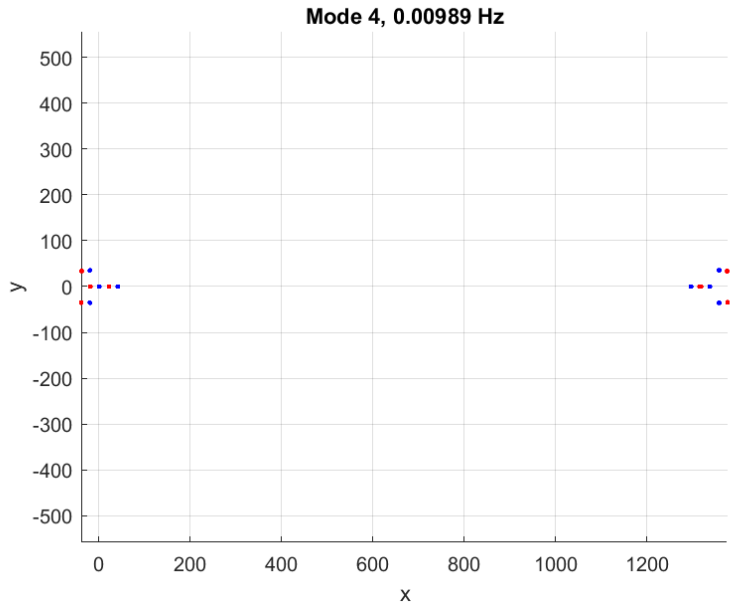

Figure 7.5: Visualization in the x-y plane of second mode corresponding to $\omega_n = 0.0098$ Hz, computed by SIMA

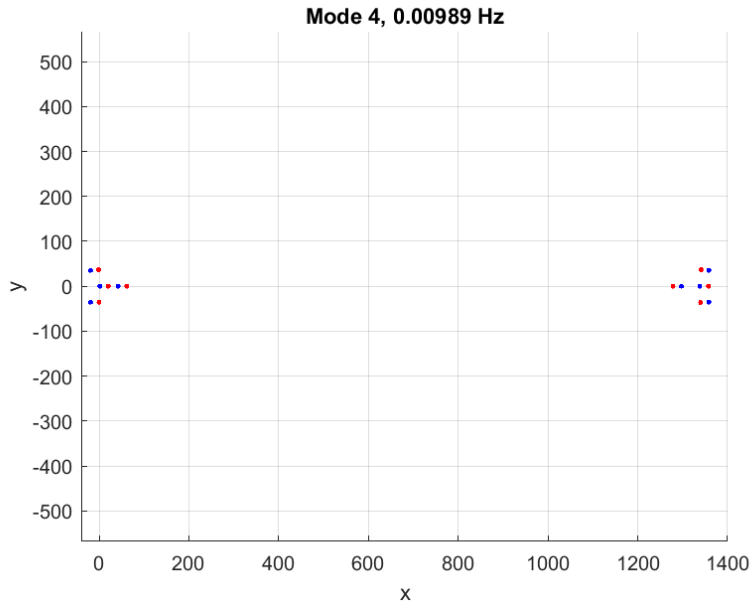

Figure 7.6: Visualization in the x-y plane of second mode corresponding to $\omega_n = 0.0098$ Hz, computed by SIMA

In the plots reported above the blue dots represent the nodes of the system in SIMA in their original position. As it is visible there are the nodes that represent the two semisumbersibles and the fairleads, for a total of 4 nodes per floater. The red dots represent instead the same nodes but in their displaced position according to the mode. Hence, Figure 7.3 and Figure 7.4 which corresponds to a frequency of $\omega_{n,1} = 0.007$ Hz, see the floaters moving in the same directions back and forth and that also explain why in the first column of Table 7.5 values with the same sign are displayed. For example looking at Figure 7.3 the red dots are all on the right side of the system which means that the floaters moved both towards the right. Looking at Figure 7.4 the red dots are on the left side, which represents the opposite situation

of the previous plot. Figure 7.5 and Figure 7.6, which correspond to a frequency of $\omega_{n,2} = 0.009$ HZ, see the floaters moving towards and far from each-other, as also indicated by the second column of Table 7.5 in which the values have opposite sign. More specifically looking at Figure 7.5 the two floaters moved far from each other while Figure 7.6 shows how the shared line moved downwards because the floaters moved towards each other.

7.3. Dynamic analysis results

The results of the dynamic analysis performed with both models are provided in the section that follows.

7.3.1. Modelling settings

Before results are displayed the modelling settings used in both models have been reported here below.

- Simulation length
  - Matlab: 1200 s
  - SIMA: 1200 s
- Time step
  - Matlab: 0.1 s
  - SIMA: 0.1 s

7.3.2. Constant force test

To begin with, an investigation applying constant forces on both models has been performed to compare the line characteristics of the two models in terms of static tension vs. offset at the top ends of the lines. Indeed, by applying constant forces to the system it is possible to estimate what is the stiffness difference between the two models. The forces have been applied to each semisubmersible in the opposite directions: a constant force towards the left was applied to the floater on the left side and a constant force towards the right was applied to the floater on the right side. The forces are meant to push the two bodies apart, as illustrated in Figure 7.7.

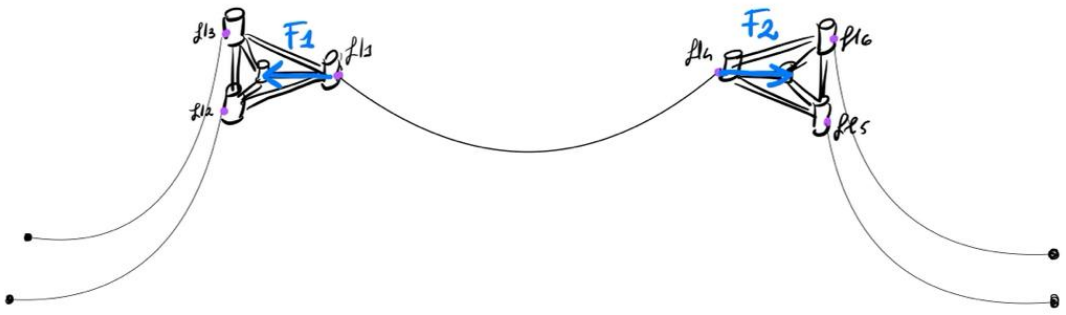

Figure 7.7: Representation of the direction of the forcing terms applied to the system

In the table below the different magnitudes of forces that have been applied to the system have been reported. In order to have force magnitudes to which the system could react in a realistic way, the amplitudes have been scaled with respect to the thrust force of the 5MW NREL wind turbine, placed on top of the floater. The thrust force is $T = 500$ kN and the values of the constant forces have been chosen to be $1/16\ T$, $1/8\ T$, $1/4\ T$, $1/2\ T$, T, $1.5\ T$ and $2\ T$.

ConditionSet	F1 [kN]	F2 [kN]
1	-31.25	31.25
2	-62.5	62.5
3	-125	125
4	-250	250
5	-500	500
6	-750	750
7	-1000	1000

Table 7.6: Constant force test values.

After applying constant forces of different magnitudes to both models, the offsets of each floater and the tensions in the lines have been measured and then compared. The results obtained from these tests are shown here below.

The first plot, Figure 7.8, shows the comparison between the displacements of Matlab and SIMA of both floaters in the x-direction x_1 and x_2. As expected, the displacement of the first floater x_1 is towards the left in the same direction of the applied force on the first floater, while the displacement of the second floater x_2 is towards the right, in the same direction of the applied force on the second floater.

Furthermore, it is visible that both the x_1, in the negative x-direction, and x_2, in the positive x-direction, increase with the higher force magnitudes. In addition, it can be observed from Figure 7.8 that the Matlab model is a linear one as the relationship between the displacement and the applied force yields to a straight line. The SIMA model on the other hand results in a curve, which implies that the model is nonlinear, which is what it is expected to be. This means that the force-displacement combination changes for each case. This also implies that for higher forces the Matlab model is overestimating the displacements.

It is also worth-mentioning that the higher the magnitude of the force applied on each of the floaters, the higher the divergence between the two models becomes. This means that for higher force-displacements relationships the stiffness of the Matlab model, which stays constant, does not approximate the stiffness of the SIMA model anymore, which is indeed possible for small displacements, where the two models overlap. This is because for higher forces acting on the system, which result in higher displacements of the floaters, there are some non-linearities that the Matlab model is not able to capture, as a linear model.

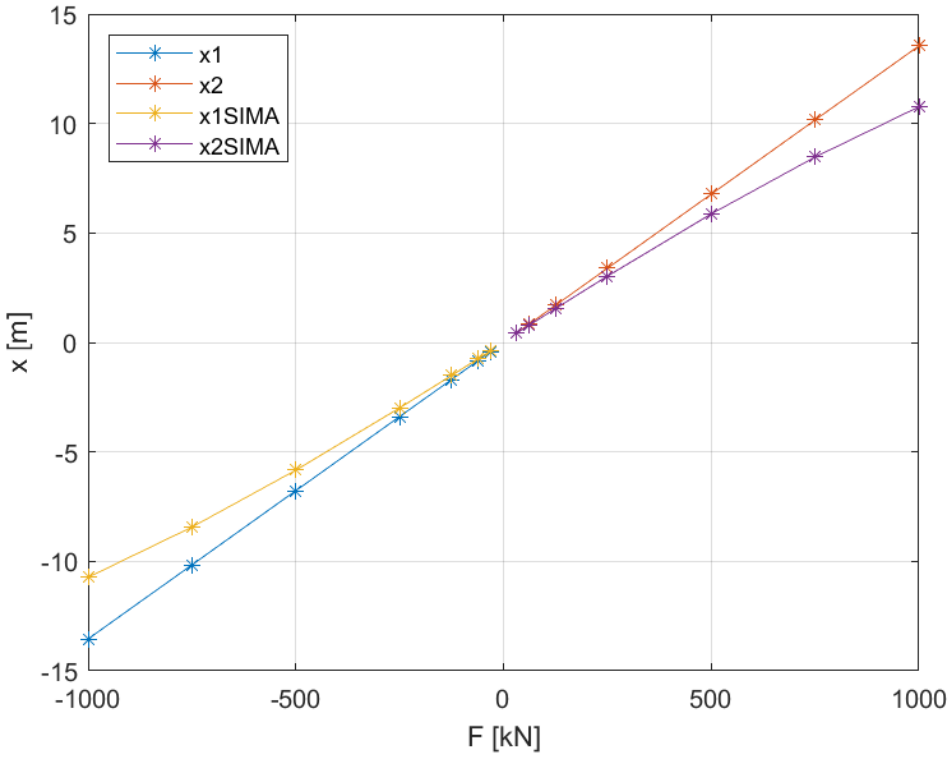

Figure 7.8: Displacement behavior of the two floaters as a function of different forcing terms from both models

Plotting the absolute value of both displacements on the same graph shows that the curves of each floater of the same model completely overlap, which means that when the same force is applied to both floaters in different directions this causes the same body responses confirming that the system is symmetric.

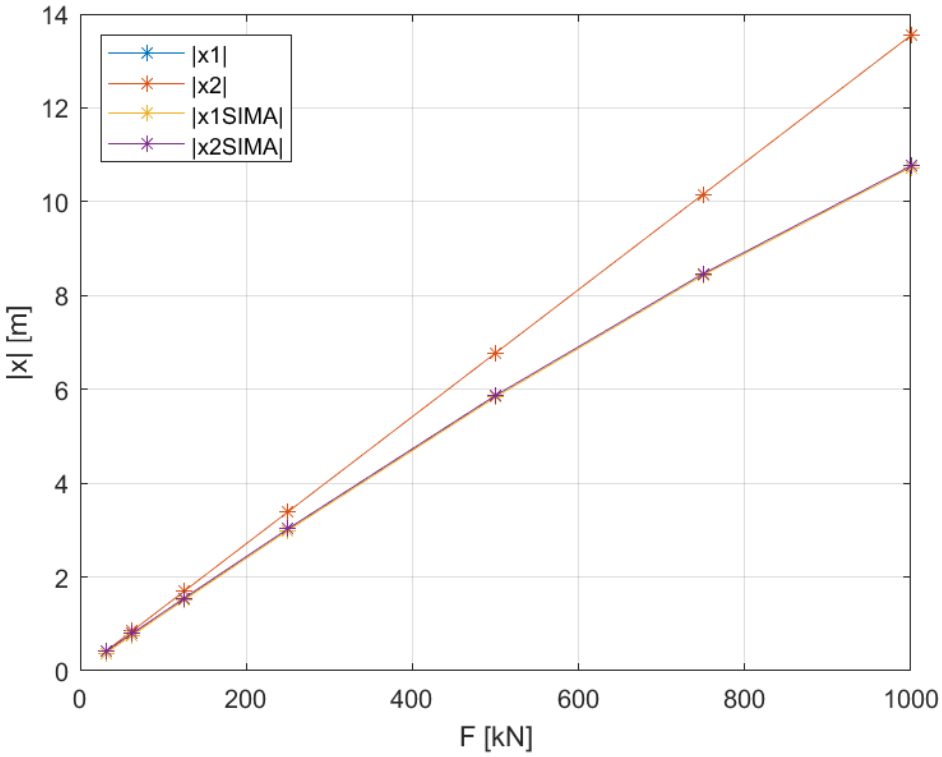

Figure 7.9: Absolute value of Figure 7.8

Regardless of which of the two graphs (Figure 7.8 or Figure 7.9) is being analyzed it is noticeable that in the first part of the graphs, when the displacements of the models small, (around 1 m) the two models display the same results. The values of the displacements have been found by applying to the system a constant force in time and letting the system reach its equilibrium position. At this point this value has been extracted and saved for the different forcing terms.

After looking at the displacements, in the following plots, the tensions at the fairleads for anchor and shared lines have been shown with respect to the displacements of each floater for both models in order to allow comparison. For the SIMA model, these values have been obtained in the same way as the displacements. The only difference is that in this case the time series of the axial tensions that came out from the SIMA model had to be decomposed first in their horizontal components with the angle ϕ at the fairlead and then only the anchor line values had to be projected in the global x-direction with the angle α. After doing this, the values at the end of the time series have been taken, which represent the values of the tensions in the lines when the system has reached its equilibrium position. For the Matlab model instead, the values of the tensions have been found as follows:

$$\begin{aligned} T_1 &= -1465.7\cos(\alpha) - k_1 x1 \cos(\alpha)^2 \text{ kN} \\ T_2 &= 1465.7\cos(\alpha) - k_2 x2 \cos(\alpha)^2 \text{ kN} \\ T_s &= 1467.7 - k_s x_{12} \text{ kN} \end{aligned} \tag{7.3}$$

These expressions have been written from the perspective of the floaters. In the case of the first floater the tension T_1 with respect to the positive global x-direction (in green in Figure 7.27) will be negative. The first floaters feels a force in the positive direction coming from the pre-tension of the line (1465.7 kN) but w.r.t the force definition given in the EOM Equation 5.4,

looking at Figure 7.16, this contribute will have the negative sign. For the second floater instead, the external force acting on the floater coming from the pre-tension in the line is in the positive direction but the contribution coming from the stiffness of the line is negative. Finally looking at the shared line tension, the pre-tension is positive and the contribution coming from the stiffness has to be subtracted to this value. In this term x_{12} has been calculated simply by taking the difference between the displacement of the first floater and the second one. These values then w.r.t the line's perspective are defined in the same way but with the opposite sign.

Here below the first two graphs show how the tension in the anchor lines changes for different offsets of each floater in both SIMA and Maltab.

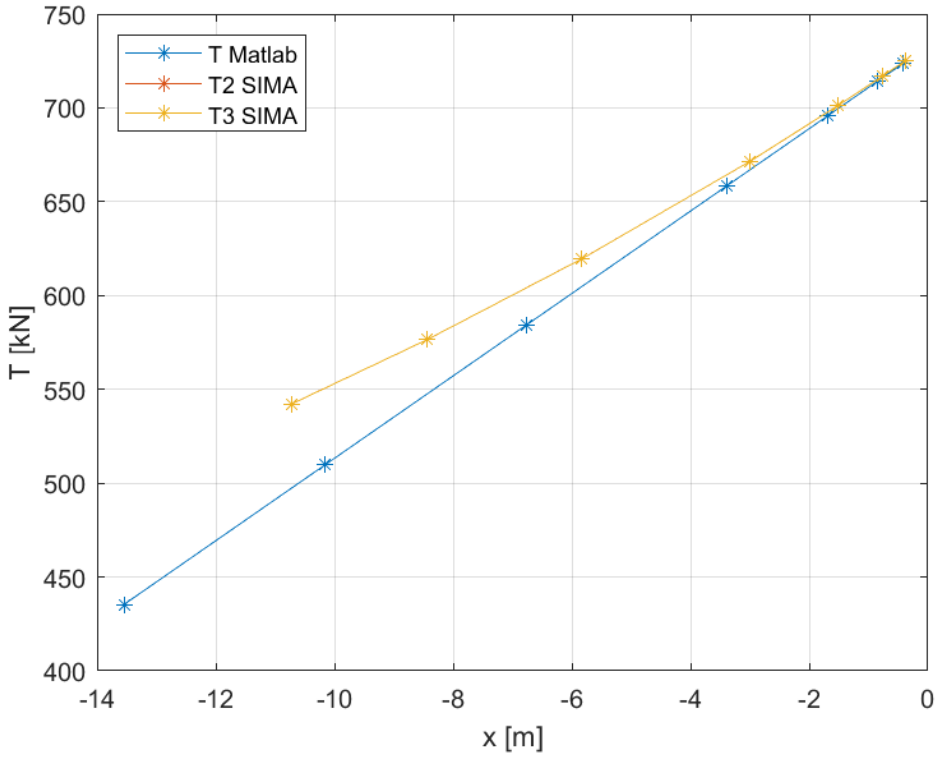

Figure 7.10: Left anchor line tensions as function of offset of first turbine

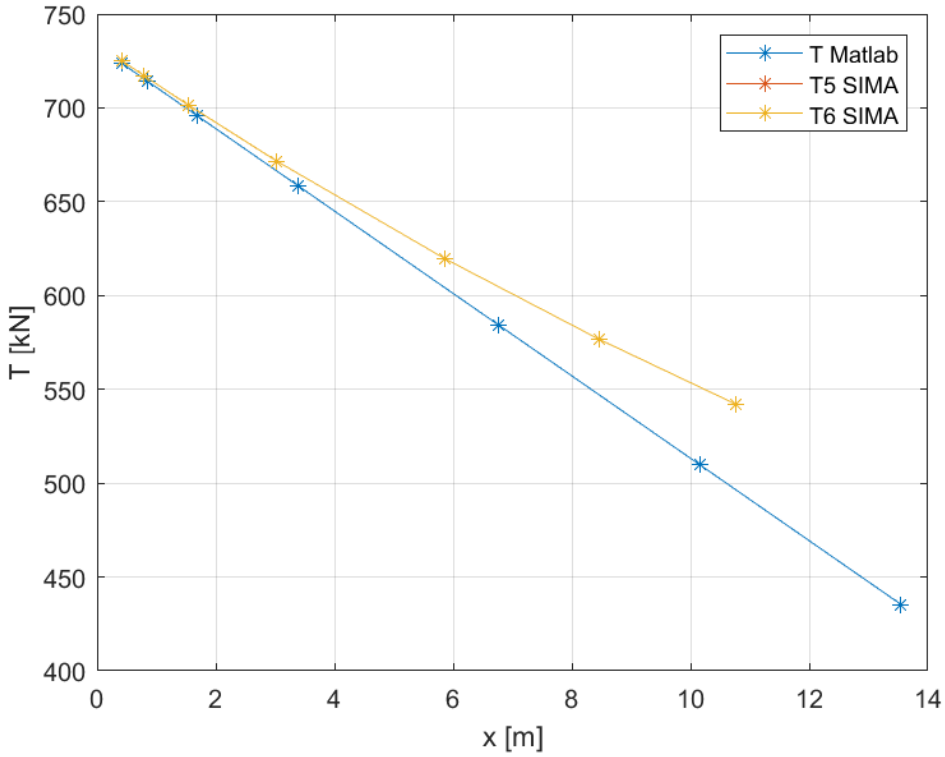

Figure 7.11: Right anchor line tensions as function of offset of second turbine

The plots show both the same trend: the higher the offset in the direction of the anchor the lower the tension in the lines becomes. This is because when the floaters move outwards the tension in the anchor lines will decrease since the pre-tension already in the lines will be relieved when the floaters are moving outwards towards the anchors and therefore the overall tension will decrease.

The graph here below Figure 7.12 instead, shows how the shared line changes with respect to different resultant offsets that the shared line sees, from both the SIMA and Matlab models.

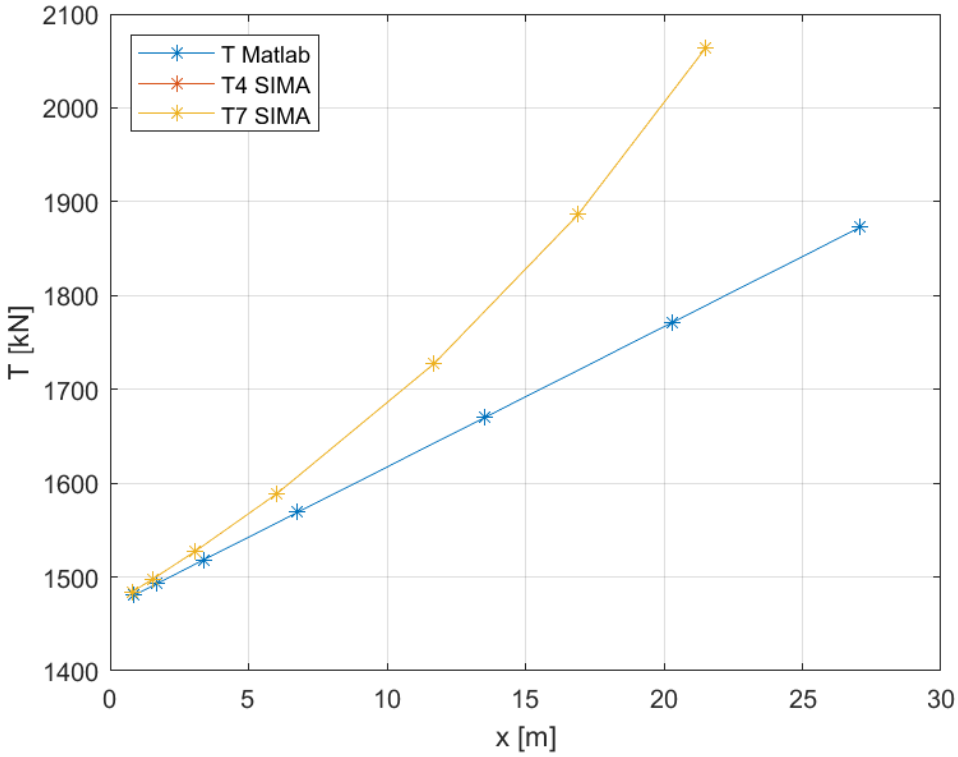

Figure 7.12: Shared line tensions as function of offset of system

This graph has the opposite trend of the one of the anchor lines. This because when the floaters are pushed outwards the tension in the shared line has to increase because the line gets pulled from both directions becoming, indeed, more tensioned.

What is visible from all the plots is that the higher the displacements the more the two models diverge. This because the Matlab model which is a linear model, is only valid for small displacements, as also seen previously with the displacement plots.

What can be concluded from this test is that the stiffness of the Matlab model matches fairly enough the one from the SIMA model when dealing with small displacements of the floaters.

Here below have been reported three graphs showing the comparison between Maltab and SIMA models when computing the shared line tension by changing the equivalent stiffness values for the Matlab model. The values used are respectively 20.8 kN/m, 24.4 kN/m and 30.6 kN/m. These are the values of the stiffness terms used for the SIMA model in three different portions of the graph. What can be observed is that when changing the value of the stiffness term it is possible to get more or less correspondence between the two models. The actual value of the stiffness for the shared line used in the Matlab model is 14.5 kN/m, which already gives good results. Looking at the graph it is noticeable that for even smaller displacements than 2 m, which is what will be achieved in the dynamic calculations, the two models show very close stiffness values. For this reason the value of this stiffness can be considered adequate. Anyways, looking at the other graphs it can be observed that for example using a shared line stiffness of 20.8 kN/m in Figure 7.13 the two models overlap for a wider interval of force-displacement combinations.

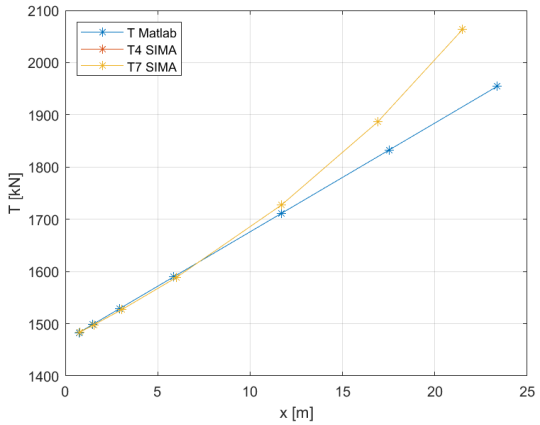

Figure 7.13: Shared line tensions as function of offset of system with $k_S = 20.8kN/m$

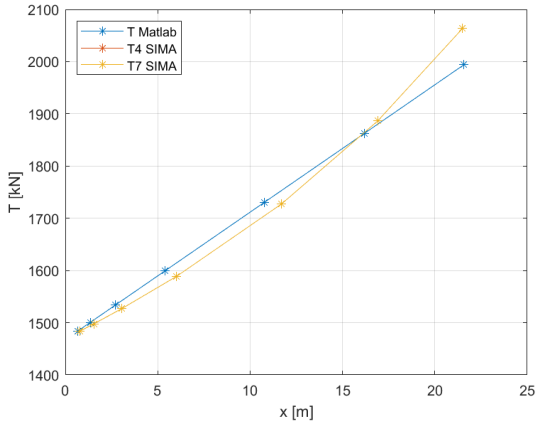

Figure 7.14: Shared line tensions as function of offset of system with $k_S = 24.4kN/m$

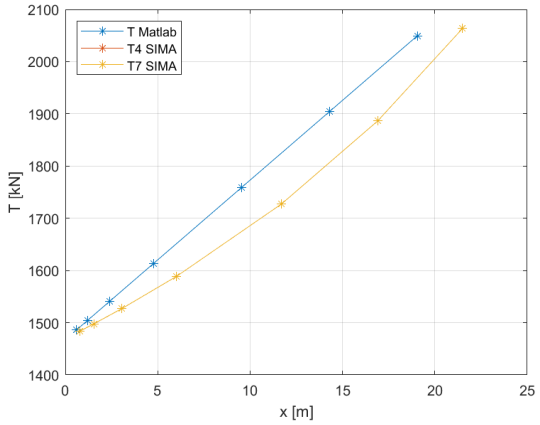

Figure 7.15: Shared line tensions as function of offset of system with $k_S = 30.5kN/m$

In the second and third plot, Figure 7.14 and Figure 7.15 for small displacement values the Matlab model is overestimating the tension values, while for higher values the second model's plot crosses the SIMA one and underestimates the tensions. Using the last value instead it is visible that Matlab over estimates the tension values for the entire range of displacements.

In the end, looking at the observations that were made, for further analysis the initial value of the $k_s = 14.5$ kN/m has been used.

Verification

In the constant force model the equilibrium between the forces in both SIMA and Matlab has been checked for each load condition. The equations used to check the equilibrium for both floaters are the following:

$$\begin{aligned} \text{Eq floater 1} &= 2 \cdot T_1 + T_s + F1 \\ \text{Eq floater 2} &= 2 \cdot T_2 - T_s + F2 \end{aligned} \tag{7.4}$$

The SIMA model for each condition ensures the equilibrium, by using Equation 7.4 the value obtained is 0 for each condition.

Regarding the Matlab model instead, the results have been reported below.

Condition	Eq floater 1 [kN]	Eq floater 2 [kN]
1	1.99999999944	-1.99999999944
2	1.99999999887	-1.99999999887
3	1.99999999774	-1.99999999774
4	1.99999999661	-1.99999999661
5	1.99999999548	-1.99999999548
6	1.99999999661	-1.99999999661
7	1.99999999548	-1.99999999548

As it is visible from the table, the resultant equilibrium on each floater gives an imbalance if 2 kN, which corresponds to the 2 kN difference between the static horizontal tensions at the fairleads as indicated in Table 7.2 between the $Tx_{shared} = 1467.7$ kN and the $Tx_{anchor} = 1465.7$ kN.

7.3.3. Dynamic load case

After applying constant load cases to the system and verifying that the models agree, in this section dynamic load cases have been applied. The values of the forces that have been applied to the two models have been reported in the table below, as a combination of F amplitudes and T_f forcing periods with the corresponding condition number. Twenty one different forcing cases have been analysed in order to have a more varied range of response of the system, to analyse more in depth the differences between the two models.

The values of the amplitudes reported in the table, have been found by interpolating the values from the first order wave transfer function in Figure 5.4, in order to find the correspondent amplitudes for each of the forcing frequencies. All of them have then been multiplied by a factor of 1.5 in order to obtain wave forces that would correspond to a 3 m wave height to obtain realistic values. This because the values from the wave transfer function are all normalized by a 1 m wave amplitude.

In the table below have been reported the 21 conditions that have been simulated with both models.

ConditionSet	Tf [s]	F [N]
1	5	5.3639e+06
2	6	7.7673e+06
3	7	4.1516e+06
4	8	4.1957e+06
5	9	5.5717e+06
6	10	6.2786e+06
7	11	6.3747e+06
8	12	6.1207e+06
9	13	5.7069e+06
10	14	5.2439e+06
11	15	4.7887e+06
12	16	4.3679e+06
13	17	3.9896e+06
14	18	3.6573e+06
15	19	3.3681e+06
16	20	3.1154e+06
17	21	2.8966e+06
18	22	2.7105e+06
19	23	2.5441e+06
20	24	2.3931e+06
21	25	2.2675e+06

Table 7.7: Specification of the condition sets that have been modelled

These amplitudes have been applied to the model as two harmonic forces, $F1 = Fcos(\omega t)$ and $F2 = Fcos(\omega t + \phi)$ as already specified in chapter 5, where the phase angle ϕ has been kept constant and equal to π. The reason why the forces have been applied in counterphase was to get the maximum effect on the mooring line tensions. In both models these regular cosinusoidal wave forces have been applied to the bodies as external point forces as showed in the following figure:

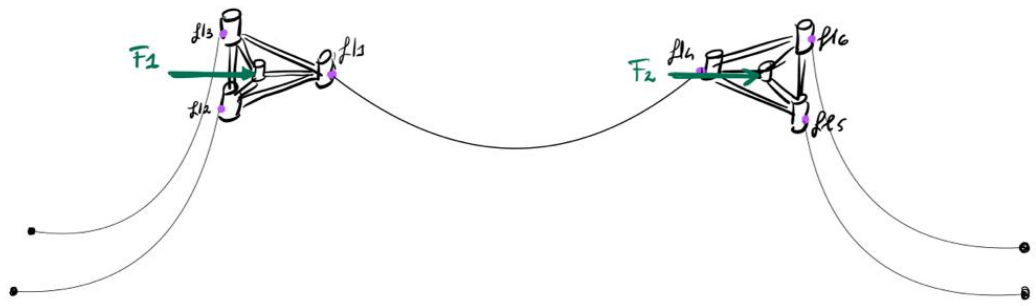

Figure 7.16: Orientation of the dynamic forces applied to the system in both models

Displacements

The initial comparison between the SIMA full dynamic model and the Matlab quasi-dynamic one has been done by examining the motion and the tension amplitudes for all the twenty one

conditions.

Here below in Figure 7.17 the amplitudes of the motions in surge as a function of the different forcing frequencies have been displayed. In order to compare these results more accurately, the values from SIMA and Matlab have been reported on the same plot, while in Figure 7.18 the percentage difference between the values has been shown as a function of the different frequencies, taking as baseline the outputs from the SIMA model.

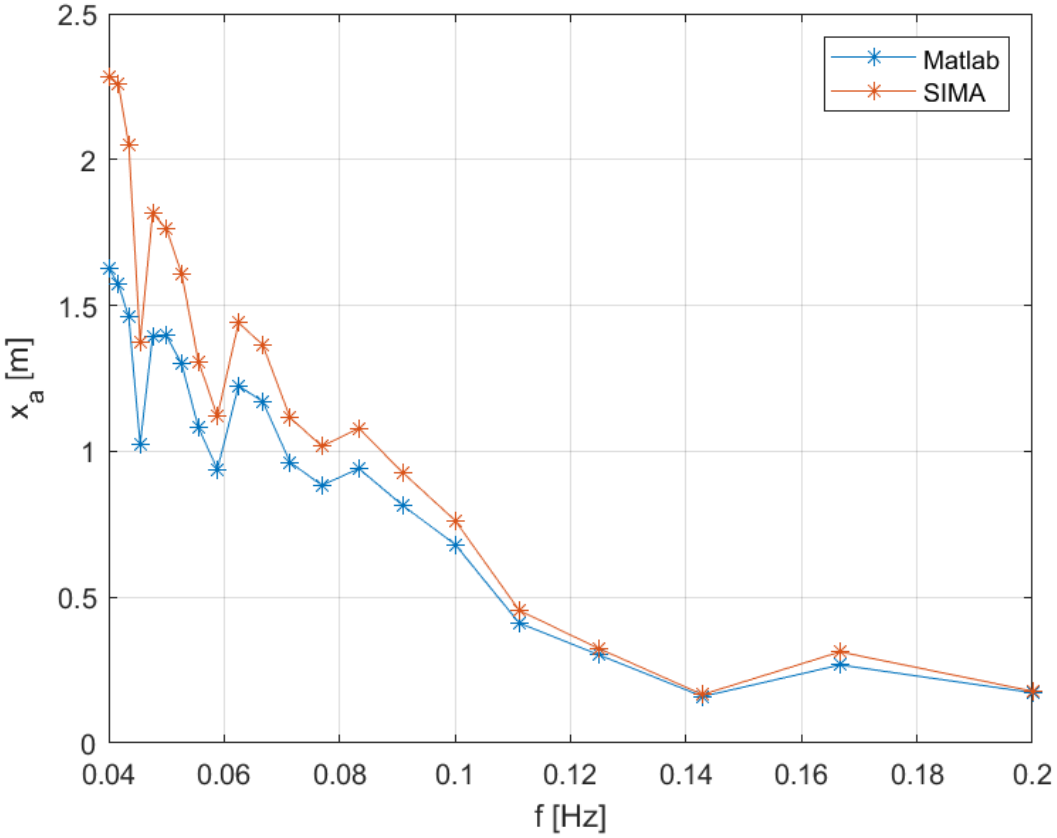

Figure 7.17: Comparison between surge amplitudes from both models

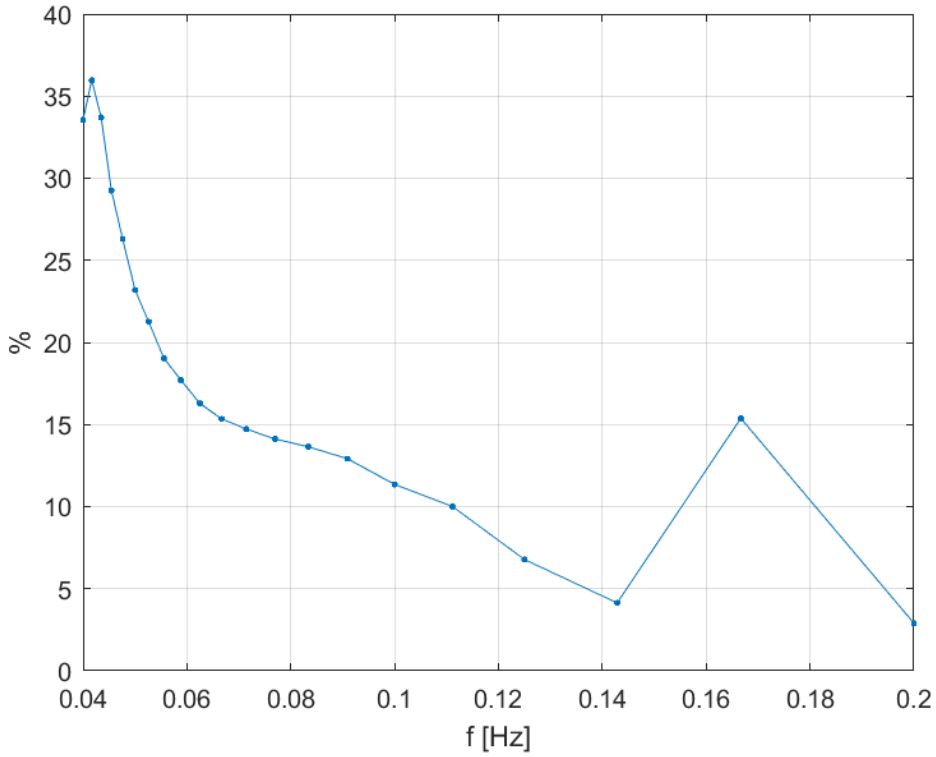

Figure 7.18: Percentage difference between the values from the two models

From Figure 7.17 it is visible that the Matlab quasi-dynamic model for higher frequencies gives a more accurate estimation of the motion amplitudes, while for lower frequencies the difference between the two models seems to increase.

The first thing to point out is that both models show the same trend, characterized by having lower displacements at higher forcing frequencies and larger displacements at lower forcing frequencies. This because to high forcing frequencies correspond high varying forcing terms which determine lower amplitudes of motion because the system has less time to react to a force that is changing rapidly in time. For lower frequencies instead, which imply slow varying forcing terms, the system has more time to react to the force and the amplitudes of motion of the masses become higher.

Together with this difference it is noticeable that for smaller displacements the two models give almost identical results and for higher displacements the two graphs diverge. This is due to the fact that for smaller surge amplitudes the quasi-dynamic model gives more accurate results, since being a linear model it is suitable for small displacements. For lower frequencies the SIMA model gives as output higher motions and the results from both models diverge.

It must be said, however, that in general, the displacements observed in these tests do not go over 2.5 m, which can still be reasonably defined as a small displacement. It is expected that the models are more accurate for small displacements, and the difference between the two becomes imperceptible for minimum displacements and increases with increasing displacement, reaching a maximum difference of 36%.

In the meantime, it is worth noticing that the fact that both models display the same pattern is a good indicator. This is due to the fact that in both models the amplitudes and frequencies of the forcing terms were chosen following the first order wave transfer function shown in Figure 5.4 and indeed the pattern reminds this curve. This would also be an indicator that the mooring system has little impact on the first-order-wave-induced motions, which should be the

case.

The results above have been obtained by calculating the amplitudes of motion from both models starting from the time series. For the Matlab model the amplitudes for x_1 and x_2 have been extracted from the respective time series, which have been filtered with the forcing frequency of interest and afterwards provided to a function that would run a fast Fourier transform in order to get the amplitudes of each signal. The same approach has been adopted with the results from the SIMA model, with the only difference that in this case the time series available from the software were calculated using as starting position the final static configuration, reported in Table 7.3. Therefore the actual surge motions have been found as:

$$\begin{aligned} x_1 &= surge_1(t) - 1.256\text{m} \\ x_2 &= surge_2(t) - (1339.3 - 1.3)\text{m} \end{aligned} \tag{7.5}$$

where $surge_1$ and $surge_2$ are the time series of the surge platform motions extracted from SIMA, 1.256 m and 1.3 m are the positions at the end of the static analysis, as also show in Table 7.3, and 1339.3 m is the x-coordinate in SIMA of the node correspondent to the second floater, as shown in table Table B.1.

Verification

To check the amplitudes of the displacements, the values were taken and then multiplied by the $cos(\omega t)$ or $cos(\omega t + \phi)$ in order to get a time series that was then compared to the original one. Then the ”artificial” time series has been overlapped to the original, showing an only a small difference in the mean value and an shift in the phase.

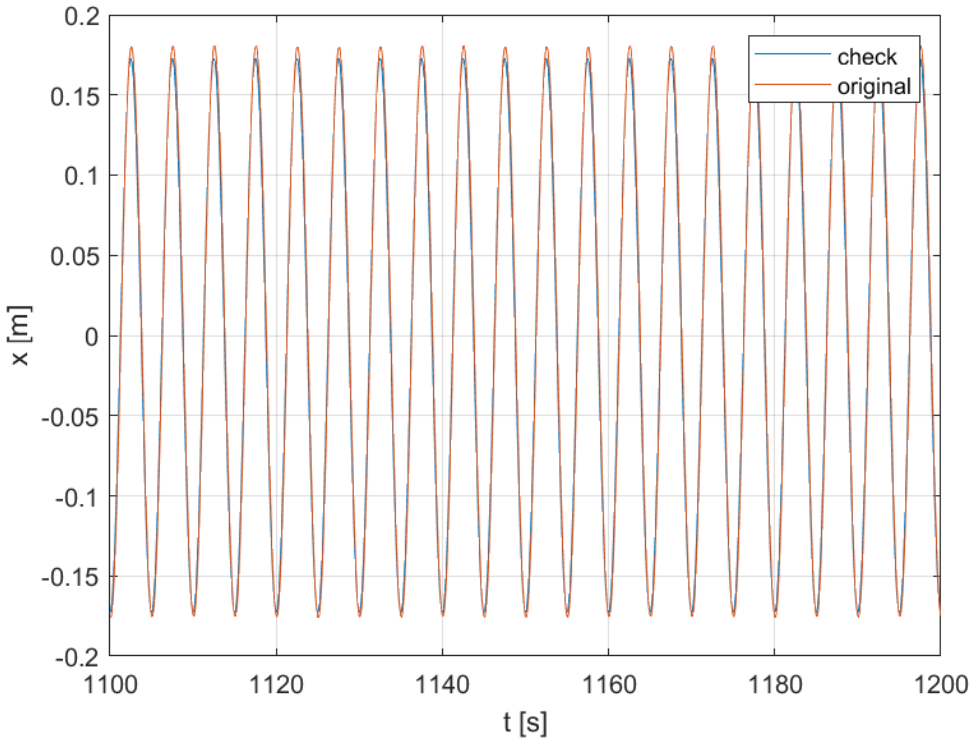

Figure 7.19: Verification of displacement amplitudes

The amplitudes of the velocities obtained in Matlab using the differential equations solver have been double checked by taking the amplitudes of the displacements and multiplying them

by the forcing frequency ω in rad/s. The values obtained are the same as the ones obtained by doing the FFT of the time series of the velocities from the ode4 function.

SIMA vs Quasi-dynamic tensions

The graphs reported in this section show the comparison between the amplitudes of the horizontal tensions projected in the global x-direction for both anchor and shared lines at their fairleads, found both with SIMA and Matlab. The values have been reported as a function of the forcing frequency and the forcing period, this because by plotting the results against the forcing periods, the points are better distributed as can be seen from the graphs and the different points are more clear to observe.

First of all, only the dynamic tension amplitudes from both models have been reported on the same graphs.

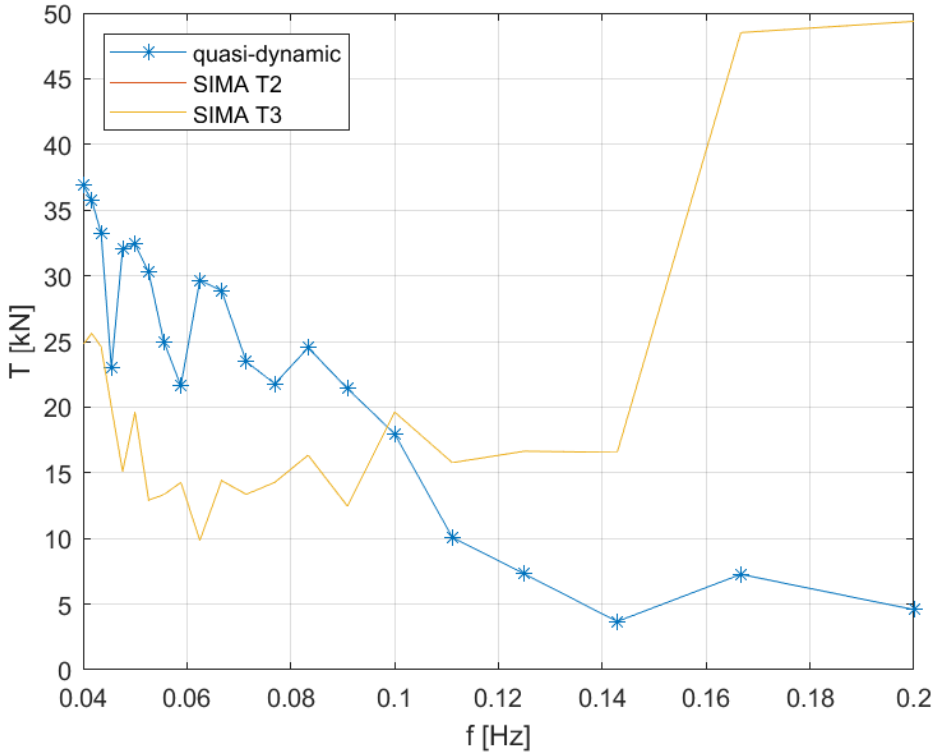

Figure 7.20: Tension amplitudes at fairleads for anchor lines on the left side

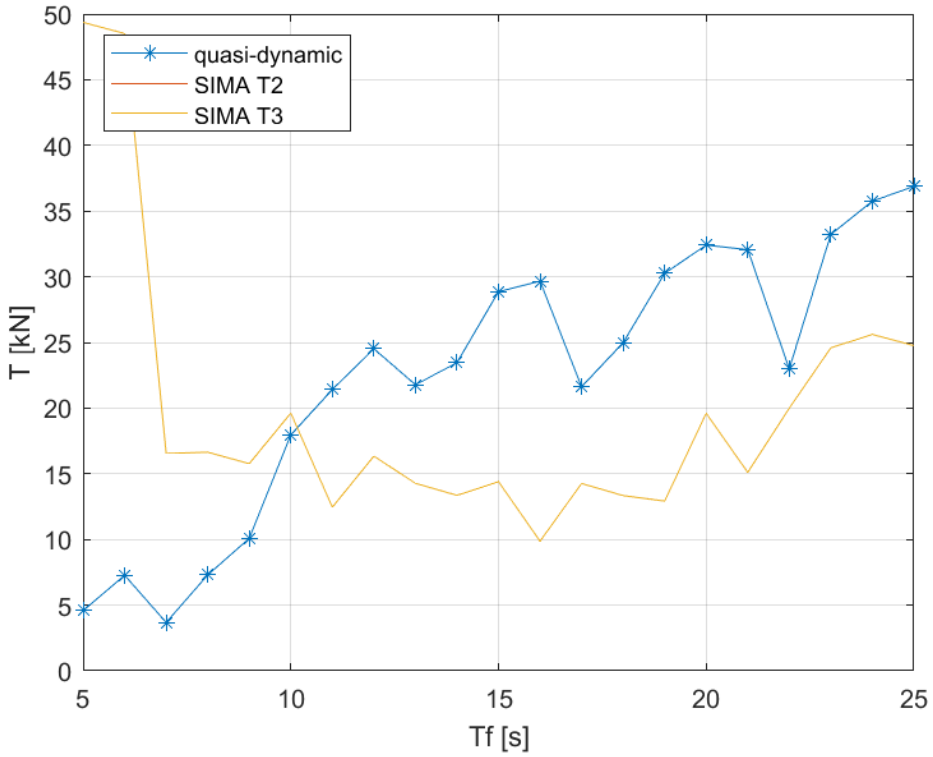

Figure 7.21: Tension amplitudes at fairleads for anchor lines on the left side

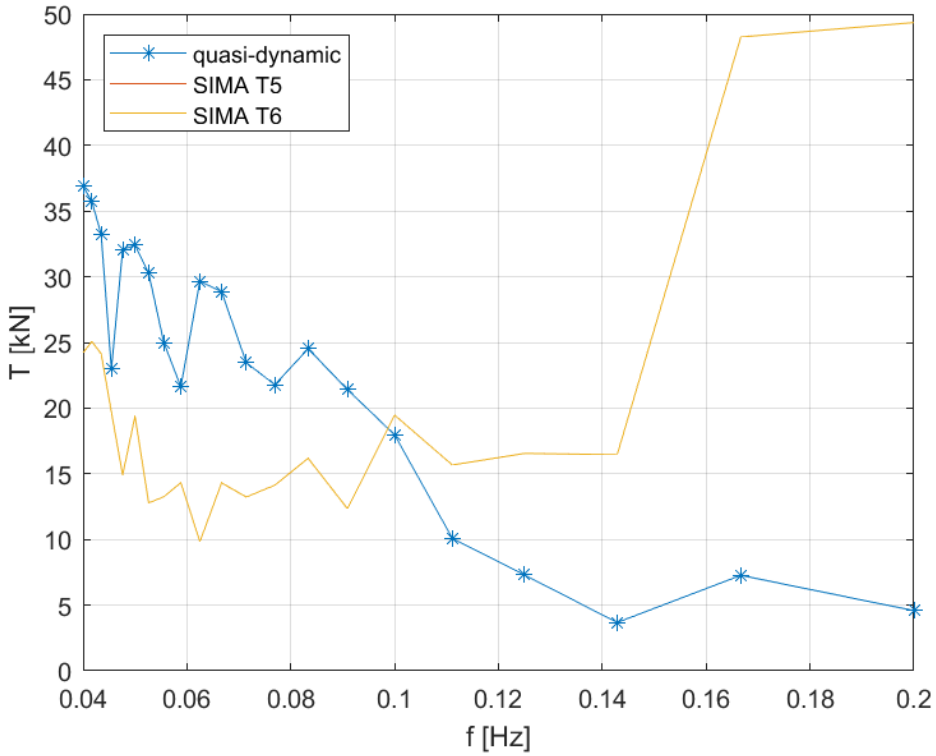

Figure 7.22: Tension amplitudes at fairleads for anchor lines on the right side

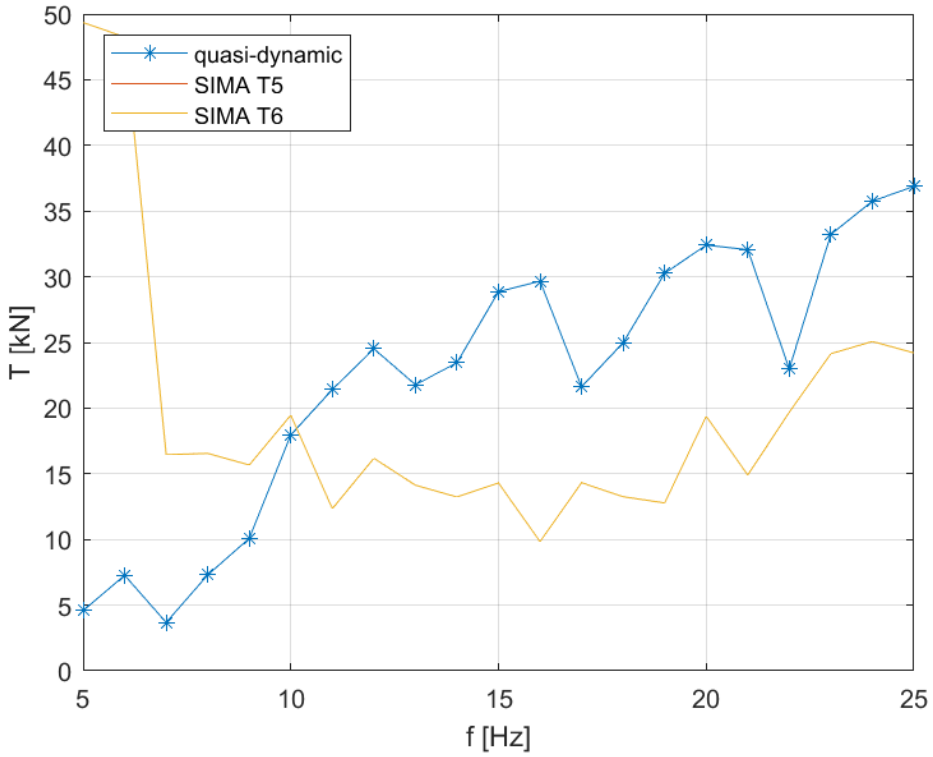

Figure 7.23: Tension amplitudes at fairleads for anchor lines on the right side

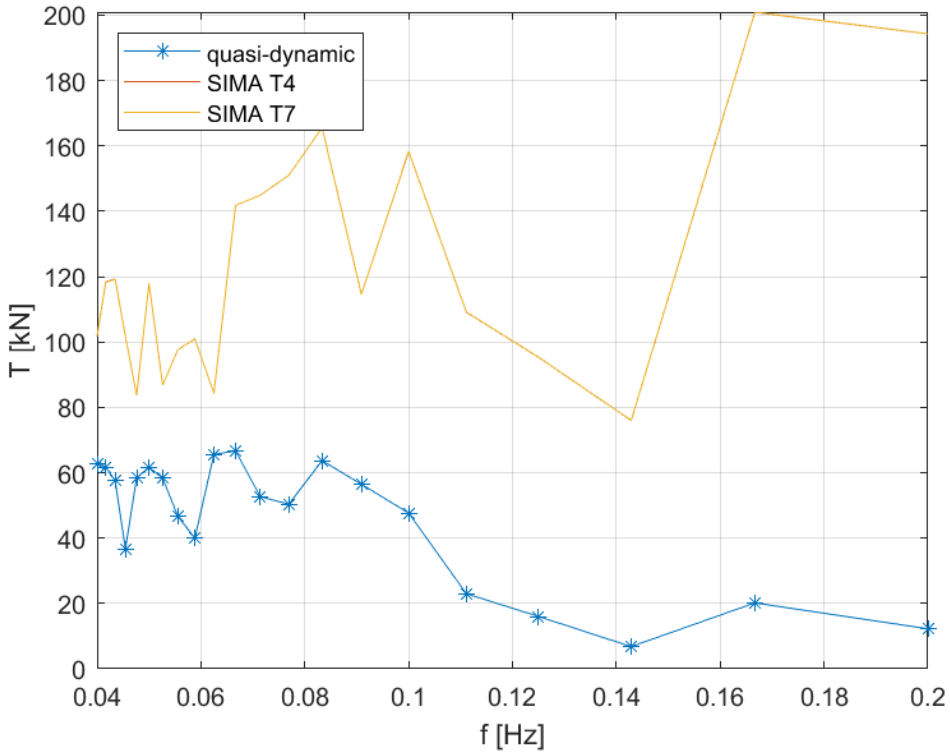

Figure 7.24: Tension amplitudes at fairleads for the shared line

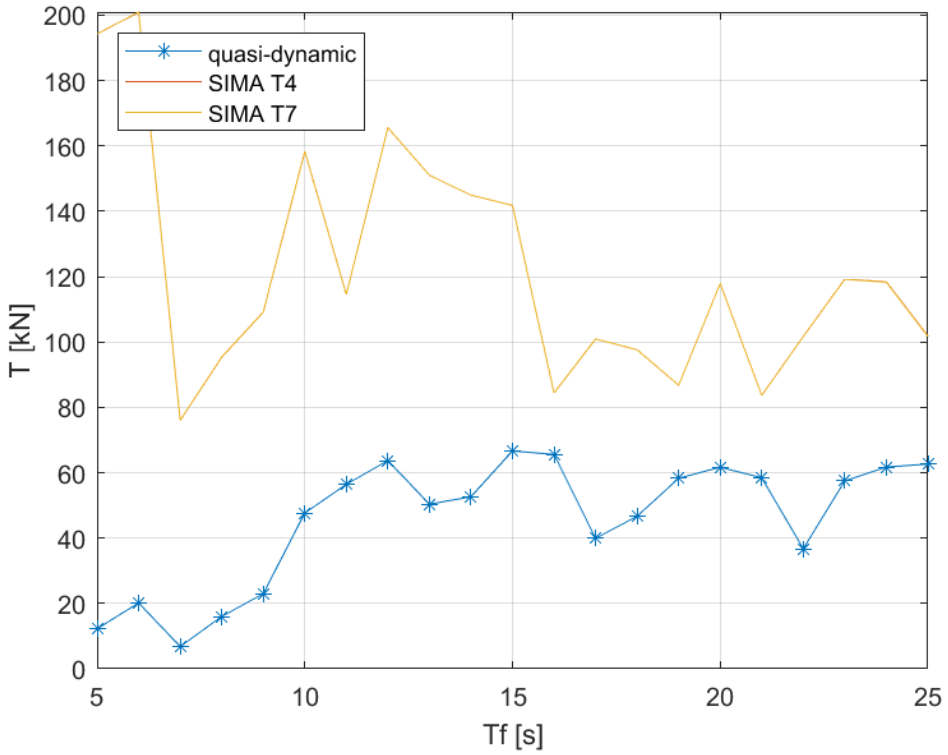

Figure 7.25: Tension amplitudes at fairleads for the shared line

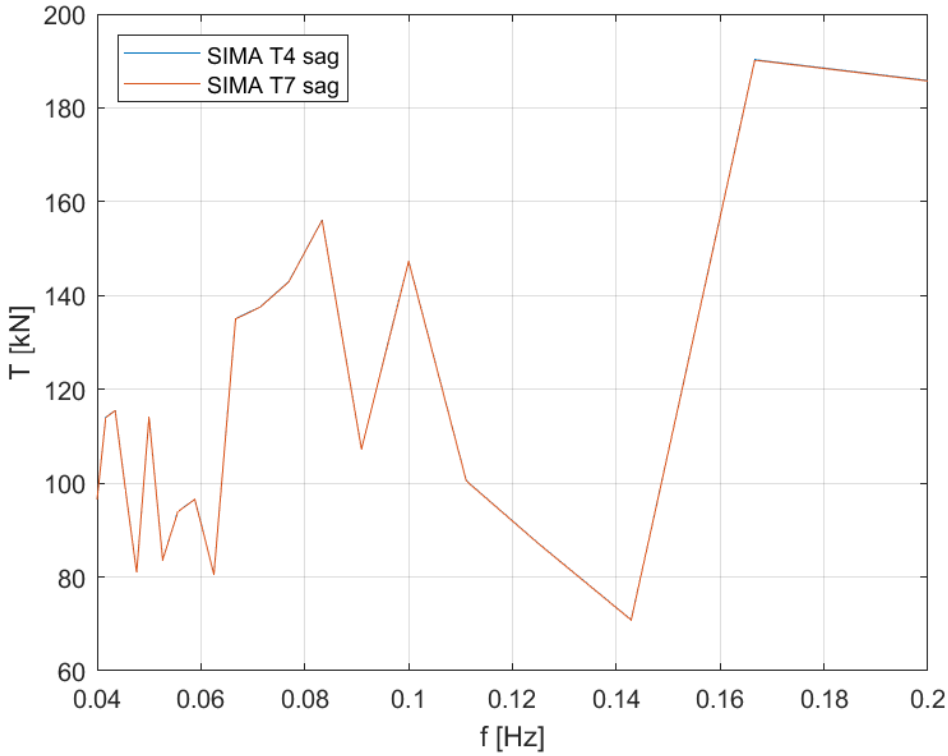

Figure 7.26: Tension amplitudes at the sag of the shared line

The tension amplitudes for the Matlab model, reported in the figures above, have been found employing the following expressions:

$$\begin{aligned} T_{a1} &= \sqrt{(k_1 x_{a1}(\cos(\alpha))^2)^2 + (c_1 \dot{x}_{a1}(\cos(\alpha))^2)^2} \\ T_{a2} &= \sqrt{(k_2 x_{a2}(\cos(\alpha))^2)^2 + (c_2 \dot{x}_{a2}(\cos(\alpha))^2)^2} \end{aligned} \tag{7.6}$$

$$T_{as} = \sqrt{(k_s x_{as})^2 + (c_s \dot{x}_{as})^2} \tag{7.7}$$

In these formulas k_1, k_2, k_s are the equivalent stiffnesses computed as shown in chapter 5, using Equation 5.2, while c_1, c_2, c_s are the equivalent dampign coefficients computed using Equation 5.3. x_{a1} and x_{a2} are the amplitudes of respectively the motions of the first and second floaters while x_{as} is the amplitude of the relative motions between the floaters that the shared line feels, computed as the amplitude of the difference between the time series $x_1(t)$ and $x_2(t)$. In the formulas for the tension amplitudes there is a $cos(\alpha)^2$ term, which appears because of the projection of the stiffness and damping coefficient terms, which are defined in the plane of the line, inclined of an angle α with respect to the global x-direction.The value of the angle α in this case has been kept constant and equal to $60°$. The formula of the amplitude for the shared line has no projection because the line is already in the global x-direction as also shown in Figure 6.2.

Regarding the SIMA tension amplitudes, these values have been found by taking the time series of the tensions at the fairleads of each anchor line and of the shared line and by filtering the signals with the respective frequency of interest to be able to extract the wanted amplitudes using the fast Fourier transform function. As already mentioned above in order to get these values the time series of the tensions that come directly out of SIMA, which represent the axial tension, have to be projected in the local horizontal direction (with the angle ϕ) and to the global x-direction (with the angle α).

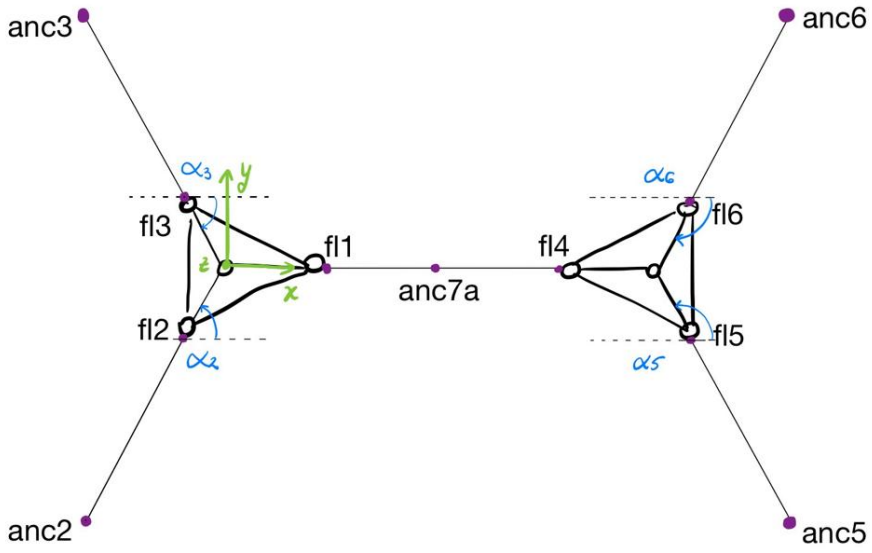

Figure 7.27: Angles of each mooring line with respect to the global x-direction

These values of the angles have been computed with the following expressions and reported in the tables below.

$$\phi = \text{arcsin}(\frac{z_{fl} - z_{node}}{||dist||}) \tag{7.8}$$

$$\alpha = \text{arctan}(\frac{y_{fl} - y_{node}}{x_{fl} - x_{node}}) \tag{7.9}$$

where z_{fl}, y_{fl}, x_{fl}, z_{node}, y_{node} and x_{node} are respectively the z,y and x coordinates of the fairleads and of the nodes right after them and $|dist|$ is the distance between the two pints.

Condition	alpha2 [°]	alpha3 [°]	alpha4 [°]	alpha5 [°]	alpha6 [°]	alpha7 [°]
1	59.9	-59.9	-180.0	120.1	-120.1	0.0
2	60.0	-60.0	-180.0	120.0	-120.0	0.0
3	59.9	-59.9	-180.0	120.1	-120.1	0.0
4	59.9	-59.9	-180.0	120.1	-120.1	0.0
5	59.9	-59.9	-180.0	120.2	-120.2	0.0
6	60.0	-60.0	-180.0	120.0	-120.0	0.0
7	59.9	-59.9	-180.0	120.1	-120.1	0.0
8	60.0	-60.0	-180.0	120.0	-120.0	0.0
9	59.6	-59.6	-180.0	120.4	-120.4	0.0
10	60.3	-60.3	-180.0	119.7	-119.7	0.0
11	59.9	-59.9	-180.0	120.1	-120.1	0.0
12	59.9	-59.9	-180.0	120.1	-120.1	0.0
13	60.1	-60.1	-180.0	119.9	-119.9	0.0
14	60.2	-60.2	-180.0	119.8	-119.8	0.0
15	59.7	-59.7	-180.0	120.3	-120.3	0.0
16	59.9	-59.9	-180.0	120.2	-120.2	0.0
17	59.8	-59.8	-180.0	120.2	-120.2	0.0
18	60.0	-60.0	-180.0	120.0	-120.0	0.0
19	59.8	-59.8	-180.0	120.2	-120.2	0.0
20	59.9	-59.9	-180.0	120.1	-120.1	0.0
21	59.9	-59.9	-180.0	120.1	-120.1	0.0

Table 7.8: Table with values of α for every mooring line

Condition	phi2 [°]	phi3 [°]	phi4 [°]	phi5 [°]	phi6 [°]	phi7 [°]
1	28.2	28.2	24.7	28.1	28.1	24.8
2	28.0	28.0	24.8	28.0	28.0	24.8
3	28.0	28.0	25.3	28.0	28.0	25.4
4	28.1	28.1	24.8	28.1	28.1	24.8
5	28.0	28.0	25.6	27.9	27.9	25.7
6	28.3	28.3	24.7	28.3	28.3	24.7
7	28.3	28.3	25.1	28.3	28.3	25.1
8	28.4	28.4	24.6	28.4	28.4	24.6
9	27.9	27.9	25.7	27.9	27.9	25.8
10	28.0	28.0	24.7	28.0	28.0	24.7
11	28.5	28.5	24.5	28.5	28.5	24.6
12	28.5	28.5	24.5	28.5	28.5	24.6
13	27.6	27.6	25.2	27.6	27.6	25.2
14	27.8	27.8	25.0	27.8	27.8	25.0
15	28.3	28.3	25.0	28.3	28.3	25.0
16	28.6	28.6	24.5	28.6	28.6	24.5
17	28.4	28.4	24.9	28.3	28.3	24.9
18	27.5	27.5	25.4	27.5	27.5	25.5
19	28.2	28.2	25.0	28.2	28.2	25.0
20	28.7	28.7	24.5	28.7	28.7	24.5
21	28.7	28.7	24.4	28.6	28.6	24.5

Table 7.9: Table with values of ϕ at every fairlead

Looking at the plots, the tensions found by SIMA of for the four anchor lines are the same. The curves entirely overlap and the tension amplitudes at the two fairleads of the shared line and in the middle are identical as well. This result confirms that the symmetry of the system has been captured but the model.

Looking at the anchor line comparison at first (Figure 7.20 and Figure 7.22), it is noticeable that for low frequencies the values found with the two models are close, with Matlab's values being slightly higher than those given by SIMA. For higher frequencies then the difference between the models increases significantly and Matlab assumes smaller values than the ones found by SIMA, following the same decreasing pattern found in the displacements.

Looking at the shared line plots (Figure 7.24), the values of the two models differ for the entire range of frequencies, showing an increasing divergence for higher frequencies as well. In this case the differences are higher than in the anchor line values and if looking at the lower frequency side of the graph, where the major correspondence between the models is expected, the values of the tension amplitudes for the SIMA model are almost twice as high as in Matlab.

In Figure 7.26, have also been reported the amplitudes of the dynamic tension computed in SIMA at the sag of the shared line. This has been included to further verify the symmetry of the system is SIMA. Not only the tension amplitudes at the fairleads for each floater correspond but also the ones computed at the sag of the shared line.

The high peaks, corresponding to the high frequencies, on the other hand are caused by the dynamic effects that SIMA takes into account more precisely than the quasi-dynamic model.

Here below have also been reported the plots showing only the damping and the stiffness contributions from both anchor and shared line for the Matlab model from Equation 7.6 and

Equation 7.7, in order to understand more in depth where the differences between the models come from.

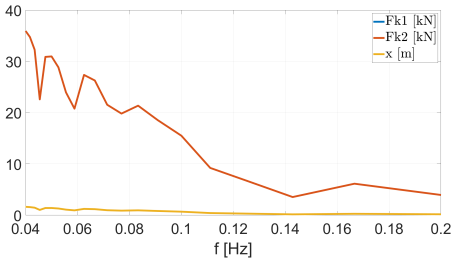

(a) Stiffness contribution from anchor lines

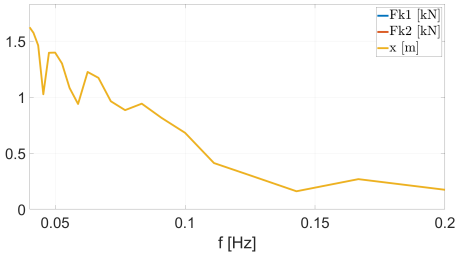

(b) Displacements

Figure 7.28

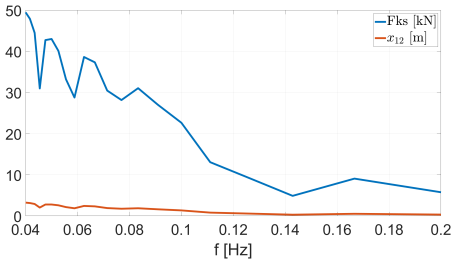

(a) Stiffness contribution from shared line

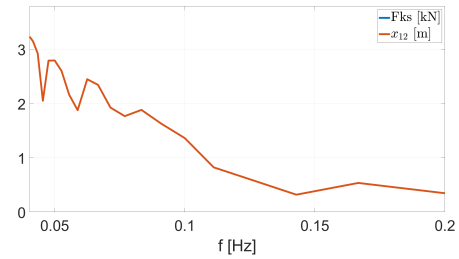

(b) Relative displacement

Figure 7.29

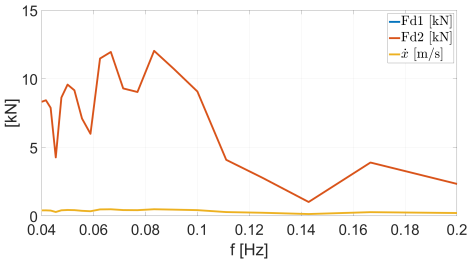

(a) Damping contribution from anchor lines

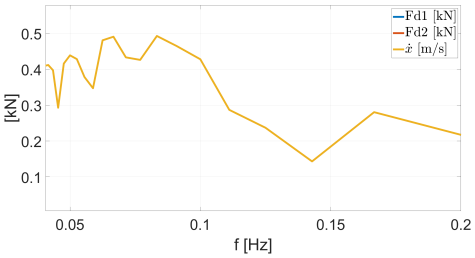

(b) Velocities

Figure 7.30

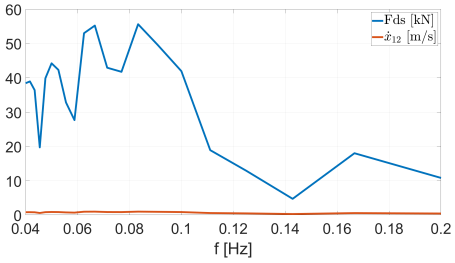

(a) Damping contribution from shared line

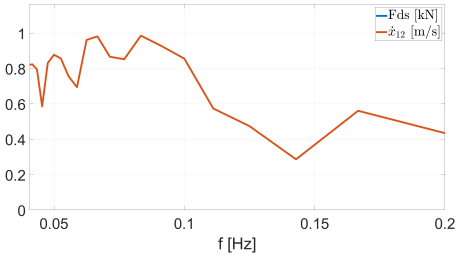

(b) Relative velocities

Figure 7.31

The damping contributions from both anchor and shared lines follow the velocity pattern, decreasing from lower to higher forcing frequencies which is the opposite trend than expected. The reason why this happens is that the Matlab model for higher frequencies is not able to take into account some non-linearities or damping effects. The shared line contribution has higher values compared to the anchor line case. This because the velocities are greater being the sum of the velocities of the single floaters and the damping force does not have to be projected in the global x-direction in the case of the shared line (already in line the the global x) decreasing its magnitude, while for the anchor line it does.

The stiffness contributions instead follow the pattern of the displacements in surge. The shared line displays higher forcing values for the same reason as mentioned for the damping contribution. It sees higher displacements compared to the single anchor lines and the stiffness is already acting the the direction of the motion, not needing to be projected and thus decreased.

The figures below represent instead the total tensions given by the summation between the total static pre-tension and the dynamic component, shown in the previous graphs. The definitions of the total terms for both models is as follows.

$$\begin{aligned} T_{2tot,SIMA} &= T_{fl2,static} + T_{2,SIMA} \\ T_{3tot,SIMA} &= T_{fl3,static} + T_{3,SIMA} \\ T_{4tot,SIMA} &= T_{fl1,static} + T_{4,SIMA} \\ T_{5tot,SIMA} &= T_{fl5,static} + T_{5,SIMA} \\ T_{6tot,SIMA} &= T_{fl6,static} + T_{6,SIMA} \\ T_{7tot,SIMA} &= T_{fl4,static} + T_{7,SIMA} \end{aligned} \tag{7.10}$$

These are the expressions used for the computation of the total tensions in SIMA. The total tensions are defined as the summation between a constant value, given by the static pre-tension in each line e.g.$T_{fl2,static}$ for fairlead 2 and a varying value, given by the frequency-dependant dynamic contribution e.g. $T_{2,SIMA}$. This last one is the amplitude of the dynamic tension, shown in Figure 7.20, Figure 7.22 and Figure 7.24. The values of the static tensions at the fairleads for each condition set are reported in the table below Table 7.10.

$$\begin{aligned} T_{1,tot} &= T_{1,static} + T_{a1} \\ T_{2,tot} &= T_{2,static} + T_{a2} \\ T_{s,tot} &= T_{s,static} + T_{as} \end{aligned} \tag{7.11}$$

The expressions above, on the other side, are the definitions of the total tensions for the Matlab model. Also in this case they are equal to the summation between a constant value, the static pre-tension e.g. $T_{1,static}$, and a dynamic one, given by amplitude of the frequency dependant quasi-dynamic tension e.g. T_{a1}, computed using Equation 7.6 and Equation 7.7. In this case the static values of the pre-tensions at the fairleads are reported in Equation 7.12 and Equation 7.13.

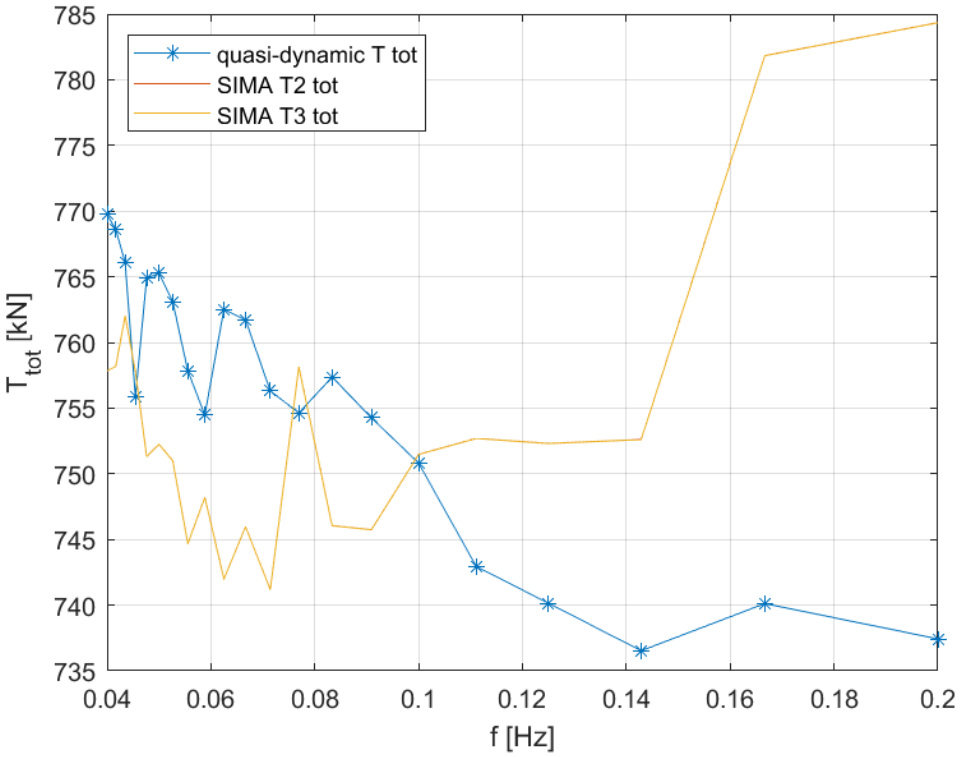

Figure 7.32: Total tensions for the anchor line on the left side for different forcing frequencies

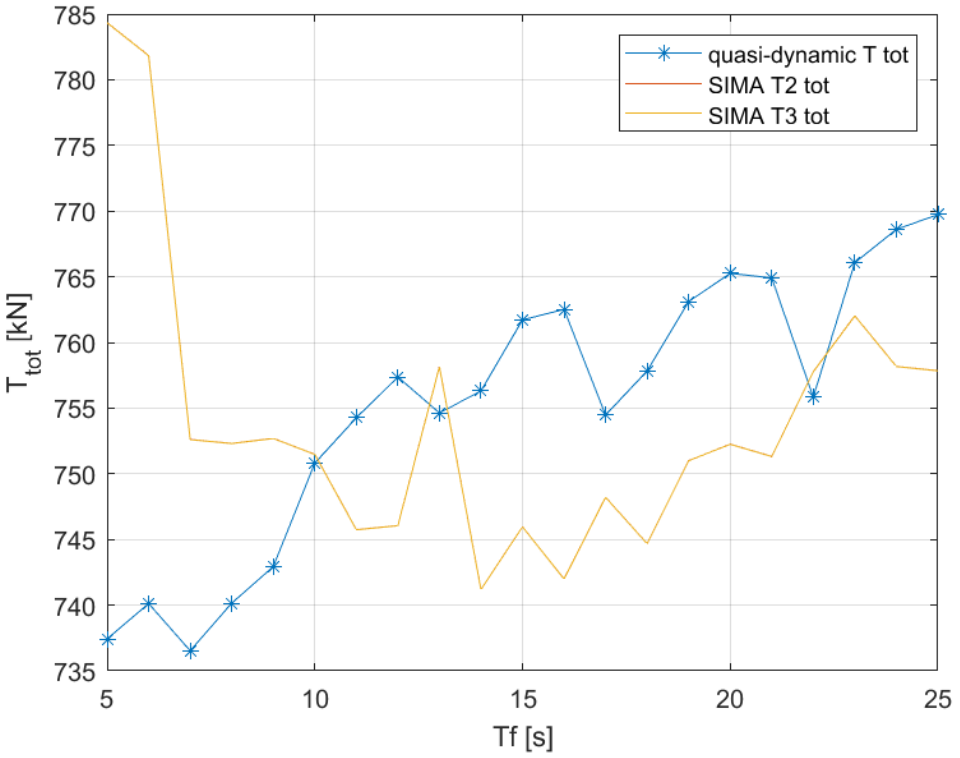

Figure 7.33: Total tensions for the anchor line on the left side for different forcing periods

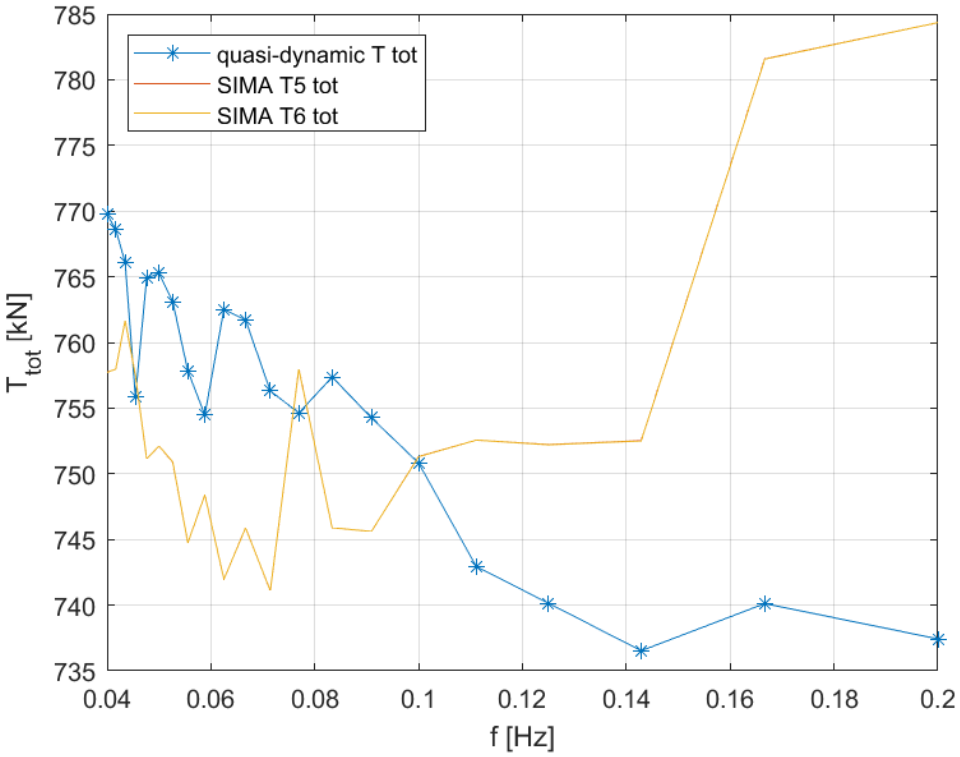

Figure 7.34: Total tensions for the anchor line on the right side for different forcing frequencies

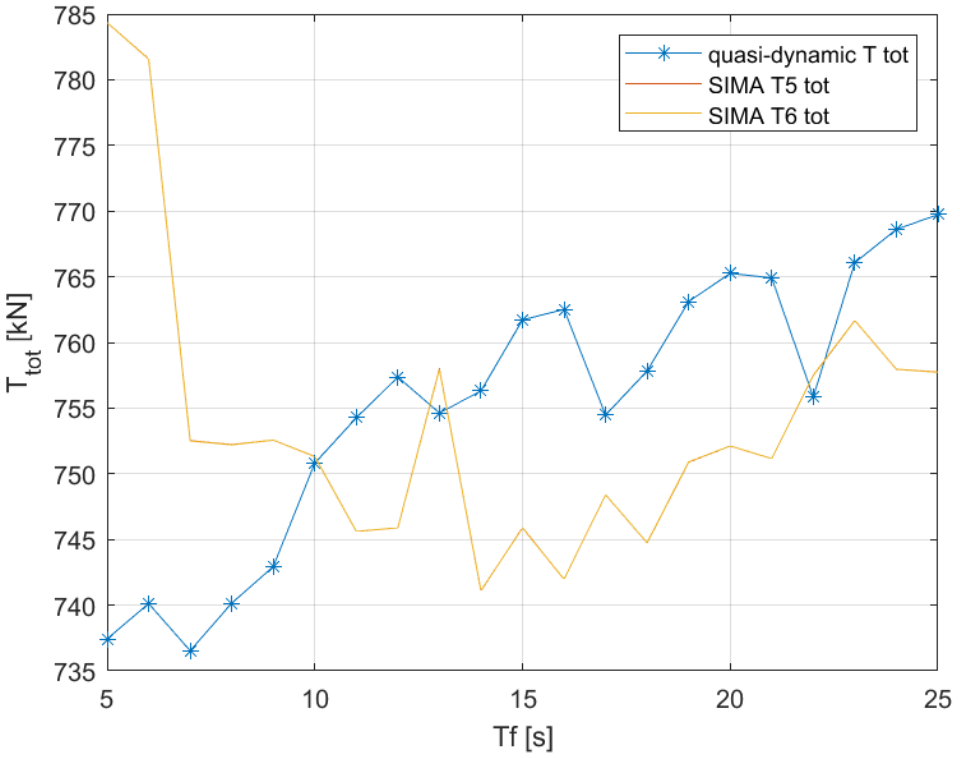

Figure 7.35: Total tensions for the anchor line on the right side for different forcing periods

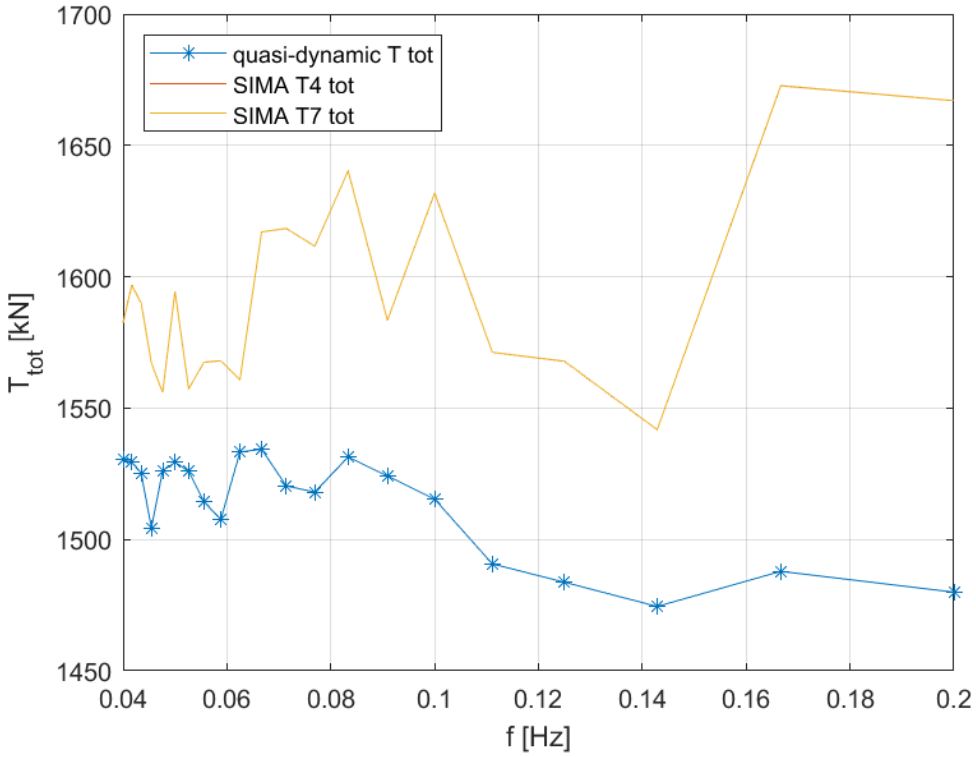

Figure 7.36: Total tensions for the shared line for different forcing frequencies

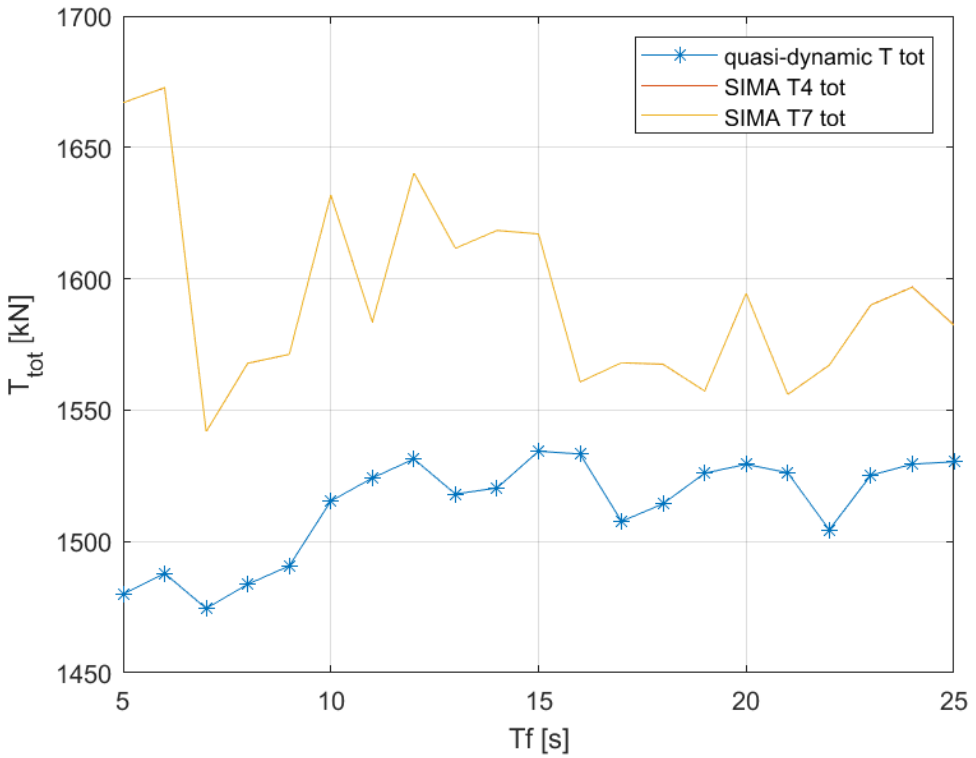

Figure 7.37: Total tensions for the shared line for different forcing periods

ConditionSet	Ts_{fl2} [kN]	Ts_{fl3} [kN]	Ts_{fl1} [kN]	Ts_{fl5} [kN]	Ts_{fl6} [kN]	Ts_{fl4} [kN]
1	734.98	734.97	1472.8	734.99	734.99	1472.8
2	733.32	733.31	1471.8	733.33	733.31	1471.8
3	736.06	736.05	1465.8	736.06	736.05	1465.8
4	735.67	735.66	1472.5	735.67	735.65	1472.5
5	736.92	736.92	1462.1	736.90	736.90	1462.1
6	731.86	731.85	1473.6	731.85	731.84	1473.6
7	733.29	733.28	1468.9	733.27	733.27	1468.9
8	729.71	729.70	1474.8	729.71	729.71	1474.8
9	743.87	743.86	1460.6	743.85	743.83	1460.6
10	727.84	727.83	1473.5	727.86	727.88	1473.5
11	731.56	731.56	1475.3	731.59	731.58	1475.3
12	732.13	732.12	1476.3	732.13	732.13	1476.4
13	733.95	733.94	1467.1	734.08	734.08	1467.1
14	731.34	731.34	1469.8	731.49	731.49	1469.9
15	738.08	738.07	1470.5	738.11	738.12	1470.5
16	732.65	732.64	1476.6	732.74	732.74	1476.6
17	736.21	736.21	1472.3	736.25	736.25	1472.3
18	737.77	737.76	1465.4	737.80	737.82	1465.5
19	737.44	737.43	1470.8	737.53	737.53	1470.8
20	732.56	732.55	1478.5	732.89	732.89	1478.5
21	733.09	733.08	1480.6	733.54	733.52	1480.6

Table 7.10: Table with the static tension values at each fairlead for each forcing conditions from SIMA

Looking at Table 7.10, it is visible that the static tensions from SIMA assume slightly different values for each condition set. This is because the model in SIMA, unlike the Matlab model, takes into account the fact that during the different dynamic analysis the angles at the fairlead between the axial and the horizontal direction in the plane of the line ϕ and the angles between the plane of the lines and the global x-direction α change as reported in Table 7.8 and Table 7.9. These changes are not overly large but they cause minor variations in the values of the amplitudes of the tensions that are reported in the table.

Regarding the Matlab model, the values of the static tension at the fairleads for both anchor and shared lines stay constant for all the different condition set. These values are found by taking the static axial tensions at the fairleads after the static analysis is performed. For the anchor lines:

$$\begin{aligned} T_1 &= 732.85 \text{ kN} \\ T_2 &= 732.85 \text{ kN} \end{aligned} \tag{7.12}$$

While for the shared line:

$$T_s = 1467.7 \text{ kN} \tag{7.13}$$

These values already represent the horizontal components of the static tensions in the global x-direction.

What it is visible in these plots is that the total tension values found by the two models are similar both for the anchor and shared lines, this because the two contributions, static and dynamic, balance each other in the two models when they are summed up. Another aspect to point out regarding these last graphs is that the patterns of curves are the same, especially

when looking at the low frequency side of the graphs. The values then diverge when going towards high forcing frequencies.

Here below is a summarizing scheme reporting all the different post-processing steps to which the the signals obtained from SIMA have been submitted in order to get the amplitudes comparable with the Matlab model.

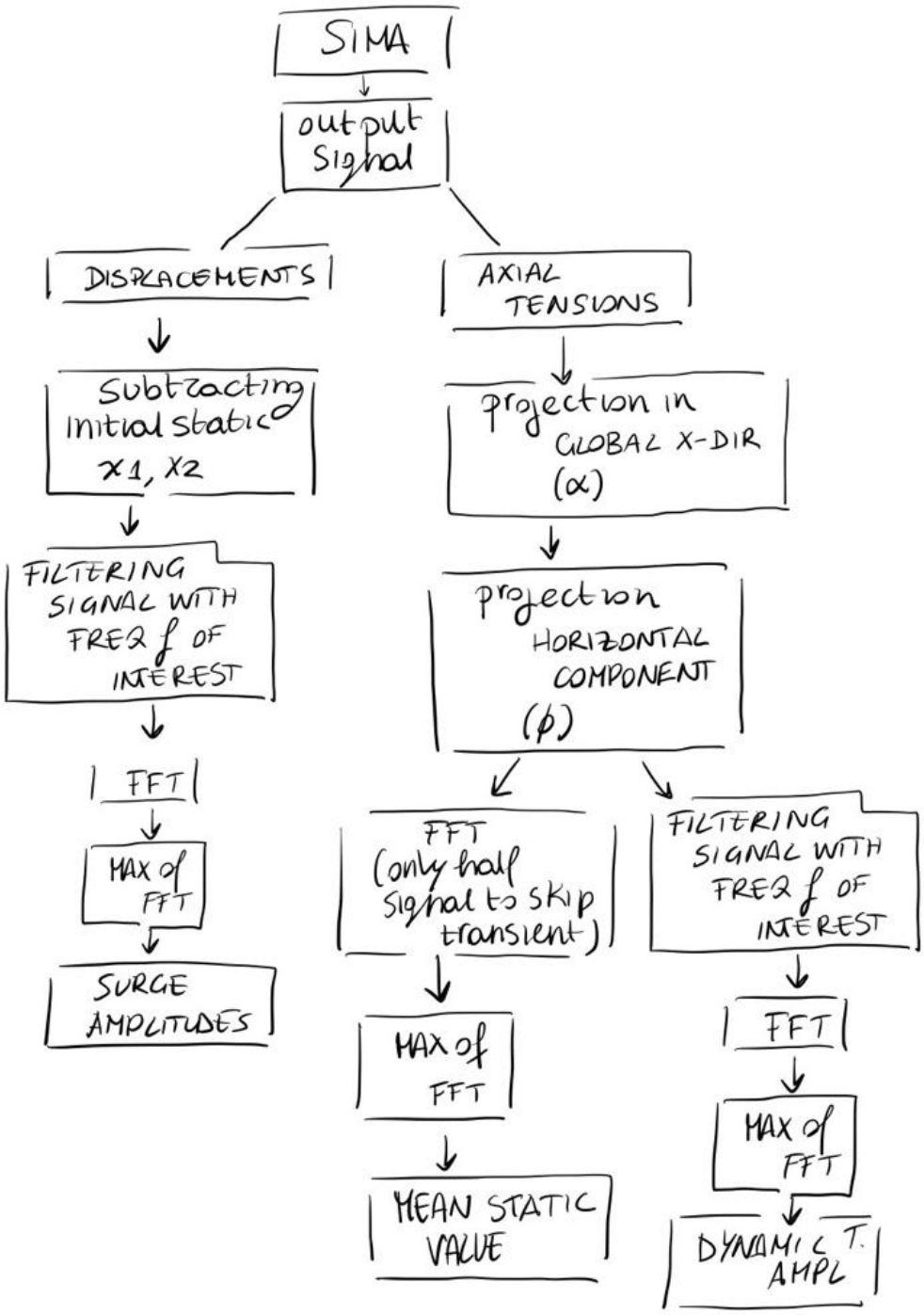

Figure 7.38: Post processing steps of SIMA signals

Verification

Also in this case, to check that the FFT function in Matlab was extracting the correct amplitudes out of the time series of the tensions and the displacements, the value of the dynamic amplitude was taken and then multiplied by the cos(ωt) or cos$(\omega t + \phi)$ and the mean value was also summed. Then the ”artificial” time series has been overlapped to the original, showing an almost complete overlapping except for a difference in the mean value.

More specifically this check has been done with all forcing frequencies but here below only the result obtained with the last forcing frequency $f = 0.04$ Hz, has been reported. The idea is to check that by creating the time series as $T_{ampl} \cdot \cos(\omega t + \pi) + T_{mean}$ this overlaps to the original time series of the axial tension that comes out of SIMA, projected in the global horizontal direction and taking int account the horizontal component of it. The same check has been done with the displacements. The time series defined as ”check” is the ”artificial” one obtained and the ”original” one is the one that comes out of SIMA computations.

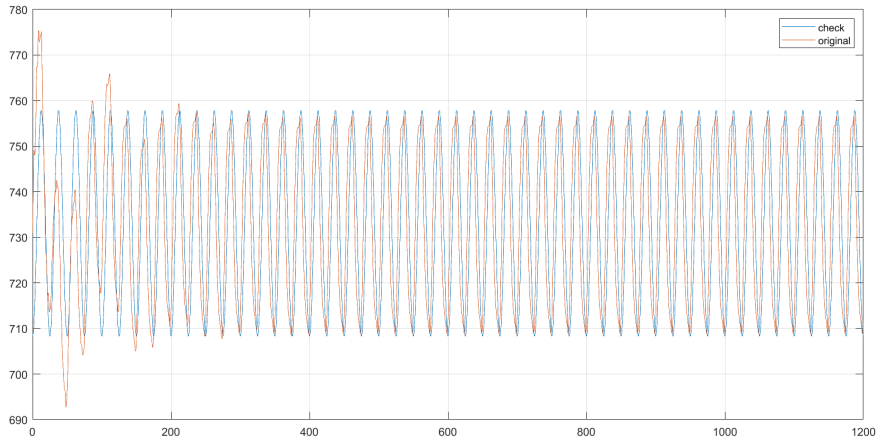

Figure 7.39: Verification of the tension value amplitudes

7.3.4. Inertia calculation

One of the main causes of the discrepancies between the Matlab quasi-dynamic and the SIMA dynamic models is due to lack of inclusion of the inertia contribution from the mooring lines in the Matlab model, especially in the shared line case. This contribution is proportional to the acceleration and therefore it tends to increase for higher frequencies, as the acceleration does since it grows quadratically with the frequency. This could explain also why the difference between the two models increases with higher frequencies. It is merely a hypothesis, and a test is conducted in the following section to verify it.

Therefore, an approximate calculation has been carried out to try to estimate the magnitude of the inertia term for the shared line case, since it is where the highest difference between the tension amplitudes is registered. To estimate this inertia force the shared line has been treated as two straight lines in the middle of which a lumped mass M has been placed, calculated as mass per unit length m, from Table 4.4 times the total length of the line $L_{tot} = 1296$ m. In order to get the inertia, this mass has been multiplied by the acceleration of the middle point of the shared line. To compute this acceleration, first the change in the sag of the line has been estimated. For a displacement of 1 m of each floater, which is the order of magnitude of the displacements observed in the dynamic calculations, the change in the sag z is around 12 m. This value has been found by using the catenary equations for a suspended line.

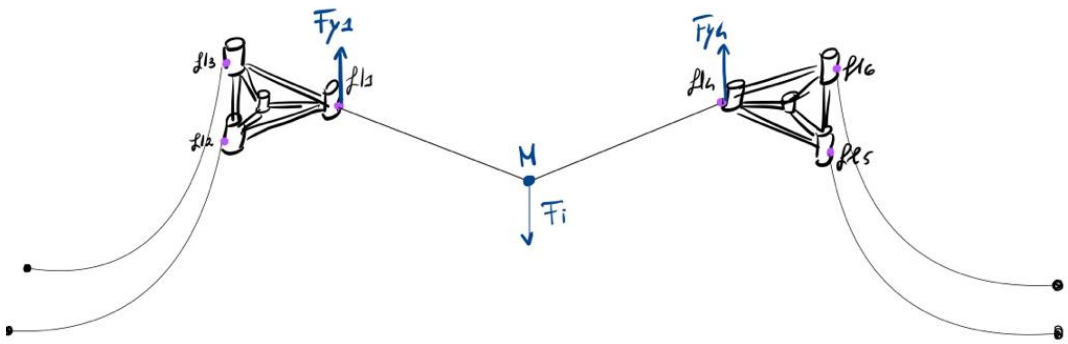

Figure 7.40: Scheme of the approximate inertia force of the shared line

To compute the inertia force of the line the following expression has been used:

$$F_i = M\ddot{z} = m\ L_{tot}\ z\ \omega^2 \tag{7.14}$$

This value changes depending on the value of ω, as reported in Table 7.11. This force applied at the mid point of the shared line is balanced at the fairleads by two vertical tensions F_{y1} and F_{y2}, as shown in Figure 7.40. The contribute given by the inertia force that should then be summed up to the dynamic tensions is in the horizontal direction. To compute these terms the expression below has been used:

$$T_{x1} = T_{x4} = F_i/2 \cdot cot(\phi) \tag{7.15}$$

Where ϕ is the angle at the fairlead between the horizontal and the axial direction.

Looking at Table 7.11, it is visible that the inertia contributions are much higher than the difference between the tension amplitudes for high frequencies visible in Figure 7.24, which fluctuates around 200 kN. The values produced are not surprising because the approximation used, by lumping all the mass of the line in the center, is as extreme as it could be. However, this demonstrates both that the absence of the inertial term of the lines may be the cause of the observed discrepancy between the models and that their proper inclusion would be required to obtain the desired order of magnitude.

f [Hz]	$F_{inertia}$ [kN]	T_{xfl} [kN]
0.200	2734.5	2906.3
0.167	1899.0	2018.3
0.143	1395.2	1482.8
0.125	1068.2	1135.3
0.111	843.98	897.02
0.100	683.63	726.58
0.091	564.98	600.48
0.083	474.74	504.57
0.077	404.51	429.93
0.071	348.79	370.71
0.067	303.83	322.93
0.063	267.04	283.82
0.059	236.55	251.41
0.056	211.00	224.25
0.053	189.37	201.27
0.050	170.91	181.65
0.048	155.02	164.76
0.045	141.25	150.12
0.043	129.23	137.35
0.042	118.69	126.14
0.040	109.38	116.25

Table 7.11: Table showing the values of the inertia force and corespondent tension at fairlead computed for each forcing frequency

Quasi-static vs. quasi-dynamic tensions

Here below the values of the tension amplitudes for both shared and anchor lines found with the quasi-dynamic Matlab model have been presented together with the quasi-static calculations also done in Matlab. This has been done to show how much the tension amplitudes calculated with the quasi-dynamic modelling differ from the conventional and more simplistic quasi-static formulation (see Figure 3.1.3).

As it is visible from both graphs the difference between the quasi-static and the quasi-dynamic approximation differs depending on the forcing frequency. For the anchor lines, see Figure 7.41 and Figure 7.42, the difference between the two models generally increases with higher frequencies. This because the quasi-dynamic, that includes damping in its calculations, increases with higher frequencies. For the shared line, see Figure 7.43, the differences are much higher with respect to the quasi-static model.

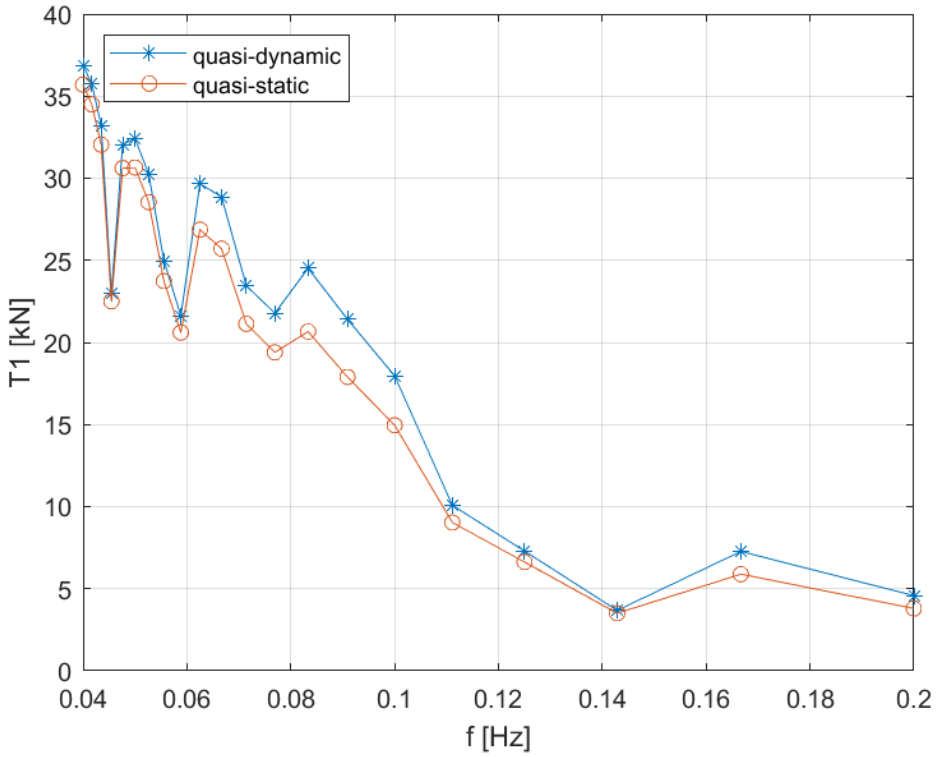

Figure 7.41: Quasi-dynamic and quasi-static total tension amplitudes for anchor lines on left side

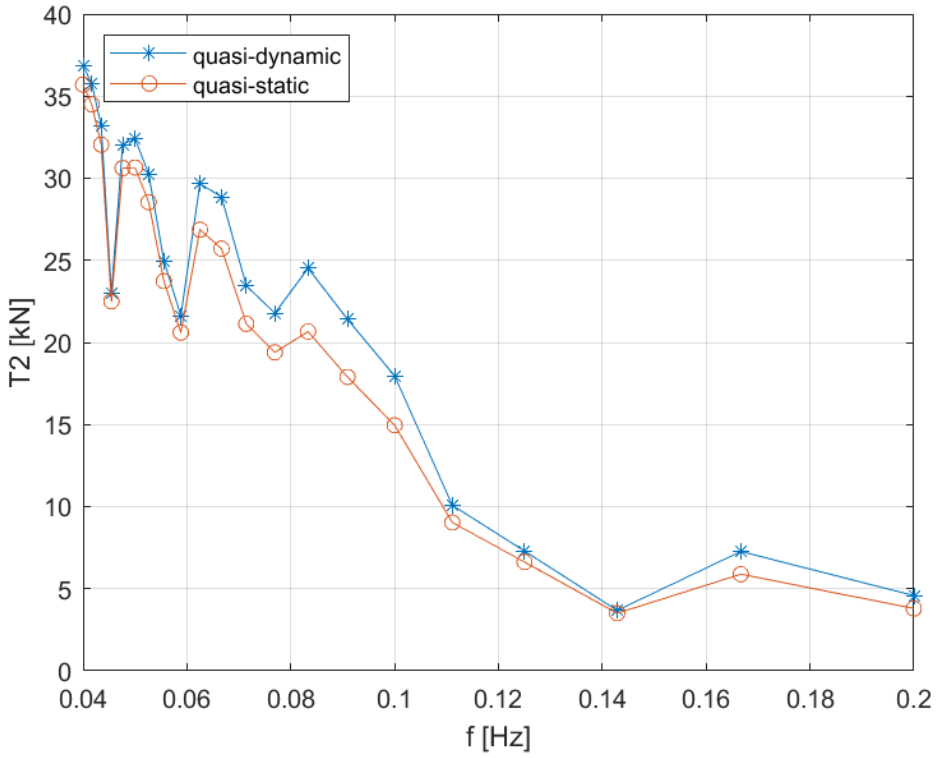

Figure 7.42: Quasi-dynamic and quasi-static tension amplitudes for anchor line on right side

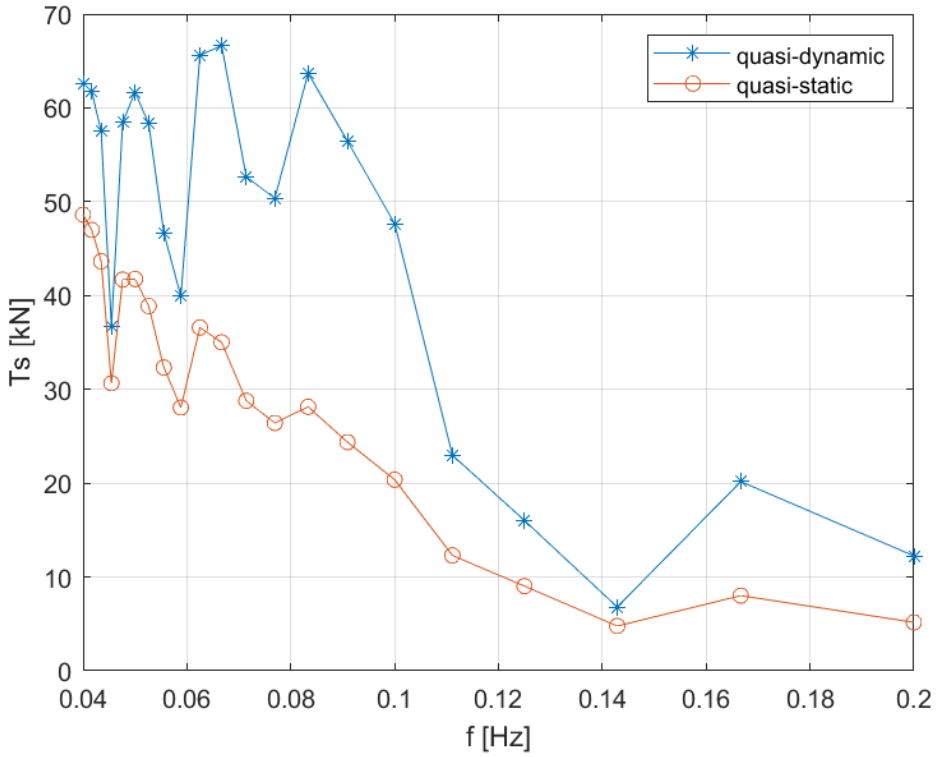

Figure 7.43: Quasi-dynamic and quasi-static tension amplitudes for shared line

Here below have been reported the figures that represent the difference in tension amplitude between the static and quasi-dynamic modelling for one anchor and one shared line considered separately as individual ones. Different forcing frequencies and motion amplitudes were also evaluated.

Figure 7.44 and Figure 7.46 are obtained respectively for an anchor and a shared line for fixed forcing frequencies, varying the motion amplitudes from 1 to 5.5 m. The values of the quasi-static tension amplitudes for each forcing frequency are represented by the continuous lines, while the dots represent the values of the quasi-dynamic one. The quasi-static tension increases with the amplitude as the quasi-dynamic does but it does not depend on the frequencies and therefore is represented by one single line. Looking at the plot it is visible that the higher the motion amplitude for a given forcing frequency the higher the quasi-dynamic values and therefore the difference between the two models. It is also visible that the higher the forcing frequency the bigger this difference becomes, indeed when the forcing frequency is 0.2 Hz the difference between the values is at its maximum, especially in the shared line case. This is because the higher the frequency, the higher the dynamic effects due to the damping term that the quasi-static model does not capture, in particular for the shared line case.

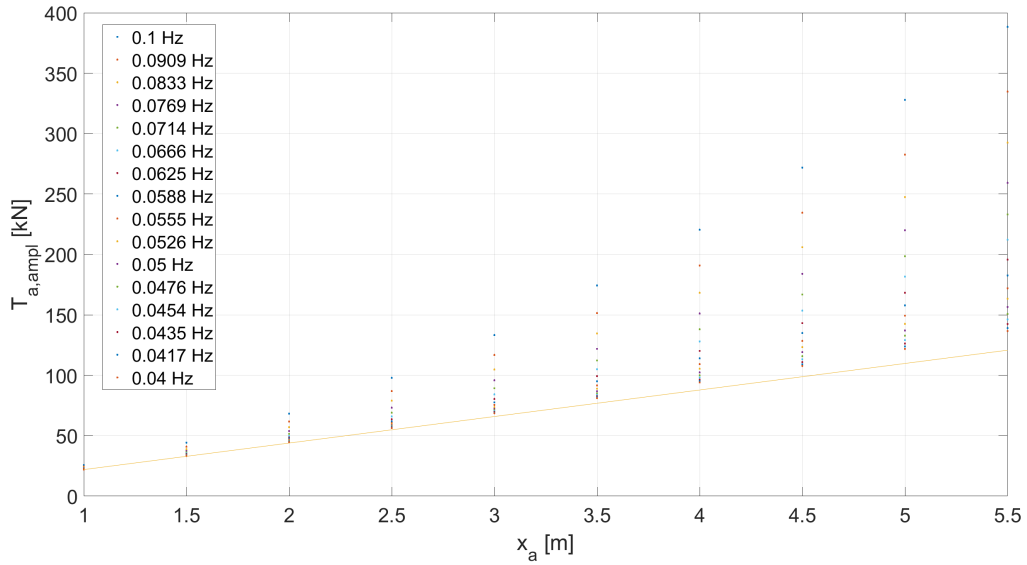

Figure 7.44: Quasi-static vs. quasi-dynamic tension amplitudes for different motion amplitudes considering one anchor line

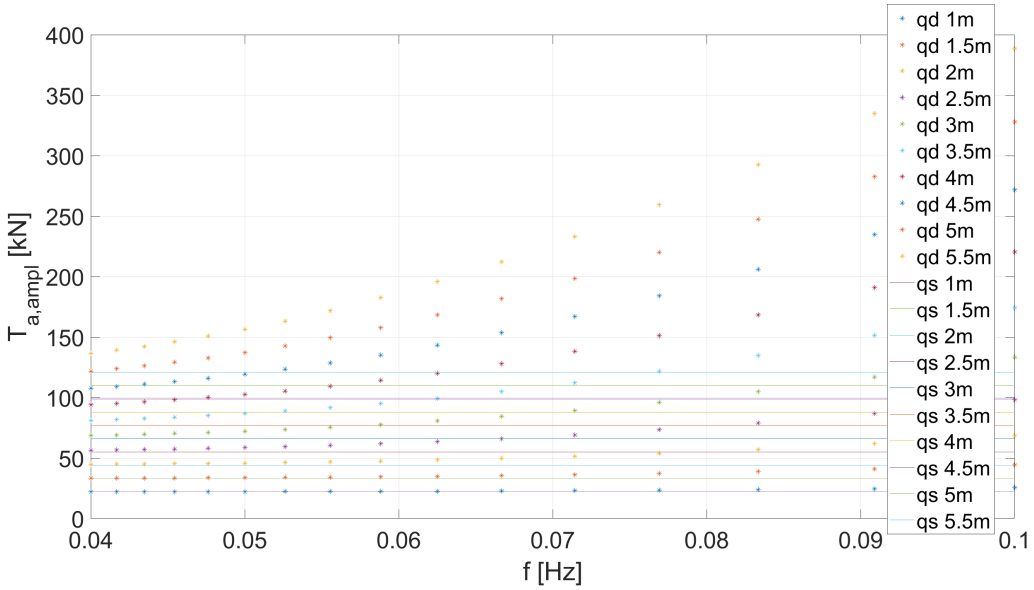

Figure 7.45: Quasi-static vs. quasi-dynamic tension amplitudes for different forcing frequencies considering one anchor line

Looking then at Figure 7.45 and Figure 7.47 it is visible again that the quasi-static tension amplitude does not depend on the forcing frequency for each amplitude motion, in fact this is represented by the continuous lines. The tension values increase with the increase of the motion amplitudes, these vary from 1 to 5.5 m starting from the first line and going up. In the case of the shared line the amplitude of the motion imposed, refers to the relative motion between the two floaters. And also in this case it is visible that the higher the frequency, the higher the difference between the two models. Even higher differences are reached with higher motion amplitudes. Also in this case the difference between quasi-static and quasi-dynamic becomes more pronounced in the shared line case.

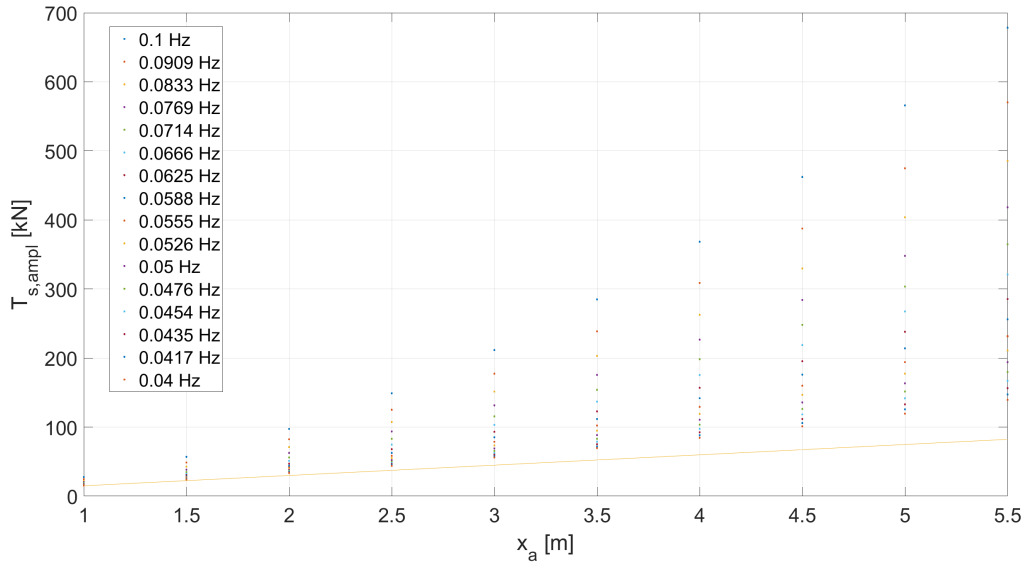

Figure 7.46: Quasi-static vs. quasi-dynamic tension amplitudes for different motion amplitudes considering one shared line

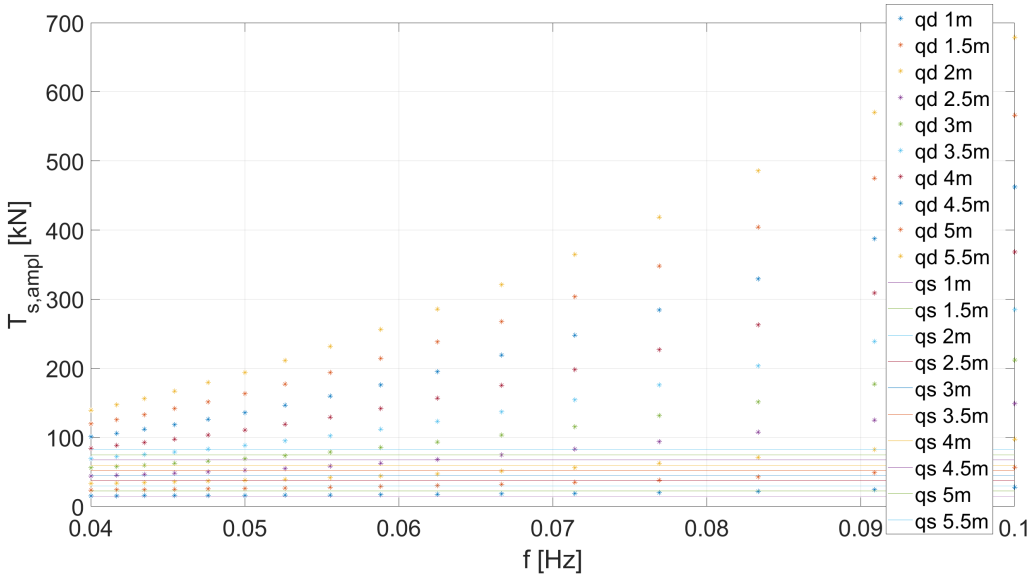

Figure 7.47: Quasi-static vs. quasi-dynamic tension amplitudes for different forcing frequencies considering one shared line

The utility of these plots is to explain the differences between the quasi-static and quasi-dynamic tensions looking at Figure 7.41 and Figure 7.43 together with Figure 7.43.

7.4. Linearization

This project was built around the idea of realising a simplified 2 DOF system based on the applied references. As showed in Figure 7.48, when building a simplified model, depending on whether or not linearization is desired, the frequency domain analysis can be carried out or not.

In this project the model used for the mooring lines is a linearized simplified 1 DOF quasi-dynamic model based on the following references [LS90] and [Heg20]. Therefore the options where to use either a time or a frequency domain analysis. In this case the linearization of the model has been done using the frequency domain, see subsection 5.1.3 and when estimating the response of the system in terms of motions and tensions the time domain analysis has been used. The focus of the project was also to compare the results with a non-linear model (SIMA), that runs its analysis in time domain. Consequently the equations of motion ended up being solved in the time domain.

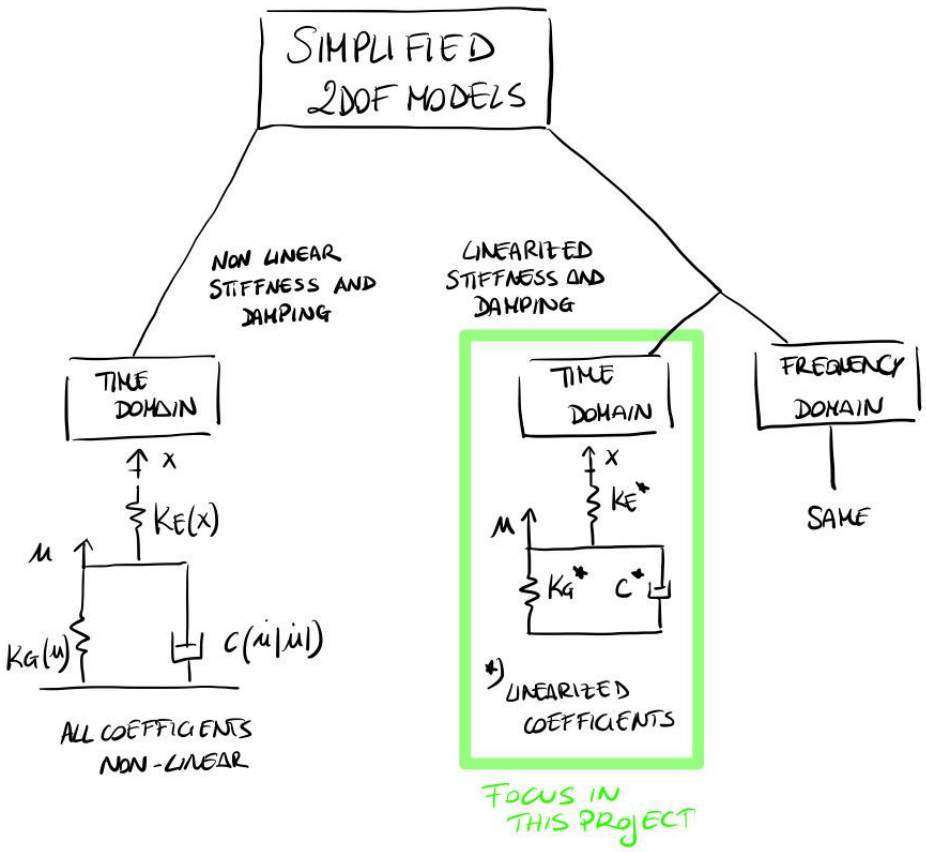

Figure 7.48: Different approaches when realising a simplified model

7.5. Discussion

The initial assumption made to compute the geometric stiffness for the shared line was to utilize the towline approximation, which is by definition a high tensioned line, as the shared line should be. At the end of the analysis the assumption regarding the towline expressions has been revised. Looking back, one of the main requisites was that the value of the horizontal component of the tensions in the line had to be much higher that the total weight of the suspended line. It turned out that the horizontal tension in the shared line was not so high as it

was thought to be compared to the total weight of the line. Indeed, the ratio $T_x/(wL)$ had to be much bigger than 1 and in this specific case this ratio was equal to 1.06, which means that the requirement was not met.

Therefore, to quantify how much the computation of the geometric stiffness was off, the k_G has been computed using the catenary equation for a suspended line and the results shown below. More specifically the expression of the horizontal coordinate according to the catenary equations for the suspended line case from Equation 3.13 has been used, without considering the elastic component and imposing $y(S) = h = 0$ in Equation 3.14.

$$l(s) = \frac{2T_0}{w}\,\text{asinh}(\frac{ws}{2T_0}) \tag{7.16}$$

and

$$k_G = \frac{1}{\partial l(s)/\partial T_x} = \frac{w\sqrt{L^2 + 4T_0^2/w^2}}{2\,\text{asinh}(\frac{wL}{2T_0})\sqrt{L^2 + 4T_0^2/w^2} - 2L} = 1.84e + 04N/m \tag{7.17}$$

Comparing this value with the one from Equation 5.14 which is $1.53e{+}04$ N/m the difference is around 18%. At this point, given the non-negligible difference between the two results, the value for the k_G given by Equation 7.17 was used in the calculation of the dynamic tensions for the shared line. The results of the amplitudes for each different forcing frequency has been reported in the figure below together with the original values (see Figure 7.50):

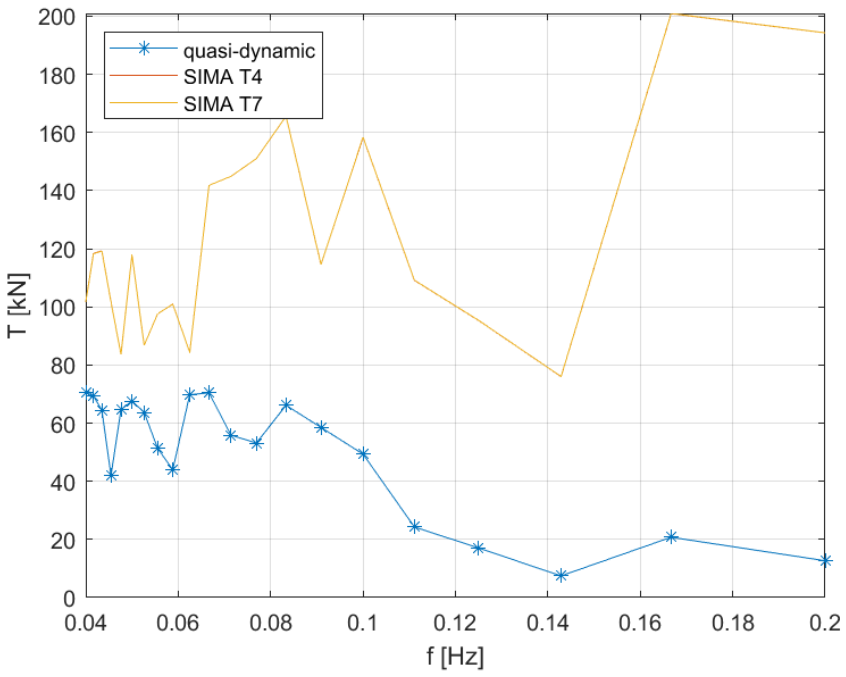

Figure 7.49: Tension amplitudes at fairleads for the shared line using the geometric stiffness found with the catenary equations

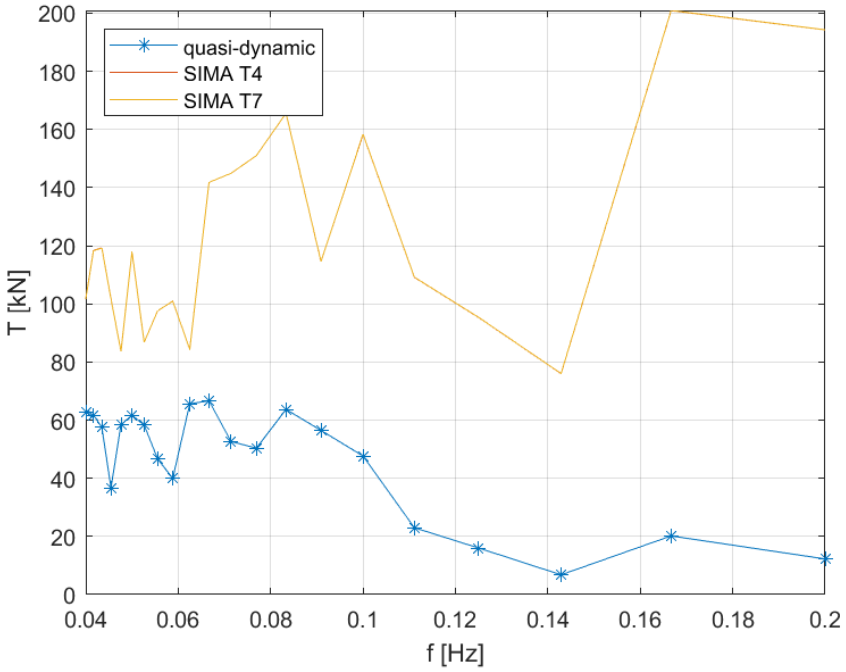

Figure 7.50: Tension amplitudes at fairleads for the shared line using the geometric stiffness found with the towline equations

Comparing this with Figure 7.24 it is visible that there are not that many differences.

Therefore, even if the values of the geometric stiffnesses were different the influence that they have on the results when plugged into the EOMs are not dramatically different. The main variation is visible for lower frequencies where in the case of using the k_G from the catenary equations the amplitudes of the dynamic tensions are slightly higher.

8

Conclusion and Recommendations

8.1. Conclusions

Shared mooring lines may be the new frontier in the field of floating offshore wind farms to substantially reduce the total costs associated with these systems by allowing the use of fewer anchors and mooring lines.

The downside of the use of shared moorings is that adjacent turbines show coupling effects, which complicate the dynamics of the whole system. This is because when two turbines are connected by a shared mooring line the motions of one platform influence those of the other.

To be able to further implement this concept and to effectively use this design it is necessary to have an in-depth understanding of what are the different scenarios that can occur when a system of this type is realized. In order to predict how floating offshore wind turbines behave dynamically mooring line modelling is crucial, especially when dealing with more complicated systems as shared mooring ones.

In order to do this a model is required that in the first place is able to carry out an accurate and fast analysis of the dynamics of these types of mooring lines to be able to conduct preliminary analysis and acknowledge the profitability of these type of systems.

For this reason, in this project a quasi-dynamic model has been proposed and implemented in a 2-floating wind turbine model in Matlab with the main purpose of obtaining faithful results but in a shorter amount of time and demanding less computational expenses with respect to a full dynamic analysis, because of the reduced number of degrees of freedom. At the same time an equivalent model has been built in SIMA, a full time domain analysis software in order to make a comparison between the results from both models.

In this simplified model the anchor lines are represented as single-degree-of-freedom systems, which include two springs, one for the geometric stiffness and the other for the elastic stiffness, together with a dashpot to account for damping contributions. However, no inertial contributions from the mooring lines were have been included in the model.

When the results of the quasi-dynamic and full dynamic models were compared in terms of motion and tension amplitudes for different forcing frequencies, it was found that for lower frequencies, there was some correspondence between the two approaches. Comparing the simplified model to the full dynamic analysis results showed that the motion amplitudes were accurately modeled. Regarding the tension values it was found that the values were not dramatically different between the two models for the low frequency forcing terms. The lack of inertia terms is most likely the cause of the discrepancies in the tension amplitudes, particularly for the shared line case, where the acceleration of the line is supposed to be greater than

the one of the anchor lines.

Therefore, based on the results it seems possible to obtain acceptable results regarding both the motion amplitudes and the tension values, in a shorter amount of time and with less computational complexity compared to a full-dynamic analysis. The main goal was to obtain reasonable tension amplitude values with the quasi-dynamic model because the motion amplitudes had already been well estimated using a quasi-static modeling approach, which was not the case for the tensions.

8.2. Recommendations

This section provides an overview of how to build on the approach and findings described in this study.

Among the things that may be added next to the model, there is the possibility to properly include the inertial contributions of the lines, which were not considered in this case due to the limited scope of the project. Probably by adding these inertia terms the correspondence between the quasi-dynamic and the fully dynamic models will increase. Especially for the shared line which would have a higher contribution with respect to the anchor lines.

Additionally, in order to make the model more realistic, it could be useful to incorporate both the mean environmental wind force and use irregular wave forcing terms, instead of regular sinusoidal waves.

Another aspect that could be implemented in the model is to include both pitch and heave motions of the two floating platforms in order to have a more complete model. A further step will be then to increase the number of wind turbines in the system, modelling a triangle layout with three shared mooring floating wind turbines. In the latter case, a further investigation should be done to choose a proper layout that would be able to optimize the wind farm efficiency, perhaps taking into account the research already done by Connolly and Hall in [CH19].

The availability of a model that is in time domain allows it to be easily extended with future work to a non-linear time domain model including non regular wave forces and non linear stiffness and damping coefficients, or, because it is a linearized model, it can be also easily extended to the frequency domain.

Extending the model to the frequency domain is a simple process that can be accomplished by utilizing the linearized transfer function to get the motion amplitudes.

$$x_a(\omega) = |H(\omega)|F_a(\omega) \tag{8.1}$$

Where $|H(\omega)|$ is the linearized transfer function matrix and $F_a(\omega)$ is the linear wave forces amplitude. Knowing the motion amplitudes to compute the dynamic axial tension amplitudes with the quasi dynamic modelling, $x_a(\omega)$ has to be projected in the inline direction.

$$T_A(\omega) = x_a(\omega)^{inline}\sqrt{(K_{eq})^2 + (\omega c_e)^2} \tag{8.2}$$

By doing so, the benefit will be the achievement of a greater knowledge in this field that can be used for further design explorations regarding this type of technology.

References

[Bha+13] Subhamoy Bhattacharya et al. “Observed dynamic soil–structure interaction in scale testing of offshore wind turbine foundations”. In: *Soil Dynamics and Earthquake Engineering* 54 (2013), pp. 47–60.

[CH19] Patrick Connolly and Matthew Hall. “Comparison of pilot-scale floating offshore wind farms with shared moorings”. In: *Ocean Engineering* 171 (2019), pp. 172–180.

[Con18] P Connolly. “Resonance in Shared Mooring Floating Offshore Wind Turbine Farms”. In: (2018).

[Cou+13] Alexander J Coulling et al. “Validation of a FAST semi-submersible floating wind turbine numerical model with DeepCwind test data”. In: *Journal of Renewable and Sustainable Energy* 5.2 (2013), p. 023116.

[CPS18] Alfonso Campanile, Vincenzo Piscopo, and Antonio Scamardella. “Mooring design and selection for floating offshore wind turbines on intermediate and deep water depths”. In: *Ocean Engineering* 148 (2018), pp. 349–360.

[Equ22] EquinorASA. *Hywind Tampen*. 2022. URL: `https://www.equinor.com/energy/hywind-tampen`.

[GM15] Marek Goldschmidt and Michael Muskulus. “Coupled mooring systems for floating wind farms”. In: *Energy Procedia* 80 (2015), pp. 255–262.

[Heg20] John Marius Hegseth. “Efficient Modelling and Design Optimization of Large Floating Wind Turbines”. In: (2020).

[Jon+09] Jason Jonkman et al. *Definition of a 5-MW reference wind turbine for offshore system development*. Tech. rep. National Renewable Energy Lab.(NREL), Golden, CO (United States), 2009.

[JSW06] L Johanning, GH Smith, and J Wolfram. “Mooring design approach for wave energy converters”. In: *Proceedings of the Institution of Mechanical Engineers, Part M: Journal of Engineering for the Maritime Environment* 220.4 (2006), pp. 159–174.

[LJM21] Guodong Liang, Zhiyu Jiang, and Karl Merz. “Mooring Analysis of a Dual-Spar Floating Wind Farm With a Shared Line”. In: *Journal of Offshore Mechanics and Arctic Engineering* 143.6 (2021).

[LKC18] Mareike Leimeister, Athanasios Kolios, and Maurizio Collu. “Critical review of floating support structures for offshore wind farm deployment”. In: *Journal of Physics: Conference Series*. Vol. 1104. 1. IOP Publishing. 2018, p. 012007.

[LS90] Kjell Larsen and Peter C Sandvik. “Efficient methods for the calculation of dynamic mooring line tension”. In: *The First ISOPE European Offshore Mechanics Symposium*. OnePetro. 1990.

[Ma+19] Kai-Tung Ma et al. *Mooring system engineering for offshore structures*. Gulf Professional Publishing, 2019.

[Ma+21] Kai-tung Ma et al. “Mooring Designs for Floating Offshore Wind Turbines Leveraging Experience From the Oil & Gas Industry”. In: *International Conference on Offshore Mechanics and Arctic Engineering*. Vol. 85116. American Society of Mechanical Engineers. 2021, V001T01A031.

[Mag14] Eivind Tørset Magnussen. “Analysis of low-Frequency damping in mooring lines for floating production units”. MA thesis. Institutt for marin teknikk, 2014.

[OED22] OEDigital. “TotalEnergies, Semar Working on ’Honeymooring’ Solution for Floating Wind”. In: *Offshore Engineer* (2022).

[Rob+14] Amy Robertson et al. *Definition of the semisubmersible floating system for phase II of OC4*. Tech. rep. National Renewable Energy Lab.(NREL), Golden, CO (United States), 2014.

[SEM] SEMARAS. *Honeymooring*™. URL: `https://semar.no/honeymooring/`.

[Wil+21] Samuel Wilson et al. “Linearized modeling and optimization of shared mooring systems”. In: *Ocean Engineering* 241 (2021), p. 110009.

A

Derivation of Equations

A.1. Amplitude of horizontal motion ua

The starting point to find the expression for this extra DOF was the expression of the tension in the elastic spring k_E has to be the same as the tension in the dashpot c_e and geometric spring k_G, see Figure 5.3a.

$$T = k_E\,(x-u) = c_e\dot{u} + k_G\,x \tag{A.1}$$

which implies:

$$c_e\dot{u} + (k_G + k_E)\,u = k_E\,x \tag{A.2}$$

Setting $x = x_a e^{i\omega t}$ and $u = u_a e^{i(\omega t+\phi)}$, Equation A.2 becomes:

$$c_e u_a i\omega e^{i(\omega t+\phi)} + (k_G+k_E)u_a e^{i(\omega t+\phi)} = k_E x_a e^{i\omega t} \tag{A.3}$$

and then dividing by $e^{i(\omega t+\phi)}$, the following expression is obtained:

$$c_e u_a i\omega + (k_G+k_E)u_a = k_E x_a e^{-i\phi} = k_E x_a(cos\phi - isin\phi) = \tag{A.4}$$

which leads to:

$$\begin{aligned} c_e u_a i\omega &= -k_E x_a isin\phi \\ (k_G+k_E)u_a &= k_E x_a cos\phi \end{aligned} \tag{A.5}$$

These two expressions combined lead to:

$$\begin{aligned} \frac{u_a^2}{x_a^2}\cdot\left(\frac{k_E+k_G}{k_e}\right)^2 &= \cos^2\phi \\ \frac{u_a^2}{x_a^2}\cdot\left(\frac{c_e\cdot w}{k_E}\right)^2 &= \sin^2\phi \end{aligned} \tag{A.6}$$

Since $sin\phi^2 + cos\phi^2 = 1$, the previous expressions summed give the following:

$$\left(\frac{u_q}{x_a}\right)^2\left[\left(\frac{k_E+k_G}{k_e}\right)^2 + \left(\frac{c_e w}{k_E}\right)^2\right] = 1 \tag{A.7}$$

$$u_a = \frac{k_E}{\sqrt{(k_E+k_G)^2 + (c_e\cdot\omega)^2}}\cdot x_a \tag{A.8}$$

A.2. Equivalent stiffness k

Starting with the requirement that the tension in the elastic spring of the quasi-dynamic model $T = k_E(x-u)$, must be equal to that of the equivalent model $T = kx + c\dot{x}$, the expressions Equation 5.2 and Equation 5.3 were obtained.
The initial step was to take the real part of the tension $T = k_E(x-u)$ in order to derive the expression for the equivalent stiffness:

$$kx = \mathrm{Re}[k_E(x-u)] = k_E x - k_E \frac{k_E}{\sqrt{(c_e\omega)^2 + (k_G+k_E)^2}} x \cos(\phi) \tag{A.9}$$

Knowing that: $\tan(\phi) = \frac{\sin\phi}{\cos\phi} = -\left(\frac{c_e\omega}{k_E+k_G}\right)$, $\sin\phi = -\frac{\omega c_e}{k_E}x_a$ from Equation A.6 and Equation A.8
Then:

$$\cos\phi = -\left(\frac{k_E+k_G}{c_e\omega}\right)\sin\phi = -\frac{(k_E+k_G)}{c_e\omega}\left(-\frac{\omega c_e}{k_E x_a}\cdot\frac{k_E}{\sqrt{(c_e\omega)^2+(k_G+k_E)^2}}\right) \tag{A.10}$$

After simplifying the expression, it becomes:

$$\cos\phi = \frac{(k_E+k_G)}{\sqrt{(c_e\omega)^2+(k_E+Kk_G)^2}} \tag{A.11}$$

Then by plugging Equation A.11 into Equation A.9:

$$kx = k_E x - \frac{k_E^2}{\sqrt{(c_e\omega)^2+(k_G+k_E)^2}}\cdot x \cdot \frac{(k_E+k_G)}{\sqrt{(c_e\omega)^2+(k_E+k_G)^2}} \tag{A.12}$$

Then finally the expression fro the equivalent stiffness k becomes the following:

$$k = k_E\left[1 - \frac{k_E(k_E+k_G)}{(k_E+k_G)^2+(c_e\omega)^2}\right] \tag{A.13}$$

Which corresponds to Equation 5.2.

A.3. Equivalent damping c

For the damping coefficient instead the initial step was to take the imaginary part of the tension $T = k_E(x-u)$ in order to derive the expression for the equivalent damping coefficient c:

$$c\dot{x} = \mathrm{Im}[k_E(x-u)] = -\frac{k_E k_E}{\sqrt{(c_e\omega)^2+(k_G+k_E)^2}} x \sin\phi \tag{A.14}$$

From before it is known that $\sin\phi = \frac{\omega c_e}{k_e x_a}\frac{k_E}{\sqrt{(c_e\omega)^2+(k_e+k_G)^2}}x_a$ and therefore:

$$c\dot{x} = \frac{\omega c_e}{\sqrt{(k_E+k_G)^2+(c_e\omega)^2}}\cdot\frac{k_E^2}{\sqrt{(k_E+k_G)^2+(c_e\omega)^2}}x \tag{A.15}$$

performing the multiplications and simplifying by $\dot{x}$ and ω:

$$c = \frac{c_e k_E^2}{(k_G+k_E)^2+(c_e\omega)^2} \tag{A.16}$$

Which corresponds to Equation 5.3.

B

SIMA nodes and lines

Here below are reported the tables containing the different nodes and lines that have been modelled in SIMA.

Node	Constraint	Master	Xg_{in} [m]	Yg_{in} [m]	Zg_{in} [m]	Xg [m]	Yg [m]	Zg [m]
fl1	slave	semi1	40.868	5.00E-15	-14	/	/	/
fl2	slave	semi1	-20.434	-35.395	-14	/	/	/
fl3	slave	semi1	-20.434	35.395	-14	/	/	/
fl4	slave	semi2	1298.5	5.00E-15	-14	/	/	/
fl5	slave	semi2	1359.8	35.395	-14	/	/	/
fl6	slave	semi2	1359.8	-35.395	-14	/	/	/
anc2	fixed	/	-406.43	-703.97	-14	-391.15	-677.5	-200
anc3	fixed	/	-406.43	703.97	-14	-391.15	677.5	-200
anc5	fixed	/	1745.8	-703.97	-14	1730.5	-677.5	-200
anc6	fixed	/	1745.8	703.97	-14	1730.5	677.5	-200
anc7a	free	/	669.67	5.00E-15	-170.57	/	/	/
semi1	fixed and freed during static analysis	/	0	0	0	0	0	0
semi2	fixed and freed during static analysis	/	1339.3	0	0	1339.3	0	0
towerlow	slave	semi1	0	0	0	/	/	/
towerup	free	/	0	0	87.6	/	/	/
towerlow1	slave	semi2	1339.3	0		/	/	/
towerup1	free	/	1339.3	0	0	/	/	/

Table B.1: Table with the super-nodes from SIMA

Name	Line type	end1	end2	L [m]
mline2	mooring	fl2	anc2	772
mline3	mooring	fl3	anc3	772
mline4	mooring_shared_half	fl1	anc7a	648
mline5	mooring	fl5	anc5	772
mline6	mooring	fl6	anc6	772
mline7	mooring_shared_half	fl4	anc7a	648
semiart	semidum	semi1	towerlow	10
semiart1	semidum	semi2	towerlow1	10
tower	tower_lt	towerlow	towerup	77.6
tower11	tower_lt	towerlow1	towerup1	77.6

Table B.2: Table with different line types modelled in the system in SIMA